



HANS WIJMANS

SYNTHETIC MEMBRANES

on the mechanism of formation of
membranes and the concentration
polarization phenomenon in
ultrafiltration

SYNTHETIC MEMBRANES

**On the formation mechanism of membranes and on the
concentration polarization phenomenon in ultrafiltration**

PROEFSCHRIFT

ter verkrijging van de graad van doctor
in de technische wetenschappen
aan de Technische Hogeschool Twente,
op gezag van de rector magnificus,
prof. ir. W. Draijer,
volgens besluit van het College van Dekanen
in het openbaar te verdedigen op
vrijdag 23 november 1984 te 16.00 uur

door

JOHANNES GERARD WIJMANS

geboren op 24 mei 1955.
te Amsterdam

© 1984 by J.G. Wijmans
cover design by Yme de Flüter
printed by Alfa, Enschede, the Netherlands

Dit proefschrift is goedgekeurd door de promotor prof. dr. C.A. Smolders
Referent: dr. ir. F.W. Altena

VOORWOORD

Het in dit proefschrift beschreven onderzoek is uitgevoerd in nauwe samenwerking met alle leden van de werkgroep Membraanfiltratie van de Technische Hogeschool Twente. De werkgroep heeft dankzij de immer enthousiaste Kees Smolders een explosieve groei doorgemaakt en inclusief studenten en stagiairs hebben zeer velen gezorgd voor een uitstekend werkklimaat met veel sfeer en kennis. Een drietal wil ik met name noemen en bedanken: Marcel Mulder, voor zijn opmerking, vele jaren geleden, dat het membranenonderzoek toch wel de moeite waard was; Frank Altena, voor de uitgebreide discussies over de vorming van membranen; en Shin-ichi Nakao, voor zijn bijdragen aan de hoofdstukken over concentratie polarisatie.

De diensten en werkplaatsen van de afdeling Chemische Technologie bedank ik voor de verrichte werkzaamheden en het daarin verwerkte meedenken en meeleven.

Tenslotte was dit boekje niet tot stand gekomen zonder het zorgvuldige typewerk van Bartie Bruggink en Julia Ardesch.

CONTENTS

	page	
CHAPTER 1	INTRODUCTION	11
1.1	Separation Processes	11
1.2	Membrane Filtration	12
1.3	Why Use Membranes?	16
1.4	Preparation of Membranes	17
1.5	Membranes at Work	18
1.6	Structure of this Thesis	20
1.7	References and Notes	22
PART I	THE MECHANISM OF FORMATION OF SYNTHETIC MEMBRANES	
CHAPTER 2	PREPARATION OF ASYMMETRIC MEMBRANES BY THE PHASE INVERSION PROCESS	27
2.1	Summary	27
2.2	Introduction	27
2.3	Phase Inversion Process: Preparation Procedures	28
2.4	Phase Separation in Polymer Systems	30
2.5	Formation of Asymmetric Membranes	38
2.6	Membrane Structures in Relation to Preparation Procedures	41
2.7	Conclusions	47
2.8	References	47

CHAPTER 3	PHASE SEPARATION PHENOMENA IN SOLUTIONS OF POLYSULFONE IN MIXTURES OF A SOLVENT AND A NONSOLVENT: RELATIONSHIP WITH MEMBRANE FORMATION	51
3.1	Summary	51
3.2	Introduction	52
3.3	Theory	52
3.4	Experiments	56
3.5	Results and Discussion	61
3.6	Preparation and Properties of Poly- sulfone Membranes	68
3.7	Conclusions	71
3.8	References	71
APPENDIX	REMOVAL OF A LOW MOLECULAR WEIGHT, CRYSTALLIZABLE POLYMER FRACTION FROM SOLUTIONS OF POLYSULFONE	73
	Summary	73
	Introduction	74
	Experimental	74
	Results and Discussion	75
	References	83
CHAPTER 4	PHASE SEPARATION PHENOMENA IN SOLUTIONS OF POLY(2,6-DIMETHYL-1,4-PHENYLENEOXIDE) IN MIXTURES OF TRICHLOROETHYLENE, 1-OCTANOL AND METHANOL: RELATIONSHIP WITH MEMBRANE FORMATION	85
4.1	Summary	85
4.2	Introduction	85
4.3	Theory	86
4.4	Experiments	91
4.5	Results and Discussion	93
4.6	Preparation and Properties of PPO Membranes	104
4.7	References	107

CHAPTER 5	THE MECHANISM OF FORMATION OF MICROPOROUS OR SKINNED MEMBRANES PRODUCED BY IMMERSION PRECIPITATION	109
5.1	Summary	109
5.2	Introduction	110
5.3	Theory	111
5.4	Experimental	114
5.5	Results and Discussion	115
5.6	Conclusions	123
5.7	References	124
CHAPTER 6	THE FORMATION OF MEMBRANES FROM TERNARY SYSTEMS: VARIATION OF PREPARATION PARAMETERS	127
6.1	Summary	127
6.2	Introduction	127
6.3	Theory	129
6.4	Experimental	133
6.5	Results and Discussion	133
6.6	Conclusions	139
6.7	References	139
APPENDIX	DIFFUSION DURING THE IMMERSION PRECIPITATION PROCESS	141
	Introduction	141
	The Model	142
	Critique of the Steady-State Assumption	146
	Discussion	148
	References	154

PART II THE CONCENTRATION POLARIZATION PHENOMENON
 IN ULTRAFILTRATION

CHAPTER 7	FLUX LIMITATION IN ULTRAFILTRATION: OSMOTIC PRESSURE MODEL AND GEL LAYER MODEL	157
7.1	Summary	157
7.2	Introduction	158
7.3	The Gel Layer Model	158
7.4	The Osmotic Pressure Model	159
7.5	Mathematical Description of the Osmotic Pressure Model	160
7.6	Calculated example of Osmotic Pressure Effect	163
7.7	Discussion and Conclusions	167
7.8	References	170
CHAPTER 8	HYDRODYNAMIC RESISTANCE OF CONCENTRATION POLARIZATION BOUNDARY LAYERS IN ULTRAFILTRATION	171
8.1	Summary	171
8.2	Introduction	171
8.3	Theory	172
8.4	Experiments	181
8.5	Results and Discussion	183
8.6	Conclusions	195
8.7	References	196
APPENDIX	THE MASS TRANSFER COEFFICIENT IN ULTRAFILTRATION	199
	Introduction	199
	Effect of Varying Diffusion Coefficient and Viscosity	200

Effect of Permeate Flux	202
Discussion	204
References and Notes	206
SUMMARY	207
SAMENVATTING	211
SAMENVATTING VOOR DE LEEK	215
LIST OF PUBLICATIONS	217
LEVENSLLOOP	219

INTRODUCTION

SEPARATION PROCESSES

The Entropy Maximization Postulate of the thermodynamics tells us that two miscible substances will mix spontaneously if they are brought together. In other words: a uniform distribution of the components in such a system is favoured over the existence of the two pure substances. There are countless examples of this rule to be found in our daily life, and one is the observation that salt dissolves in water. Here the thermodynamics are kind to those who like to enjoy a seasoned soup, but they constitute a major problem to those who rely on the seas for their drinking water supply. According to thermodynamics again the separation of a mixture into its pure components is possible, but it will take a certain amount of energy to achieve this. In order to actually perform the separation a device is needed that makes use of one or more differences in chemical or physical nature of the components to be separated. In the past a whole series of separation processes has been developed and in Table 1 they are classified with respect to the properties employed. Two substances that are very alike in almost all properties will be difficult to separate and if it is possible at all the efficiency will be low.

TABLE 1

Physical or chemical property	Separation Process
Size	Filtration, Microfiltration, Ultrafiltration, Gas Separation, Dialysis
Vapour Pressure	Distillation, Evaporation
Freezing Point	Crystallization
Affinity	Hyperfiltration, Gas Separation, Pervaporation, Adsorption, Absorption, Extraction, Perstraction
Charge	Ion Exchange, Electrodialysis, Electrophoresis
Density	Centrifugation, Flotation
Chemical nature	Complexation

If one faces the necessity to perform a certain separation, it must be examined whether the available separation processes meet the following criteria:

- 1) the separation must be feasible technically, and
- 2) the separation must be feasible economically.

It is not necessary that this evaluation leads to the use of one distinct process, a combination of two or more different processes may be more attractive. Furthermore, the result of the evaluation is strongly influenced by the current state of the technology and the current market value of chemicals and energy and not in the least by the current valuation of the environment as expressed in anti-pollution regulations.

MEMBRANE FILTRATION

A class of separation processes that has emerged in the last 25 years is Membrane Filtration Technology. The word

'filtration' has a much longer history and is commonly used to describe the removal of solids from a liquid or gas by means of a sieve or filter. In the case of 'membrane filtration' the system to be separated is not a two-phase system but consists of a true mixture at the molecular level. In some cases the membrane by which the separation is achieved can be viewed as a very fine filter, but the mechanism of separation may also differ from conventional sieving.

A generalized description of the membrane filtration process is as follows. A feed is brought in contact with a membrane and a difference in chemical potential is applied over the membrane. This driving force causes the components present in the feed to permeate through the membrane to the permeate side. In general the membrane acts as a selective barrier and therefore the trans-membrane velocity differs for different components. Consequently the permeate will have a composition differing from the feed, see Figure 1. There are several ways to create a chemical potential gradient over the membrane, and in Table 2 the corresponding membrane filtration processes are tabulated. From the same table it is clear that the membranes used in the various processes have specific structures and accordingly have specific properties.

With respect to their cross sections there are two distinct types of membrane structures: symmetric and asym-

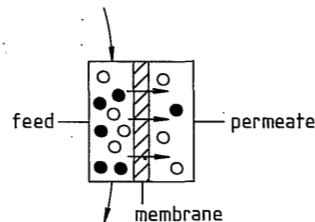


FIGURE 1. Schematic representation of a membrane filtration process.







TABLE 2.

Membrane processes and their characteristics

Membrane Process	Feed	Permeate	Driving Force	Membrane Structure	Field of Application
Microfiltration	Liquid	Liquid	Pressure	Porous	Removal of cells
Ultrafiltration	Liquid	Liquid	Pressure	Asymmetric	Separation of Macromolecules
Hyperfiltration	Liquid	Liquid	Pressure	Asymmetric or Composite	Separation of low Molecular Weight Molecules
Gas separation	Gas	Gas	Pressure	Homogeneous, Asymmetric or Composite	Separation of Gases
Pervaporation	Liquid	Vapour	Activity (Concentration)	Homogeneous, Asymmetric or Composite	Separation of Azeotropic Mixtures, of Organics from Water
Electrodialysis	Liquid	Liquid	Electric Potential	Symmetric	Separation of Ions from Neutral Molecules
Trans Membrane Distillation	Liquid	Liquid	Temperature	Porous	Removal of the Volatile Component(s)

TABLE 3

Schematic representation of cross sections of membranes

Symmetric			
	cylindrical pores	porous	dense
Asymmetric			
	porous	skinned	composite

metric membranes. In Table 3 examples of both kind are given. The transport through porous membranes takes place by convective flow, whereas the solution/diffusion mechanism determines the transport through dense membranes. The development of the asymmetric skinned membranes was responsible for the growth of membrane separation technology since the early sixties. These membranes combine the high selectivity of a dense membrane with a high permeation rate. The reason for this high permeation rate is the thickness of the selective layer, the 'skin', which is at least a hundred times smaller than the thickness of the total membrane. The resistance of the porous layer under the skin, the porous substructure, is small compared to the resistance of the dense skin. Composite membranes are (skinned) membranes on which a top layer of a different materials is coated. The vast majority of the membranes are polymeric films with a total thickness of about 0.15 mm and, if present, a skin of 0.1 to 0.5 microns in thickness.

WHY USE MEMBRANES?

As pointed out previously, the question which kind of separation process should be used to solve a certain separation problem, can only be answered after careful consideration of sometimes many alternatives. It is therefore not very sensible to search for advantages of membrane filtration processes in general. Below we give four specific merits of membrane filtration technology and indicate in which field these are useful.

(1) The energy consumption of the process is moderate compared to distillation. Useful in desalination by hyperfiltration or electrodialysis.

(2) Separation is achieved at a moderate temperature. Useful in dewatering of temperature sensitive process streams in the food and starch industry by ultra- and hyperfiltration.

(3) Breaking of azeotropic mixtures is possible. Useful in production of pure ethanol by pervaporation in combination with distillation.

(4) Continuous separation is easy. Useful in continuous removal of products from bioreactors by means of micro-, ultra- or hyperfiltration membranes.

The number of membrane applications is increasing and as a result the membrane-based industry is growing. Lonsdale [1] estimated that in this industry sales in 1981 amounted to at least \$ 500 million. It will be clear that substantial improvements of membrane performance increases the potential of membrane technology. Worldwide there are numerous research programs [2] aimed at the development of membranes with specific properties, the so-called 'tailor-made' membranes designed to meet the demands of well defined separation problems. Understanding the phenomena that determine the membrane structure and thus the membrane properties is crucial to the successful application of membrane technology. Basic research into the formation of membranes and the characterization of their structure is

therefore a necessity.

TABLE 4

Major Technologies to Emerge in the 1990s [4]

. Microelectronics and Computers		
. New Materials	→	. Fine Structure Ceramics
. Biotechnologies		. Functional Polymers
		→
		. Membranes
		. Conductive Polymers
		. High Crystalline Polymers
		. Bioerodible Polymers
		. Composite Materials
		. Amorphous Alloys

PREPARATION OF MEMBRANES

There are a number of different preparation techniques of synthetic membranes. The survey given below is limited to polymeric membranes and excludes inorganic membranes, dynamic membranes and liquid membranes. At the moment the latter are still of small economical importance, but especially the prospects for the liquid membranes and inorganic membranes are very promising.

Preparation techniques of polymeric membranes [3].

(1) *Sintering*. A polymer powder (Polytetrafluorethylene, Polyethylene, Polypropylene) is pressed and sintered to form a porous structure.

(2) *Stretching*. A crystalline film or foil (Polytetrafluorethylene, Polyethylene, Polypropylene) is stretched in the direction traverse to the orientation of the crys-

talline regions. In between these regions ruptures will occur which form pores and an irregular porous structure is obtained.

(3) *Track etching*. A Polycarbonate film or foil is subjected to a high energy particle radiation (metal ions) perpendicular to the film. The particles damage the polymer matrix and create tracks with increased reactivity. The film is then immersed in an acid bath and the polymeric material is etched away along these tracks. Cylindrical pores with a very narrow pore radius distribution are obtained.

(4) *Phase inversion*. The vast majority of the commercially available membranes is made by the phase inversion process. In Chapter 2 an extensive description of this process will be given. Within the class of phase inversion processes the immersion precipitation technique is the most important one and the investigations into the mechanism of formation by immersion precipitation form part I of this thesis.

(5) *Coating*. In this procedure an ultrafiltration membrane is coated with a top layer of a polymeric material to obtain a composite hyperfiltration membrane. There are three ways to create this top layer:

- (i) dip coating;
- (ii) interfacial polymerization, and
- (iii) plasma polymerization.

MEMBRANES AT WORK

Making the (perfect) membrane is only one part of the solution of a separation problem. The second part is the design of the membrane module. The trans membrane permeation flux is usually small, so in order to create an installation with a certain capacity a large membrane surface area must be installed. In the past twenty years a number of sophisticated membrane configurations has been developed to

obtain high ratios of membrane surface area to volume occupied by a module. The latest configuration is the hollow fiber membrane of which the inner and the outer diameters may be as small as respectively 70 and 165 microns, making it possible to have 6000 square meters of membrane area in each cubic meter of a module.

It is required that the flow conditions in the module are such that the phenomenon called concentration polarization is reduced to an acceptable level. Concentration polarization occurs in every membrane separation process and the phenomenon is illustrated in Figure 2. Suppose the transmembrane flux has a value J and the component A which is to be rejected by the membrane is present in the feed with a concentration c_b . If the membrane works properly the concentration of A in the permeate, c_p , is smaller than c_b . This implies that there is a net convective flow of component A towards the membrane equal to $J \cdot (c_b - c_p)$. This accumulation leads to an increased concentration of A at the

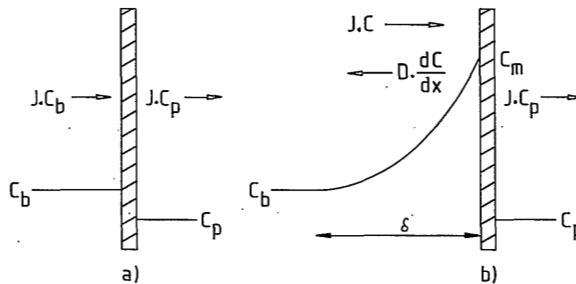


FIGURE 2. Concentration polarization.

(a): Onset of separation.

(b): Steady state concentration profile:

c_b : concentration in the bulk; c_p : concentration in the permeate;
 c_m : concentration at the membrane surface; δ : boundary layer thickness; J : permeate flux; D : diffusion coefficient.

membrane surface, which generates a diffusive flow back to the bulk of the feed. If the flow conditions in the feed compartment are such that the feed can be considered as completely mixed at a distance δ from the membrane and beyond, a steady-state concentration profile is developed and a constant concentration at the membrane surface, c_m , is reached. The values of δ and c_m depend on the degree of mixing near the membrane surface.

In the case of hyperfiltration the concentration polarization, i.e. the increased concentration at the membrane surface, decreases both the transmembrane flux and the rejection performance of the membrane. In ultrafiltration applications mainly a decrease in the permeate flux is observed and the reduction may be a factor of ten or worse. In part II of this thesis attention will be paid to the concentration polarization phenomenon in ultrafiltration and it is discussed how to account for its effect on the magnitude of the permeate flux.

STRUCTURE OF THIS THESIS

At first sight two unrelated subjects are addressed in this thesis. Both are, however, relevant to the practical importance of membrane separation processes. The first subject is the preparation of the membrane, or more specifically the physico-chemical processes that lead to characteristic membrane structures. The second subject is the concentration polarization phenomenon which may drastically reduce the rejection and permeation performance of the membrane.

Part I (Chapters 2 to 6) deals with the mechanism of formation of phase inversion membranes. Part II (Chapters 7 and 8) is concerned with the phenomenon of concentration

polarization and its effect on the ultrafiltration permeate flux.

In *Chapter 2* the preparation of membranes by the phase inversion process is discussed and the hypothesis on the formation of membranes as adopted in our laboratory is introduced.

In *Chapter 3* the phase separation phenomena in membrane forming systems consisting of the polymer Polysulfone, the solvent Dimethylacetamide and the nonsolvent Water are investigated in relation with the final properties of Polysulfone membranes. In the *Appendix* the instability of Polysulfone-solvent solutions due to the presence of oligomers is described.

In *Chapter 4* the phase separation phenomena in membrane forming systems consisting of the polymer Polyphenyleneoxide (PPO), the solvent Trichloroethylene and the nonsolvents n-Octanol and Methanol are investigated. Since PPO is a crystalline polymer, attention is paid to the kinetics of crystallization. The results are interpreted again in relation to the final properties of PPO membranes.

In *Chapter 5* it is shown that addition of solvent to the coagulation bath changes the structure of the top layer of the membranes formed: the top layer becomes more and more porous. An explanation for this phenomenon is given, which is in accordance with the formation mechanism of membranes, postulated in Chapter 2.

In *Chapter 6* the effect of polymer concentration and nonsolvent concentration in the casting solution on the membrane structure is investigated. Special attention is paid to the effect on the top layer. The results are in agreement with the findings presented in Chapter 5.

In an *Appendix to Part I* a model for the diffusive exchange of solvent and nonsolvent during immersion precipitation as put forward in the literature is discussed and partly criticized.

In *Chapter 7* it is advocated that osmotic pressure plays an important role in ultrafiltration applications. Using a

simple model it is shown that the osmotic pressure may limit the value of the permeate flux and that its effect on the permeate flux strongly resembles the effect of the formation of a gel layer.

In *Chapter 8* the results of ultrafiltration experiments are analyzed. It is shown that the concentration polarization boundary layer creates a hydrodynamic resistance which can be calculated if sedimentation and diffusion data are available and if the mass transfer coefficient is known. This so-called Boundary Layer Resistance Model is proven to be fully equivalent to the Osmotic Pressure Model. In an *Appendix* the apparent values of the mass transfer coefficient are compared with the values predicted by the semi-empirical Deissler equation. Some comments are made regarding the possible origin of the observed discrepancies.

REFERENCES AND NOTES

- [1] H.K. Lonsdale, *J. Membrane Sci.* 10 (1982) 81-181.
- [2] These research programs are in many occasions initiated and/or encouraged and financially supported by government bodies. The first decisive push for desalination by membrane filtration was given by a large scale research effort in the United States of America in the late sixties, coordinated by the Office of Saline Water of the Department of the Interior. The Ministry of International Trade and Industry of Japan, which is the driving force behind the long term strategies of Japanese industry, has given Membrane Technology a high priority as being important to the 'next generation industries'. In Table 4 [4] Membrane Science and Technology is shown to be a part of new technologies to be developed for the next generation.

In Germany the BMFT (Bundesministerium für Forschung und Technologie) has an active program on membrane science and technology since the late seventies.

In the Netherlands a national program has brought together industries, research institutes and universities to maintain and strengthen the position of the Dutch industry in the field of Membrane Technology [5].

- [3] H. Strathmann, *Trennung von molekularen Mischungen mit Hilfe synthetischer Membranen*. Steinkopf Verlag, Darmstadt, 1979.
- [4] S. Takaoka, *Emerging Technologies in the 1990s*. CHEMRAWN III Conference, The Hague, The Netherlands, 1984.
- [5] *Membraantechnologie in Nederland*. Verslag van de Programmacommissie Membraantechnologie, september 1983.

PART I

THE MECHANISM OF FORMATION OF SYNTHETIC MEMBRANES

PREPARATION OF ASYMMETRIC MEMBRANES BY THE PHASE INVERSION PROCESS

J.G. Wijmans and C.A. Smolders

SUMMARY

The formation of membranes by the phase inversion process is discussed. In this process a polymer solution is brought to phase separation by an exchange of solvent and nonsolvent. The structure of the membrane is the result of an interplay of phase separation and mass transfer. Typical morphological features of the membrane (skin, sponge structure, conical voids) are discussed in relation with the preparation procedure. It is shown that the skin layer is formed by gelation at increased polymer concentration, while liquid-liquid phase separation is responsible for the porous sublayer.

INTRODUCTION

Since the beginning of this century, when the first microporous membranes were prepared by Bechold [1], the potential of synthetic membranes for the separation of dissolved and suspended solutes from the solvent has been recognized. Industrial-scale applications remained limited until Loeb and Sourirajan [2] developed the first asymmetric skinned membranes in 1962. These membranes owe their practical value to the presence of a skin: a very thin (0.1 to 0.5 μm) and very

dense layer which possesses selective properties. The skin is supported by a porous sublayer of 0.1 to 0.2 mm thickness which gives the membrane mechanical stability. Due to the thin skin layer the hydrodynamic resistance is low compared with symmetric membranes having the same selectivity.

Synthetic membranes can be prepared in various ways. In this article we will focus on the so-called phase inversion process, by which the majority of the commercially available membranes are produced. The concept phase inversion is introduced by Kesting [3] and it can be defined in the following way: a homogeneous polymer solution is transformed into a two-phase system in which a solidified polymer phase forms the porous membrane structure, while a liquid phase, poor in polymer, fills the pores.

The next sections include a discussion of the various preparation procedures of phase inversion membranes and the phenomena which are characteristic of the phase inversion process; these phenomena are then correlated with the resulting membrane structure in a discussion of the mechanism of membrane formation.

PHASE INVERSION PROCESS: PREPARATION PROCEDURES

The membranes produced by phase inversion are polymeric. To obtain these membranes the polymer is dissolved in a solvent which can be a single component solvent or a mixture of solvents and nonsolvents. Generally this solution is cast on a support, i.e. a glass or metal plate or a non-woven textile fabric, and then treated in a specific way (see (a) to (d) below) in order to precipitate the polymer. In this way flat or tubular membranes are obtained. In an other procedure the polymer solution is spun through a spinneret which has an extra outlet for pressurized air or liquid in the centre of the opening, resulting in hollow fiber membranes. For all these membranes the structure formation

phenomena are basically the same.

Within the phase inversion process four different techniques can be distinguished:

(a) Precipitation from the vapour phase [4,5]. In this very early developed technique membrane formation is accomplished by penetration of a precipitant for the polymer into the solution film from the vapour phase, which is saturated with the solvent used. A porous membrane is produced without a skin and with an even distribution of pores over the membrane thickness.

(b) Precipitation by controlled evaporation [6-8]. The polymer is dissolved in a mixture of a good and a poor solvent, of which the solvent mixture shifts in composition during evaporation to a higher nonsolvent content. A skinned membrane can be the result.

(c) Immersion precipitation [5,9-12]. This technique, which was first used successfully by Loeb and Sourirajan for the preparation of a reverse osmosis membrane, has been studied and exploited most for the production of skinned membranes. The characteristic feature is the immersion of the cast polymer film in a nonsolvent bath. The polymer precipitates as a result of solvent loss and nonsolvent penetration.

(d) Thermal precipitation [12]. Here a solution of polymer in a mixed solvent, which is on the verge of precipitation, is brought to separation by a cooling step. When evaporation of the solvent has not been prevented the membrane can have a skin.

From these procedures we can infer that for the phase inversion process at least the following features are characteristic:

(i) A ternary system. The process involves at least one polymer component, one solvent and one nonsolvent. The latter two must be miscible.

(ii) Mass transfer. The polymer solution is subject to a transfer of solvent and nonsolvent in such a way that the nonsolvent concentration in the film increases. Mass trans-

fer starts at the interface between the polymer film and the coagulation medium (vapour or liquid). The changes in composition in the film are governed by diffusion. No mass transfer takes place in thermal precipitation without evaporation.

(iii) Precipitation. As a result of the increase of non-solvent content the polymer solution becomes thermodynamically unstable and phase separation will occur. So an important aspect of the phase inversion process is formed by the demixing phenomena possible in ternary polymer systems. These phenomena include not only the phase equilibria but also the kinetics of phase separation, as the formation of membranes is a dynamic process.

PHASE SEPARATION IN POLYMER SYSTEMS

Thermodynamics

Information on the stability of a solution can be obtained from the Gibbs free energy of mixing. For the system of our interest, a mixture of polymer, solvent and nonsolvent, we will use the Flory-Huggins [13] expression as derived by the lattice model:

$$\Delta G_m / RT = n_1 \cdot \ln(\phi_1) + n_2 \cdot \ln(\phi_2) + n_3 \cdot \ln(\phi_3) \\ + g_{12} \cdot n_1 \cdot \phi_2 + g_{13} \cdot n_1 \cdot \phi_3 + g_{23} \cdot n_2 \cdot \phi_3 \quad (1)$$

ΔG_m is the Gibbs free energy of mixing; R is the gas constant and T the temperature in Kelvin. The subscripts refer to nonsolvent (1), solvent (2) and polymer (3). The number of moles and the volume fraction of component i are n_i and ϕ_i respectively. The g_{ij} parameter is the component i - component j interaction parameter.

The first three terms on the right hand side of eq. (1)

represent the ideal entropy of mixing of the solution, divided by R. The last three terms describe the enthalpy of mixing of the solution (divided by RT) when only binary interactions have been taken into account. If eq. (1) has to describe the free enthalpy of mixing accurately, then the interaction terms will also have to incorporate the inevitable deviations from the ideal entropy terms. This is one of the reasons why the interaction parameters are assumed to be concentration dependent [14].

In the last two decades other expressions for ΔG_m have been derived using equation-of-state theories [15]. These formulations are certainly improvements in the theoretical sense but require the knowledge of properties of the components which are available only for a limited number of compounds. On the other hand, information on the interaction parameters can be deduced from ΔG_m measurements easily. These measurements have been compiled for binary low molecular weight mixtures [16]. For mixtures containing a polymer component some data are available, but relatively simple techniques exist which yield interaction parameter values: vapour pressure osmometry, high pressure membrane osmometry and swelling experiments.

From eq. (1) the expressions for the chemical potentials of the components can be derived, using

$$\Delta\mu_i = \partial\Delta G_m / \partial n_i \quad (2)$$

In the differentiation procedure the eventual concentration dependence of the g parameters has to be accounted for. Every system will try to minimize its Gibbs free energy. The entropy terms of eq. (1) will always be negative, whereas the enthalpy terms are positive in the case of positive interaction parameters. If the g parameters become too large demixing will occur. The equilibrium state is reached when the chemical potentials in each phase formed are equal for all components.

Liquid-liquid phase separation

If a solution becomes thermodynamically unstable it is possible that it can lower its free enthalpy of mixing by separating into two liquid phases. These two phases have different compositions but are in equilibrium with each other. The reason for the solution to become unstable could be a decrease in temperature, a loss of solvent or an increase in nonsolvent content.

In order to make the mechanism of liquid-liquid (L-L) phase separation clear, we will first consider a binary system: a polymer and a solvent. Figure 1 shows the dependence of ΔG_m on concentration in such a system for two temperatures. At temperature T_a the system is completely miscible over the whole concentration range. If one lowers the temperature the interaction parameter g will increase and for a certain temperature T_b the ΔG_m vs concentration curve is displayed in Figure 1b. The upward bend in the curve is the result of the increased enthalpy term. From this figure it can be seen that all compositions between ϕ'

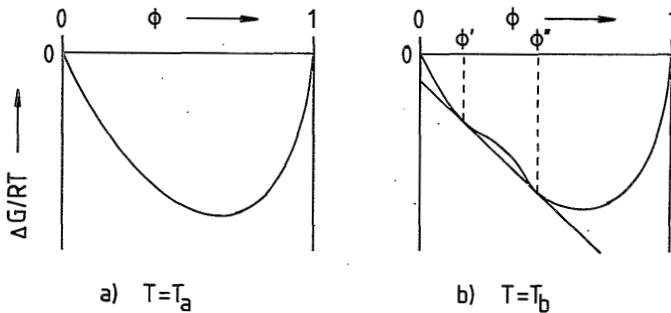


FIGURE 1. ΔG_m vs composition curves for a binary system. $T_a > T_b$. ϕ : polymer volume fractions.

and ϕ'' can lower their free enthalpy by demixing into two phases. The compositions of those two phases are ϕ' and ϕ'' respectively and the phases are in equilibrium with each other since they lie on the same tangent to the ΔG_m curve.

There are two different kinetic ways for L-L separation to occur, see Figure 2. Within the composition range $\phi^1 - \phi^2$ the curvature is such that

$$\partial^2 \Delta G_m / \partial \phi^2 < 0 \quad (\phi^1 < \phi < \phi^2) \quad (3)$$

Condition (3) implies that the solution is unstable with respect to even the smallest amplitude of certain concentration fluctuations. The solution will then separate spontaneously [17,18] into very small, interconnected regions with compositions ϕ' and ϕ'' : the so-called spinodal decomposition. In the composition regions $\phi' < \phi < \phi^1$ and $\phi^2 < \phi < \phi''$ the second derivative of ΔG_m with respect to ϕ is positive which means that there are no spontaneously growing concen-

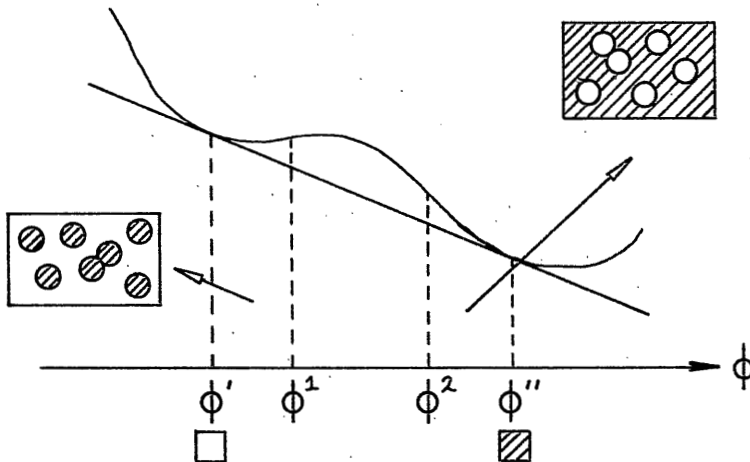


FIGURE 2. Part of the ΔG_m vs ϕ graph of figure 1b. \circ and \square : composition ϕ' ; \bullet and \blacksquare : composition ϕ'' .

tration fluctuations, so there is no spontaneous phase separation. Demixing can only start if the concentration fluctuations have generated at least one stable nucleus, i.e. the decomposition regions are metastable. A nucleus is stable if it lowers the total free enthalpy of the system, hence in the range $\phi' < \phi < \phi^1$ the nucleus must have a composition near ϕ'' and in the range $\phi^2 < \phi < \phi''$ it must have a composition near ϕ' . After the nucleation of the 'second phase' the nuclei will grow while the surrounding phase gradually moves towards the composition of the other equilibrium phase. The two possibilities indicated above are illustrated in Figure 2. In a relatively diluted solution the dispersed phase will have composition ϕ'' and in a more concentrated solution the dispersed phase will have composition ϕ' .

In a three component system the phenomena are basically the same, but here a decrease in temperature is not necessary to induce L-L phase separation, a change in composition is sufficient. In Figure 3 the ΔG_m surface for a ternary system is schematically drawn. All pairs of compositions with a common tangent plane to the ΔG_m surface together constitute the solid line in the phase diagram at the bottom of Figure 3. This line is the L-L boundary, the binodal. The dotted line is the spinodal, inside which all compositions are unstable. The point in which the spinodal and binodal touch is the critical composition. It is the location of the critical point in the phase diagram that determines whether the nuclei formed will have a composition high or low in polymer concentration. If one wants to reach the spinodal area by a change in composition, the composition has to travel first through the metastable region where nucleation and growth take place. In our opinion the latter process is fast compared with the rate of mass transfer and in that case the spinodal region is not reached. Therefore we think it is highly improbable that spinodal decomposition has a role in membrane formation.

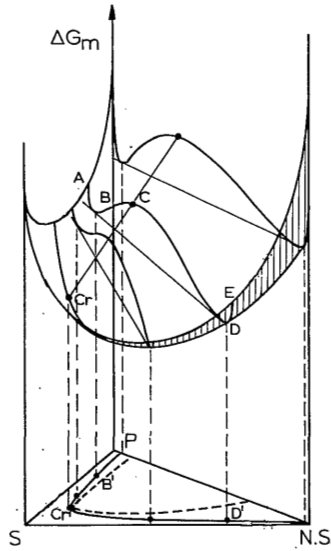


FIGURE 3. Sketch of ΔG_m surface and miscibility gap for the system polymer (P), solvent (S), nonsolvent (NS). Cr: critical composition.

Crystallization and gelation

When the thermodynamic quality of a polymer solution is decreasing which may occur by loss of solvent, by lowering of the temperature or by the introduction of a nonsolvent, most polymers are able to form ordered agglomerates. In very dilute solutions the polymer molecules can form single crystals of lamellar type, being only a few hundred Angströms thick and often many microns in the lateral direction. From solutions of medium concentration more complex morphologies occur i.e. dendrites or spherulites. These latter structures may contain, except for the ordered regions, appreciable amounts of amorphous polymeric material.

In the preparation of membranes polymer solutions of medium and high concentrations are used. In these systems the

time available for the crystallization becomes important since this process takes place through nucleation and growth. Especially if crystallization is induced by a change in composition, i.e. by mass transfer, there will be a competition between the rate of the mass transfer and the rate of nucleation. A transfer, slow compared with the nucleation process, will induce crystallization at a low level of supersaturation and there will be a limited number of nuclei which will grow considerably. A rapid mass transfer will lead to crystallization at high polymer concentrations: many nuclei are present because of the high supersaturation, but their change to grow will be limited. At high concentrations the numerous microcrystalline regions act as physical crosslinks in the solution and a thermoreversible gel is formed.

In Figure 4 we have given a schematic representation of the free enthalpy behaviour in the region of high polymer/low nonsolvent content of the three component system. One

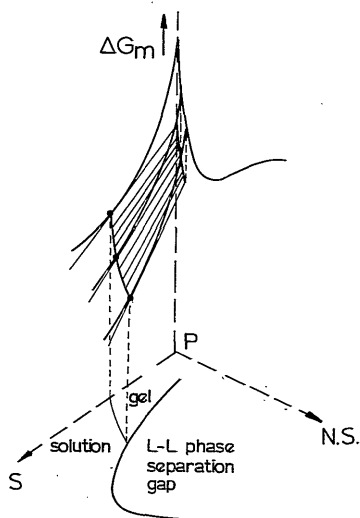


FIGURE 4. Free enthalpy behaviour at high polymer/low nonsolvent content, explaining the solution-crystal transition.

sees that at higher concentrations the free enthalpy of mixing of the solution can be lowered by the formation of solid, crystalline polymer in equilibrium with a solution of a certain lower polymer content. At a lower (or higher) temperature the ΔG_m surface will change its shape and the crystalline polymer will be in equilibrium with a solution of lower (or higher) polymer concentration.

As can be seen from Figure 4, at high polymer and high nonsolvent concentrations both L-L phase separation and crystallization are possible thermodynamically. In these regions the kinetics of the two phenomena will determine which one actually takes place.

Some polymers are completely amorphous, i.e. there is no ordered structure which lowers the free enthalpy with respect to the amorphous state. In these systems there is no liquid-solid transition in the thermodynamic sense, but nevertheless at very high polymer concentrations the fluidity of the solution becomes zero. The polymer molecules are so densely packed and there are so many entanglements that in effect a gel has formed. The solution-gel boundary is a viscosity boundary in this case.

Experimental data on phase separation

Liquid-liquid phase separation is readily detected by turbidity measurements [19] and light scattering methods [20]. If the interaction parameters of a system are available, one can calculate the L-L demixing gap, using the thermodynamic equilibrium expressions. Altena [21] has shown that for most systems consisting of a polymer, a solvent and a nonsolvent, L-L phase separation should be expected.

Crystallinity in gels is hard to demonstrate when diffraction techniques are used, since the crystalline entities are of submicroscopic order. If surface effects are

not too large, calorimetric measurements can be used [22]. Data on the kinetics of crystallization can be obtained from Pulse Induced Critical Scattering [23].

FORMATION OF ASYMMETRIC MEMBRANES

The origin of the asymmetric structure of membranes, i.e. the presence of the skin, has received much attention in membrane research. There are three views on the formation of the skin:

a) The asymmetry is already present in the cast film of the concentrated polymer solution before precipitation takes place, due to surface tension effects. Further steps in the preparation process, such as coagulation and heat treatment, will only fix the already existing asymmetry. Representatives of this approach are Panar [24] (nodular morphology) and Tanny [12]. Since it is possible to obtain both skinned and nonskinned membranes from one and the same polymer solution [25], we think this view cannot be true.

b) The skin is formed through evaporation from the upper layer of the cast film. The duration and the conditions of the evaporation step determine to a great extent the resulting properties of the membrane. This approach is followed by Sourirajan [26] and Kunst [29] (solution structure-evaporation rate concept), Kesting [3] and Anderson [28]. We do not agree that solvent evaporation in general is a necessary step to induce the formation of the asymmetric structure. The following objections can be made:

- one can prepare excellent asymmetric membranes from polymer/solvent/nonsolvent systems in which evaporation of the solvent is negligible, e.g. polysulfone/DMF/water and cellulose acetate/dioxane/water.

- also systems with a volatile solvent (CA/acetone-formamide/water) cast and coagulated under circumstances that the atmosphere is saturated with the solvent acetone give

excellent asymmetric membranes (Sarbolouki [29]).

- asymmetric hollow fibers with a skin at the interior can be made which have had no contact with air during the preparation (Strathmann [30]).

c) The coagulation process is responsible for the formation of the asymmetry. Skin formation and formation of the porous sublayer are the result of a complex interplay of phase separation and diffusional processes. Authors who have made important contributions are Frommer [31], Strathmann [5] and Koenhen [11].

The formation of asymmetric membranes according to approach c) is described below.

Mechanism of formation

In the immersion precipitation process a polymer solution, cast on a support, is immersed in a bath containing a nonsolvent. As was first suggested by Koenhen [11] we assume that the skin formed by gelation and that the porous sublayer is the result of liquid-liquid phase separation by nucleation and growth. The factor determining the type of phase separation at any point in the cast film is the local polymer concentration at the moment of precipitation. In the first split second after immersion there is a rapid depletion of solvent from the film and a relatively small penetration of nonsolvent. This means that the polymer concentration at the film/bath interface increases and that the gel boundary is crossed (see Figure 4). The thin and dense gel layer that is formed in this way, the skin, will act as a resistance to the outdiffusion of solvent and at the positions beneath the top layer demixing will occur at lower polymer and higher nonsolvent concentrations. So here the type of demixing will be liquid-liquid phase separation (see Figure 4). The demixing gap is entered at the polymer-rich side of the critical point, so the nuclei consist of the polymer-poor phase and the result is a porous structure,

the pores of which are filled with the dilute solvent/non-solvent phase. The porous structure will be fixed by gelation of the concentrated, continuous polymer phase.

The approximate changes of composition for the top layer and the substructure, the so-called 'coagulation paths', are given in Figure 5. A more detailed description of the concentration profiles in a precipitating casting solution can be found in the paper by Bokhorst *et al.* [32].

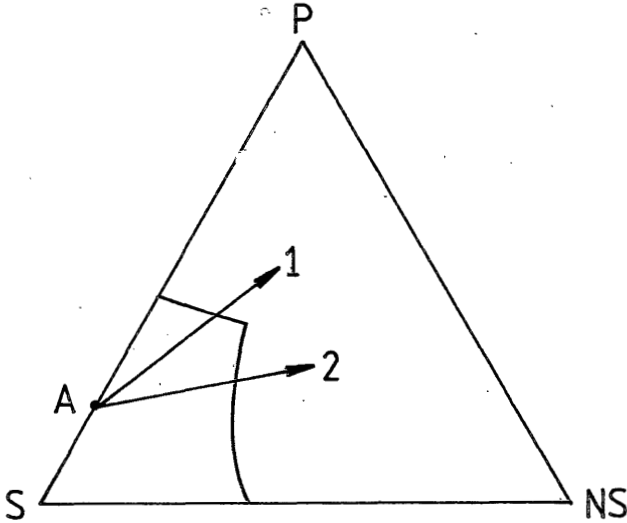


FIGURE 5. Schematic course of the composition for the skinlayer (1) and the bottom layer (2) of a polymer film with initial composition A upon immersion in a nonsolvent bath.

Precipitation from the vapour phase

The polymer solution is subject to a nonsolvent inflow, while the solvent saturated vapour phase prevents the outflow of solvent: the polymer concentration decreases gradually. The only possible demixing mechanism is L-L phase separation and a microporous membrane without a skin is the result. The mass transfer at the solution/vapour interface is slow compared to the diffusion in the polymer solution, so the concentration profile inside the film is very flat. This implies that in the whole polymer film demixing takes place at approximately the same time and at the same polymer concentration. The result is an even pore distribution over the cross-section of the membrane: they are essentially symmetric.

The size of the pores can be controlled by the preparation variables. In general the pore radius will increase when the temperature is increased (gelation at higher concentrations) or when the polymer concentration of the casting solution is decreased. The polymer content should not be too small, however, since for a porous structure it is necessary that the L-L demixing gap is entered at the polymer rich side of the critical point.

Precipitation by controlled evaporation

When a polymer-solvent solution, without nonsolvent, loses solvent through evaporation, the polymer concentration gradually increases and gelation will take place. In this manner dense polymer films are obtained which are useful in pervaporation [33]. If gelation occurs through crystallization, the properties of the film depend on the rate of evaporation and diffusion, i.e. the degree of supersaturation.

Porous structures are formed when one or more nonsolvents are added to the solution. In this case the precipitation is determined by the volatility of the compounds used, the initial concentrations in the solution and the phase boundaries of the system. Kesting [34] has utilized controlled evaporation to produce asymmetric membranes with reverse osmosis properties: the 'Dry-RO' membranes. In this procedure the solvent must have a boiling temperature which lies at least 30°C under the boiling temperatures of the nonsolvents used. In order to obtain high flux membranes more than one nonsolvent must be present in the casting solution [34]. The asymmetry of the membranes is the result of the fast evaporation of the solvent from the upper layer of the polymer solution.

Immersion precipitation

In the section on the formation of asymmetric membranes the phenomenon immersion precipitation has been discussed. Because this process is used in the production of the majority of the asymmetric membranes we will focus here to some extent on the variables determining the membrane morphology.

The ultimate determining factor for the skin formation is the local polymer concentration in the top layer in the polymer solution at the moment of precipitation. In the immersion technique the solvent depletion from the top layer of the solution film is extremely fast. An increase in polymer concentration in the top layer is the result. This increase improves the conditions for gelation to occur. The gelation will be favoured by the penetration of nonsolvent. The higher the polymer concentration has become before nucleation in the skin sets in, the more numerous and the smaller will be the nuclei because of higher supersaturation.

It will be clear now which factors favour the formation of a more finely structured, i.e. denser skin and therefore a more selective membrane:

- a higher initial polymer concentration of the solution will favour the conditions for a large supersaturation in the top layer before nucleation sets in;

- a lower tendency of the nonsolvent to induce L-L separation in the system or to penetrate the cast film will delay the onset of gelation until sufficient solvent depletion has been obtained and again supersaturation is favoured. A proper choice of nonsolvent type and the use of certain additives to the coagulation bath (salt, glycerin, etc.) will serve these purposes;

- lowering the temperature of the coagulation bath will increase supersaturation while decreasing growth kinetics for the nuclei.

The skin is formed due to a high outflow of the solvent. When the solvent used is added to the nonsolvent bath this outflow is decreased as well as the rate of penetration of the nonsolvent. It appears that in every ternary system, which yields skinned membranes when the coagulation bath is pure nonsolvent, microporous membranes without a skin are obtained if sufficient solvent is added to the coagulation bath [25]. Each system has its own minimum solvent concentration, which can be more than 80 percent by weight of solvent. On the basis of thermodynamic evaluations it seems plausible that the addition of solvent to the bath relatively favours the penetration of nonsolvent into the polymer solution [25] and thus favours L-L phase separation in the top layer.

Under the skin we find a porous substructure, see figure 6. It will be clear that the pores in this sponge structure are the grown-out nuclei of the dilute phase dispersed within the matrix of the polymer solution, and that the matrix has solidified by gelation at a certain stage. If the concentration of the polymer at the locus where

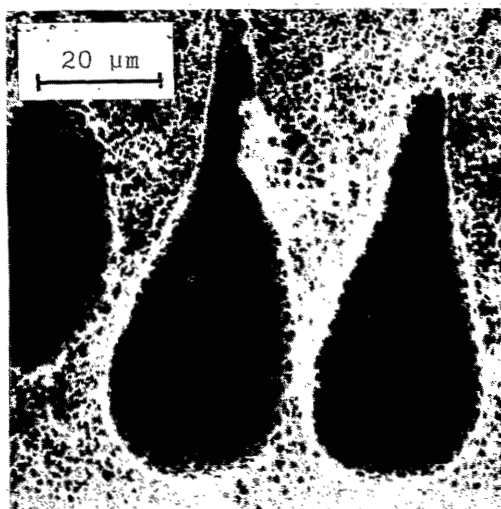


FIGURE 6. Cross section of a PSf membrane, showing voids with open walls.

L-L phase separation sets in does not vary too much with the depth of the solution layer, the nucleation density will also not vary very much across the film and a uniform pore structure will be the result. In order to obtain an 'open pore' sponge structure, a certain amount of coalescence of the drops should occur before the walls of concentrated polymer solution between the pores solidify by gelation. This can be monitored by choosing the proper initial polymer concentration (not too high), or by adding a nonsolvent to the polymer solution. Bokhorst [32] has obtained membranes with an open, very regular sponge structure by adding maleic acid to the Cellulose Acetate - Dioxane casting solution. The absence of very small pores directly under the skin layer makes these membranes wet-dry reversible (in small pores the capillary forces are large upon drying).

A very important feature in immersion-coagulated membranes (in UF membranes as well as in RO types) is the presence of

the large voids with a length from several microns to, sometimes, the total thickness of the membrane. The cavities were first observed in wet-spun fibres [35-39]. The absence of the voids in dry-spun fibres [38] and in dry RO-membranes [34] indicates that their formation only occurs in the case of immersion precipitation.

At first it was assumed that the formation was associated with volume changes in the precipitated polymer phase [36]. Later Graig [35] proposed the mechanism of penetration of nonsolvent through defects (cracks) on the surface of the spinning filament. The same mechanism in the case of immersion-coagulated membranes was proposed by Strathmann [30]. In a systematic study of the kinetics of void formation in PAN fibre spinning, Gröbe [37] came to the conclusion that diffusion of both solvent and nonsolvent to certain areas was the basis for void formation. In our opinion the available experimental data are consistent with this mechanism. Some typical facts remain interesting for further consideration:

- through optical microscopy one observes that the voids move inward faster than the diffusion controlled, coagulation front;
- the boundary of the voids does not solidify by gelation during its growth, since coalescence with small pores remains possible (Figure 6);
- often the growth of the voids slows down and the coagulation front for L-L separation passes beyond the lower end of the cavity.

Smolders [40] has proposed the following mechanism for the appearance of the conical voids:

- When the skin is formed, nonsolvent penetrates into the underlying polymer solution faster at certain spots in the skin, e.g. a thinner part of the skin or a local loose arrangement of the structural units in the skin, giving a more favourable pathway for diffusion. Only in systems with a large driving force for solvent/nonsolvent mixing is this heterogeneous type of nucleus formed;

- Solvent is expelled from the surrounding polymer solution (syneresis) to these statistically spread loci and a gradient in nonsolvent concentration is set up in the void, ranging from a rather low value near the interface with the polymer solution to a high value near the skin surface. There is a fluid interface between the polymer solution and the void;

- Because of the syneresis effect and the more rapid diffusion in the void in comparison with the polymer solution phase, the void may grow faster initially than the coagulation front proceeds. When the syneresis becomes less effective the growth of the voids depends solely on the diffusion of solvent over larger distances to the voids, so that the growth of the voids may slow down and the coagulation front may proceed beyond the void.

Up to this part we have focussed on the preparation procedures rather than on the compounds used in the procedure. There are countless combinations of a polymer, a solvent and a nonsolvent which constitute a membrane forming system, but only some will yield membranes with commercially interesting properties. For a typical polymer widely used in membrane fabrication, Cellulose Acetate, the influence of the choice of the solvent on membrane properties is illustrated in Table 1.

TABLE 1. Influence of solvent used in membrane preparation on membrane properties. Polymer: Cellulose Acetate. Nonsolvent: Water.

Solvent	Membrane structure and properties
Dioxane	Skinned, Reverse Osmosis
Acetone	Homogeneous, Dense
Acetone/Formamide	Skinned, Reverse Osmosis
Triethylphosphate	Homogeneous, Finely Porous
N,N Dimethylformamide	Skinned, Ultrafiltration

Thermal precipitation

The polymer is dissolved at a high temperature in a mixture of a solvent and a nonsolvent. Upon lowering the temperature the solution becomes unstable with respect to L-L phase separation and a porous structure is formed. If at the solution/vapour interface concentration of the polymer through evaporation takes place, a skin layer might be the result. A mixture of a polymer and low molecular weight compounds is not always employed. Polymer blends, miscible at high temperatures, will also yield porous structures if the temperature is decreased. In that case one polymer component, which is dispersed in the matrix, is washed away. This procedure is used in the dry-spinning of porous hollow fibers.

CONCLUSIONS

It has been shown that in membrane forming systems the skin is formed by gelation of the top layer, at increased polymer concentration due to solvent loss, whereas liquid-liquid phase separation is responsible for the formation of the porous sublayer. The diffusive exchange of solvent and nonsolvent determines at which place in the polymer solution and at what time these demixing processes take place. Although in different systems the membrane structure and properties may differ, the basic phenomena responsible for the membrane formation are the same.

REFERENCES

- [1] H. Bechold, *Biochem. Z.*, 6 (1907) 379.
- [2] S. Loeb and S. Sourirajan, *Advan. Chem. Ser.*, (1962)

- [3] R.E. Kesting, "Synthetic Polymer Membranes", McGraw Hill, New York, 1972.
- [4] R. Zsigmondy and W. Bachman, *Z. Anorg. Allgem. Chem.*, 103 (1981) 109.
- [5] H. Strathmann and K. Kock, *Desalination*, 21 (1977) 241.
- [6] J.D. Ferry, *Chem. Rev.*, 18 (1936) 373.
- [7] K. Maier and E. Scheuermann, *Kolloid Z.*, 171 (1960) 122.
- [8] R.E. Kesting, *J. Appl. Polym. Sci.*, 17 (1973) 1771.
- [9] a) S. Sourirajan, "Reverse Osmosis", Acad. Press, New York, 1970.
 b) R.E. Kesting, "Synthetic Polymeric Membranes", McGraw Hill, New York, 1971.
 c) H.K. Lonsdale and H.E. Podall, eds., "Reverse Osmosis Membrane Research", Plenum Press, New York, 1972.
- [10] M. Guillotin, C. Lemoyne, C. Noel and L. Monnerie, *Desalination*, 21 (1977) 165.
- [11] D.M. Koenhen, M.H.V. Mulder and C.A. Smolders, *J. Appl. Polym. Sci.*, 21 (1977) 199.
- [12] G.B. Tanny, *J. Appl. Polym. Sci.*, 18 (1974) 2149.
- [13] P.J. Flory, "Principles of Polymer Chemistry", Cornell University Press, 1953.
- [14] R. Koningsveld, Thesis, Leiden University, The Netherlands, 1967.
- [15] P.J. Flory, *J. Am. Chem. Soc.*, 87 (1965) 1833.
- [16] J. Wisniak and A. Tamir, "Mixing and Excess Thermodynamic Properties", Elsevier, Amsterdam, 1978.
- [17] J.W. Cahn, *J. Chem. Phys.*, 42 (1965) 93.
- [18] C.A. Smolders, J.J. van Aartsen and A. Steenbergen, *Kolloid Z. Z. Polym.*, 243 (1971) 14.
- [19] P.T. van Emmerik and C.A. Smolders, *Eur. Polym. J.*, 3 (1973) 293.
- [20] K.W. Derham, J. Goldsbrough and M. Gordon, *J. Pure and Appl. Chem.*, 38 (1974) 97.

- [21] F.W. Altena and C.A. Smolders, *Macromolecules*, 15 (1982) 1491.
- [22] F.W. Altena and C.A. Smolders, *J. Polym. Sci., Polym. Symp.*, (1981) 69.
- [23] D.M. Koenhen, C.A. Smolders and M. Gordon, *J. Polym. Sci., Polym. Symp.*, 61 (1977) 93.
- [24] M. Panar, H.H. Hoehn and R.R. Hebert, *Macromolecules*, 6 (1973) 777.
- [25] J.G. Wijmans, J.P.B. Baaij and C.A. Smolders, *J. Membr. Sci.*, 14 (1983) 263.
- [26] S. Sourirajan and B. Kunst, in *Synthetic Membranes*, S. Sourirajan, ed., National Research Council, Canada, Ottawa, pp. 129-, 1977.
- [27] B. Kunst and Z. Vajnaht, *J. Appl. Polym. Sci.*, 21 (1974) 2505.
- [28] J.E. Anderson and R. Ullman, *J. Appl. Phys.*, 44 (1973) 4303.
- [29] Sarbolouki, *J. Polym. Sci., Polym. Lett.*, 11 (1973) 753.
- [30] H. Strathmann, K. Kock, P. Amar and R.W. Baker, *Desalination*, 16 (1975) 179.
- [31] M.A. Frommer and D. Lancet, in *Reverse Osmosis Membrane Research*, H.K. Lonsdale and H.E. Podall, Eds., Plenum Press, New York, pp. 85- , 1972.
- [32] H. Bokhorst, F.W. Altena and C.A. Smolders, *Desalination*, 38 (1981) 349.
- [33] M.H.V. Mulder, F. Kruitiz and C.A. Smolders, *J. Membr. Sci.*, 11 (1982) 349.
- [34] R.E. Kesting, *United States Patent*, 3 884 801, May 20, 1975.
- [35] J.P. Graig, J.P. Knudsen and V.F. Holland, *Textile Res. J.*, 32 (1962) 435.
- [36] V. Gröbe and K. Meyer, *Faserforsch. Textiltechn.*, 10 (1959) 214.
- [37] V. Gröbe, G. Mann and G. Duve, *Faserforsch. Textiltechn.*, 17 (1966) 142.

- [38] Ziabicki, *Fundamentals of Fibre Formation*, John Wiley, London, 1976.
- [39] J.P. Knudsen, *Textile Res. J.*, 33 (1963) 13.
- [40] C.A. Smolders, in *Ultrafiltration Membranes and Applications*, A.R. Cooper, Ed., Plenum Press, New York, 1980.

PHASE SEPARATION PHENOMENA IN SOLUTIONS OF POLYSULFONE IN MIXTURES OF A SOLVENT AND A NONSOLVENT: RELATIONSHIP WITH MEMBRANE FORMATION*

J.G. Wijmans, J. Kant, M.H.V. Mulder and C.A. Smolders

SUMMARY

The phase separation phenomena in ternary solutions of Polysulfone in mixtures of a solvent and a nonsolvent (N,N-dimethylacetamide and water, in most cases) are investigated. The liquid-liquid demixing gap is determined and it is shown that its location in the ternary phase diagram is mainly determined by the PSf-nonsolvent interaction parameter. The critical point in the PSf/DMAc/water system lies at a high polymer concentration of about 8% by weight.

Calorimetric measurements with very concentrated PSf/DMAc/water solutions (prepared through liquid-liquid demixing, polymer concentration of the polymer rich phase up to 60%) showed no heat effects in the temperature range of -20 °C to 50 °C. It is suggested that gelation in PSf systems is completely amorphous.

The results are incorporated into a discussion of the formation of Polysulfone membranes.

*A part of this work was presented at the Fourth Symposium on Synthetic Membranes in Science and Industry, Tübingen, FRG, September 6-9, 1983.

INTRODUCTION

The field of Membrane Filtration covers a broad range of different separation techniques such as: hyperfiltration, reverse osmosis, ultrafiltration, microfiltration, gas separation and pervaporation. Each process makes use of specific membranes which must be suited for the desired separation. This implies that many different membranes with optimized properties have to be made and consequently it means that there is a strong interest among membrane manufacturers in the parameters that govern these membrane properties.

In our laboratory we try to obtain a coherent view on the formation of membranes. In this mechanism of formation an important role is played by the phase transition phenomena (gelation and liquid-liquid demixing) in ternary polymer solutions. An introduction into the formation mechanism will be given in the theory section.

The phase separation phenomena in the membrane forming system consisting of cellulose acetate, dioxane and water have been studied by Altena [1]. In the present work we will focus on systems which contain the polymer Polysulfone. Polysulfone is an important polymer in commercial membrane fabrication, especially as an Ultrafiltration membrane and as a support for composite membranes. The system studied most thoroughly consists of Polysulfone, N,N-dimethylacetamide (a solvent) and water (a nonsolvent). We will determine the liquid-liquid demixing gap and we will investigate whether the transition from a fluid to a solid state (gelation) in this system is accompanied by crystallization.

THEORY

Membrane formation

In the phase inversion process a membrane is made by casting a polymer solution on a support and then bringing

the solution to phase separation by means of solvent outflow and/or nonsolvent inflow. Thus, in most cases at least three components are involved: a polymer, a solvent and a nonsolvent. Exchange of the latter two leads to a phase transition in the at first homogeneous polymer solution and the membrane structure is formed. The cross section of this structure is asymmetric in many cases: a thin and dense skin layer is supported by a porous sublayer. In our view two different types of phase separation are responsible for these two layers [1-5]:

- gelation (possibly induced by crystallization) for the formation of the skin layer;
- liquid-liquid phase separation followed by gelation of the concentrated phase for the formation of the porous sublayer.

Gelation will take place at high polymer concentrations whereas liquid-liquid phase separation is expected to occur at low polymer concentrations. In Figure 1 the phase boundaries are schematically drawn in a ternary phase diagram.

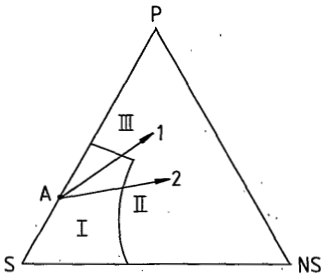


FIGURE 1. Schematic representation of a ternary phase diagram.
 I : homogeneous solution;
 II : liquid-liquid demixing;
 III: gelation.
 The arrows are possible coagulation paths, see text.

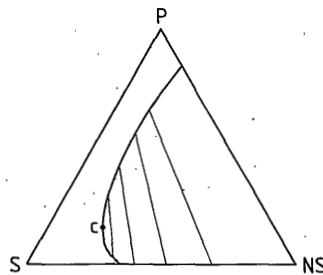


FIGURE 2. Liquid-liquid demixing gap in a ternary phase diagram. The straight lines in the demixing gap are tie lines. C is the critical point.

The arrows 1 and 2 represent the change in composition for respectively the skin layer and the sublayer if a polymer film with initial composition A is immersed in a nonsolvent bath. In this approach it is assumed that the ratio of solvent outflow to nonsolvent inflow is larger for the skin layer (in direct contact with the coagulation bath) than for the sublayer.

Liquid-liquid phase separation

Altena [6] has shown that in virtually every system consisting of a polymer, a solvent and a nonsolvent liquid-liquid demixing can be expected. The exact location of the demixing gap is determined by the interactions between the three components. The liquid-liquid phase boundary is the so-called binodal. Every composition inside the binodal will demix into two liquid phases which differ in compositions but which are in thermodynamic equilibrium with each other. The line which connects a pair of equilibrium compositions in the phase diagram is called a tie line, see Figure 2. The two compositions are identical in the critical point. Liquid-liquid demixing is reasonably well described by the Flory-Huggins thermodynamics [7] for ternary systems. In this description the interactions between the components are represented by three binary interaction parameters: $\chi_{\text{polymer/solvent}}$, $\chi_{\text{solvent/nonsolvent}}$ and $\chi_{\text{polymer/nonsolvent}}$. These interaction parameters incorporate both enthalpy and entropy contributions.

There are three different ways for liquid-liquid demixing to set in: *i*) by nucleation and growth of the concentrated phase (rich in polymer), *ii*) by nucleation and growth of the diluted phase (poor in polymer), and *iii*) by spinodal decomposition. The second phenomenon is the most important to membrane formation. It leads to a continuous polymer matrix in which spheres filled with the diluted

phase (in general with an extremely low polymer content) are dispersed. For an effective membrane the dilute phase forms also a continuous phase (by coalescence of the spheres).

Gelation

At high polymer concentrations polymer solutions are able to form a three dimensional network and in that case the fluid system is transformed into a gel. The nature of the cross links which form the network may differ from system to system [8]. For crystalline or semicrystalline polymers the cross links are micro-crystallites and the thermoreversible gelation can be described by the theory of melting point depression [7]. Gelation in the membrane forming system Cellulose Acetate/Dioxane/water has been analyzed in this way [1].

Recently attention has been paid to gelation phenomena in solutions of noncrystalline polymers by Tan *et al.* [9,10]. Both in solutions of atactic Polystyrenes [9] and of some chlorinated Polyethylenes [10] thermoreversible gelation is observed. The melting of these gels is even accompanied by a very small endothermic peak in DSC experiments. These findings raise interesting questions regarding the nature of the interchain connections in gels of amorphous polymers and these are addressed in the papers by Tan *et al.* They suggest that chain overlap is a necessary condition for gel formation and that the network junctions are stabilized through local ordering. The physical picture of the latter process is not clear at the moment.

EXPERIMENTS

Materials

The polymer Polysulfone P3500 (PSf) is purchased from Union Carbide. It is characterized by $M_n = 14,000$, $M_w = 46,000$ and $M_z = 75,000$ (determined with HPLC). The solvents and nonsolvents used are of reagent grade and were used without further purification, except for drying on molecular sieves.

Cloud points

The cloud points in ternary systems are determined in two ways:

1) By a rapid titration method and 2) by turbidity measurements upon cooling a ternary solution. The second method is the more accurate one.

1) A solution of the polymer in the solvent is brought in a vessel which is kept at a constant temperature (25°C normally). To this solution the pure nonsolvent or a mixture of the solvent and the nonsolvent is slowly added, see Figure 3. This is continued until permanent turbidity is

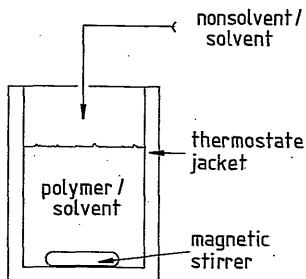


FIGURE 3. Determination of cloud points by the titration method.

detected visually. The composition of the solution in the vessel at that moment is computed from the total amounts of polymer, solvent and nonsolvent present. The addition of mixtures containing a considerable fraction of solvent is favoured over the addition of pure nonsolvent since in the latter case every drop added will cause local coagulation in the polymer solution. To allow the solution to become homogeneous again may take a long time.

2) A method described earlier by van Emmerik [11] has been modified to make the procedure less laborious. The experimental setup is shown in Figure 4. The temperature of the thermostate bath is decreased by an external cooling unit with a constant rate of 1 °C per 10 minutes. In the bath a slowly rotating wheel is placed, on which a number of capillary tubes is attached. Each tube is filled with a polymer/solvent/nonsolvent mixture of a certain composition. The tubes have been sealed under vacuum at liquid nitrogen temperature. Due to the rotation of the wheel each tube intersects the laser beam every 5 minutes. The intensity of the transmitted laser light is continuously

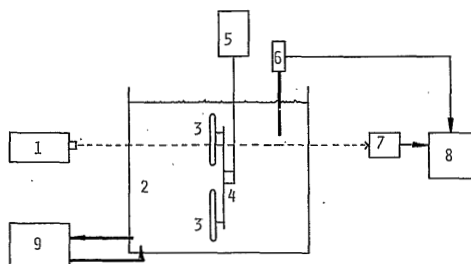


FIGURE 4. Detection of cloud point temperature by turbidity measurements.

- | | | |
|---------------------|---------------|-------------|
| 1: laser | 5: motor | 9: cryostat |
| 2: thermostate bath | 6: thermistor | |
| 3: capillary tubes | 7: detector | |
| 4: rotating wheel | 8: recorder | |

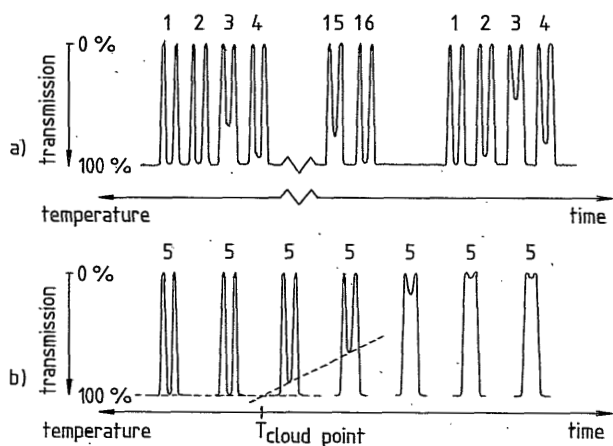


FIGURE 5. (a) Trace of recorder output of turbidity experiment. Numbers identify separate tubes.
 (b) Determination of the cloud point temperature of tube no. 5 through interpolation.

monitored on a recorder together with the temperature of the bath. The at first homogeneous solutions in the tubes will demix as a result of the decrease in temperature and this is observed in the recorder output as illustrated in Figure 5. Part a) of this figure displays the recorder output. If there is no tube between the laser and the detector the transmission is 100%. At the moment the wall of a tube intersects the laser beam, all the light is reflected and the transmission is zero. One moment later the laser beam passes through the center of the tube and if the solution is clear the transmission is 100% or a little bit less. The transmission is zero again at the moment the tube leaves the beam. After a short time the next tube appears, etc. In part b) it is shown how the cloud point temperature of a certain tube is determined by interpolation. The compositions in the tubes belong to a homologous series. These series can be made *i*) by adding different

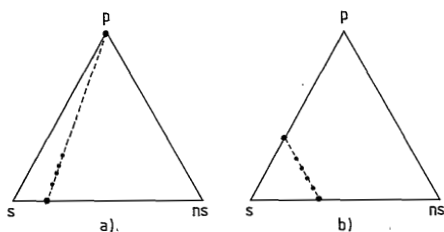


FIGURE 6. Pseudo-binary series of compositions.

amounts of polymer to a certain solvent/nonsolvent mixture (see Figure 6 a.), or *ii*) by mixing a solution of the polymer in the solvent in different ratios with a solvent/nonsolvent mixture, see Figure 6 b. For each series the cloud point temperatures are plotted as a function of the polymer concentration and through interpolation the compositions which demix at a certain temperature (25 °C normally) are determined. The choice of the concentration range to be examined is facilitated if some titration experiments as described above are performed previously.

Tie lines

If the polymer/solvent/nonsolvent mixture in a tube has been subjected to liquid-liquid phase separation, it is in principle possible to separate the two equilibrium phases from each other by centrifugation. Problems arise if gelation of the concentrated phase occurs. This is not the case in PSf systems and centrifugation (2000 rpm) yields two completely clear phases with a distinct interface. The more viscous the concentrated phase the more tedious this procedure will be. The tube is then placed vertically with the concentrated phase in top. The diluted phase flows to

the bottom of the tube, whereas the concentrated phase remains in the upper part. Upon breaking the tube, from both phases a sample can be taken and the polymer concentrations can be determined by evaporation of the solvent and the nonsolvent.

Differential Scanning Calorimetry

The apparatus used is a Perkin Elmer DSC model II, equipped with an external cooling unit (liquid nitrogen) to make experiments possible at subambient temperatures. The DSC samples can be prepared in two different ways.

1) The appropriate amounts of PSf (powder) and solvent/nonsolvent mixture are weighed into the aluminium sample pans. The PSf granules were converted into a powder as described recently [12]. The pans are sealed and are stored at a temperature of 90 °C or 120 °C for several days. After this period the sample is weighed again and only sample pans that showed no weight loss are used in the experiments. For the present purpose of the DSC experiments, this preparation method has the following disadvantages: *i*) PSf concentrations higher than 35% by weight are difficult to obtain, and *ii*) there is no direct proof that the samples have become completely homogeneous during the waiting period at elevated temperatures, molecular diffusion being the sole mixing mechanism.

2) During the determination of the tie lines, see the Results section, it became clear that the concentrated phase of liquid-liquid demixed systems had high to very high PSf concentrations. This has been used to prepare concentrated samples for the DSC experiments.

As in the determination of the tie lines, the concentrated phase of a demixed PSf/DMAc/water is isolated. From this phase a small amount (about 10 mg) is put in a sample pan and another part is used to determine the PSf concentra-

tion. In this way it is possible to prepare samples with PSf concentrations up to 60% by weight of which it is certain that they are homogeneous at room temperature. All DSC experiments presented in this paper have been carried out with samples prepared by method 2.

The samples are cooled from 50 °C to -20 °C or -70 °C with a rate of 10 °C per minute. After a waiting period at the lower temperature (varying from 0 to 20 hours) the sample is reheated to 50 °C at a rate of 10 °C per minute. During the heating run the DSC signal is recorded in order to detect heat effects.

RESULTS AND DISCUSSION

Polysulfone/solvent mixtures

The solvent DMAc is a good solvent for Polysulfone, so it is expected that binary PSf/DMAc mixtures are thermodynamically stable upto high PSf concentrations. Contrary to this is the fact that solutions of PSf in DMAc and in other solvents become turbid after a certain time and that a white precipitate is formed. In a recent publication [12] we have shown that this instability is due to crystallization of a small oligomer fraction of the Polysulfone. Once this fraction is removed, the solutions are stable at least longer than 6 months. In solutions of PSf in DMAc this oligomer crystallization does not set in within one day if the PSf concentration is lower than 15%.

Cloud points

The cloud point temperatures of homologous series of PSf/DMAc/water mixtures have been determined by the turbid-

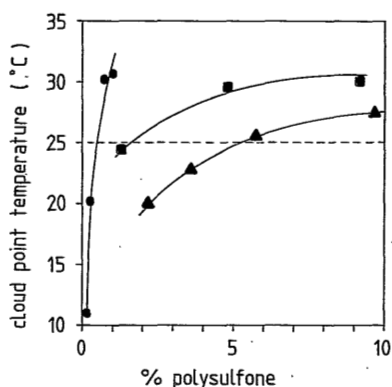


FIGURE 7. Cloud point temperatures of three pseudo-binary series.
 ● H₂O/DMAc ratio = 4.42/95.58; ■ H₂O/DMAc ratio = 4.27/95.73;
 ▲ H₂O/DMAc ratio = 4.22/95.78.

dity method. In Figure 7 the demixing temperatures are displayed for three different series. Through interpolation the compositions which demix at 25 °C are obtained and these compositions are shown in the phase diagram of Figure 8. The water concentration varies from 3.0% to 4.2% when the PSf concentration goes from 25% to 1%. In this range the cloud points lie on a straight line with very little deviation. At PSf concentrations lower than 1% the binodal bends sharply towards higher water concentrations and vanishes in the water-DMAc axis for water concentrations larger than 5%. The six cloud points with very low PSf concentrations have been determined by the titration method and the compositions are given in Table 1. At such low polymer concentrations the detection of the cloud point is not very accurate and the values of Table 1 are the mean values of in total 24 experiments.

Polysulfone is a very hydrophobic polymer, so the PSf-water interaction parameter will have a large positive value. This parameter has been determined by swelling ex-

FIGURE 8. Cloud points in the system consisting of Polysulfone, DMAC and water at 25 °C.

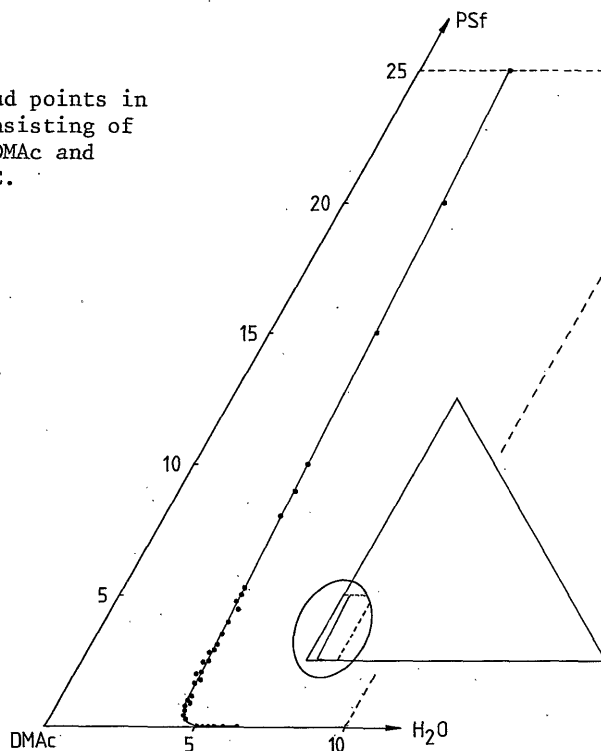


TABLE 1
Cloud points at low PSf concentrations

% PSf	% H ₂ O	% DMAC
0.042	5.10	94.86
0.024	5.30	94.68
0.015	5.50	94.49
0.0095	5.70	94.29
0.0060	6.00	93.99
0.0018	6.45	93.55

periments and a value of 5.9 was obtained [13]. The theoretical phase diagrams, as calculated by Altena [6] for ternary systems with a large polymer-nonsolvent interaction parameter, display a binodal located close to the

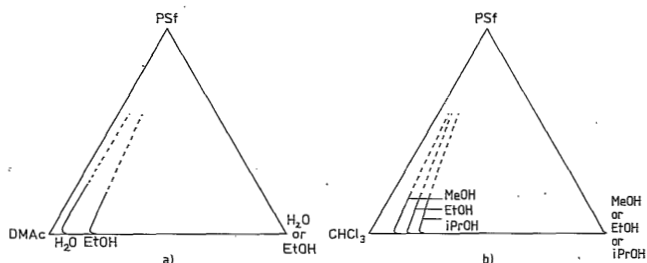


FIGURE 9. Binodals in five different systems with Polysulfone and varying solvents and nonsolvents. $T = 25\text{ }^{\circ}\text{C}$.

polymer-solvent axis, regardless of the choice of the solvent. The experimentally determined binodal is in agreement with this observation.

Next to the PSf/DMAC/water system the binodals in other Polysulfone systems have been determined by the titration method. The binodals are shown in Figure 9 (a: PSf/DMAC/water or ethanol, and b: PSf/ CHCl_3 /methanol or ethanol or iso-propanol). Figure 9 has previously been published by Mulder *et al.* [14] in their study of the preparation of asymmetric pervaporation membranes. The binodals of the systems PSf/DMAC/EtOH and PSf/ CHCl_3 /EtOH are almost identical. This once again shows that the polymer-nonsolvent interaction is very important in these systems. In the homologous series of nonsolvents, the binodal shifts to higher nonsolvent concentrations going from water to iso-propanol. In the same series the Polysulfone-nonsolvent repulsion, and thus $\chi_{\text{PSf/nonsolvent}}$, decreases ($\chi_{\text{PSf/EtOH}} = 2.5$ [13]). From these observations it is clear that in ternary systems with strong polymer-nonsolvent repulsions the value of $\chi_{\text{polymer/nonsolvent}}$ determines to a large extent the location of the liquid-liquid demixing gap.

Tie lines

The determination of the polymer concentration in the concentrated and diluted phases is not very accurate. This is illustrated by the fact that an increase in the PSf concentration in the concentrated phase is not always accompanied by a decrease in the PSf concentration in the diluted phase. In a truly ternary system this should be the case. The presence of a polymer component makes our system a pseudo-ternary system, but at present we feel that the molecular weight distribution of the polymer is not very relevant. The uncertainty in the experiments is probably due to the fact that during the centrifugation step no temperature control was possible.

In Figure 10 the PSf concentration in the concentrated phase is plotted as a function of the PSf concentration in the corresponding diluted phase in

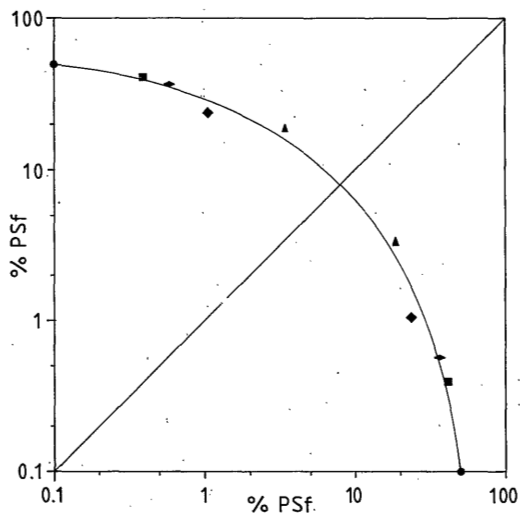


FIGURE 10. PSf concentration in the concentrated phase as a function of the PSf concentration in the corresponding diluted phase. The points on either side of the diagonal are identical.

the diluted phase for five different experiments. The points above and under the diagonal are identical. Figure 10 shows *i)* that the PSf concentrations in the concentrated phase are very high upto 60%, *ii)* that the tie lines are extremely steep, i.e. they are almost parallel to the PSf-DMac axis, and *iii)* that the critical point, where the two concentrations are identical, probably lies at a PSf concentration around 8%.

In the first part of this section, attention has been paid to the oligomer crystallization in concentrated PSf solutions. The concentrated phase of a liquid-liquid demixed system does not show this behaviour, since the oligomer fraction accumulates in the PSf poor phase [12].

Gelation

Samples with PSf concentrations ranging from 40% to 60% have been examined. Due to the preparation method these samples are known to be fluid at 25 °C and they contain a small percentage of water. Extrapolation of the binodal to high PSf concentrations suggests that the water concentration is about 2%.

All samples were cooled from 50 °C to -70 °C and then immediately reheated to 50 °C. In the heating run melting endotherms were detected in the range of -40 °C to -25 °C, see Figure 11. The melting peak is larger and sharper than expected for the melting of a polymer and this raises the question whether low molecular weight components are responsible for this transition energy. That this indeed is the case is proven by the following experiment: the corresponding diluted phase is cooled to -70 °C and then reheated to 50 °C. A very large melting effect is observed in the same temperature range as the endotherm of the concentrated sample. The fact that the melting effect is larger for the polymer poor phase indicates that not the Poly-

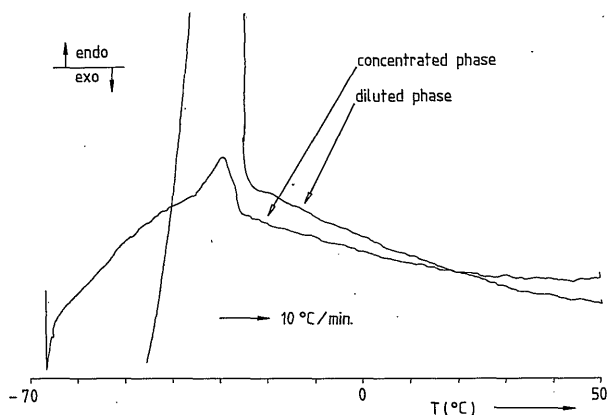


FIGURE 11. DSC thermogram of a concentrated phase and of the corresponding diluted phase. The PSf concentration in the concentrated phase is about 60%.

sulfone but the DMAC/water mixture crystallizes. This conclusion is supported by the observation that the melting point of a binary DMAC/water mixture with a DMAC concentration of 95% is about -30°C . The two peaks in Figure 11 coincide in temperature because the two samples are in thermodynamic equilibrium with each other.

In order to avoid the crystallization of the solvent and the nonsolvent the lower temperature boundary is set at -20°C in the next series of experiments. The samples are cooled to -20°C and reheated to 50°C after a waiting period of 0 to 20 hours. In none of the heating runs heat effects could be detected and there is no significant influence of the waiting time.

Thus, according to the DSC experiments no crystallization or local ordering has been demonstrated in the concentrated PSf solutions. To our knowledge no evidence of crystallinity has been reported in the literature for the class of the Polysulfones, with the exception of solvent-induced crystallization of Poly(ethersulphone) [15]. Nev-

ertheless, in a certain concentration range there must be a solution-gel transition since there do exist PSf films and membranes. Apparently in PSf solutions this gelation is not induced by crystalline regions. The possibility of amorphous local ordering, as proposed by Tan *et al.* [9,10] will not be addressed here since this concept is not yet described in physical terms. Another possibility is to view the solution-gel boundary as a viscosity boundary. In very concentrated solutions the overlap between the polymer molecules is large and the entanglements are numerous. This drastically reduces the fluidity of the solution and as disentanglement will be slow, the system has viscoelastic properties. In this case the solution-gel transition is not a thermodynamic equilibrium and one does not expect a sharp, thermoreversible, gel point.

PREPARATION AND PROPERTIES OF POLYSULFONE MEMBRANES

The most important result in relation to membrane formation is the observation that gelation in the PSf system is not accompanied by any large scale ordering. This means that the molecules in a gelled PSf film are evenly distributed and that transport through such a layer must take place via molecular diffusion using the free volume of the PSf molecules. Thus, in asymmetric PSf membranes with a skin layer formed by gelation the transport mechanism will be the solution-diffusion mechanism.

In Table 2 the characteristic properties of some Polysulfone membranes are collected. Coagulation of a 15% PSf-DMAC solution in water yields a typical ultrafiltration membrane with a reasonable permeability for water. Considering the hydrophobic nature of the polymer, we assume that in the skin layer there must be pores present through which a convective flow is possible. This is supported by the pervaporation experiments: the permeability is so high that

TABLE 2.

Properties of Polysulfone membranes. The data have been taken from the reference 14 (pervaporation) and from an internal report (ultrafiltration).

No.	solvent	% PSf	nonsolvent	$J_{H_2O}^a$ (cm/hr)	J^b (10^{-2} cm/hr)	$\alpha_{H_2O}^c$
I	DMAC	15	water	18 (3 atm)	\bar{d}	-
II	DMAC	35	water	0 (40 atm)	1.5	3.0
III	DMAC	15	ethanol		7.0	1.0
IV	CHCl ₃	15	ethanol		0.1	58

^a pure water flux, pressure indicated is trans membrane difference

^b pervaporation permeate flux, feed: 50% water/50% ethanol

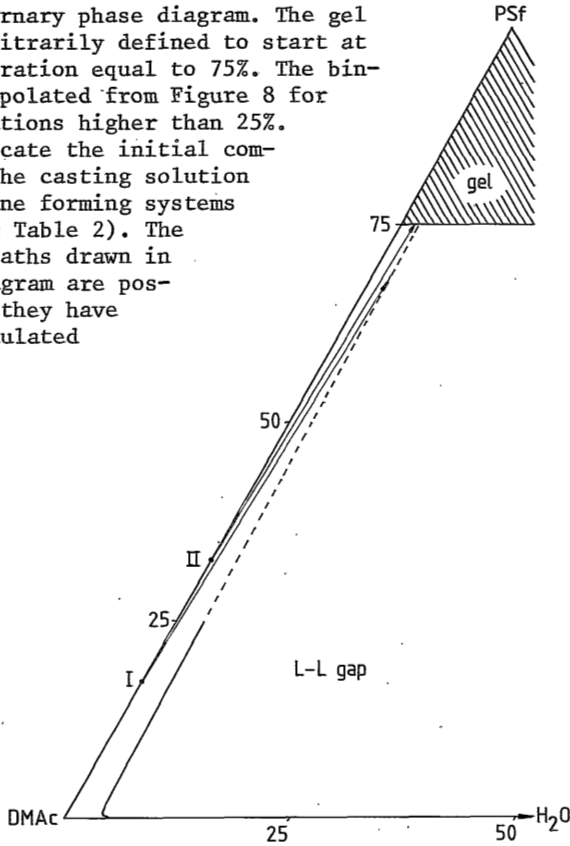
^c selectivity for water

^d permeability is too high; no proper vacuum is attained

no vacuum on the permeate side of the membrane is attained. If the PSf concentration in the casting solution is increased to 35%, a pressure driven transport of water through the membrane is not possible. In pervaporation experiments this membrane shows a reasonable flux and a moderate selectivity for water. In our opinion this points at transport by diffusion and certainly not by convection. There are two reasons why in this case the filtration water flux is zero and the pervaporation flux is not: *i*) a concentration gradient represents a much larger gradient in chemical potential (the true driving force) compared to a pressure gradient, and *ii*) the water uptake by the Polysulfone is facilitated by the presence of the ethanol [13].

The difference in structure of the skin layer of the membranes I and II (see Table 2) can be explained with the ternary phase diagram given in Figure 12. In the skin layer of membrane II no pores are present, so the coagulation path responsible for the skin formation does not cross the binodal. Lowering of the PSf concentration in the casting solution increases the possibility of liquid-liquid

FIGURE 12. Ternary phase diagram. The gel region is arbitrarily defined to start at a PSf concentration equal to 75%. The binodal is extrapolated from Figure 8 for PSf concentrations higher than 25%. I and II indicate the initial composition of the casting solution in the membrane forming systems I and II (see Table 2). The coagulation paths drawn in the phase diagram are possible paths, they have not been calculated nor measured.



demixing in the skin layer, if we assume that the direction of the coagulation path is unchanged. The coagulation path for the skin layer of membrane I crosses the binodal at a very high polymer concentration and this leads to pores with very small radii.

From the analysis given above it is clear that the location of the binodal is important with respect to the formation of the skin layer. In the Polysulfone systems discussed here the binodal is determined mainly by the polymer-nonsolvent interaction. Nevertheless, the choice of the solvent remains crucial. The nature of the solvent may influence *i*) the ratio of the solvent outflow and of the nonsolvent inflow, i.e. the direction of the coagula-

tion path, and *ii*) the structure of the formed gel. This is illustrated by the two last columns of Table 2. The membrane forming systems III and IV have almost the same location of the binodal, see Figure 9, but the membranes III and IV clearly differ in properties, the skin of membrane IV obviously being much denser.

CONCLUSIONS

The experimentally determined binodals of Polysulfone/solvent/nonsolvent systems are in qualitative agreement with the Flory-Huggins lattice theory for polymer solutions. No evidence for crystallization has been found in concentrated solutions of Polysulfone, so gelation in these systems is considered to be amorphous.

Gelation is responsible for the formation of the skin of asymmetric Polysulfone pervaporation membranes, whereas liquid-liquid demixing creates the pores in the skin of Polysulfone ultrafiltration membranes.

REFERENCES

- [1] F.W. Altena, *PhD Thesis*, chapters 3 and 4, Twente University of Technology, Enschede, The Netherlands, 1982.
- [2] L. Broens, F.W. Altena, C.A. Smolders and D.M. Koenhen, *Desalination*, 32 (1980) 33.
- [3] D.M. Koenhen, M.H.V. Mulder and C.A. Smolders, *J. Appl. Polym. Sci.*, 21 (1977) 199.
- [4] C.A. Smolders, in "Ultrafiltration Membranes and Applications", A.R. Cooper, Ed., Plenum Press, New York, 1980.
- [5] J.G. Wijmans and C.A. Smolders, to be published in

the NATO ASI Series, Reidel Publishing Company, chapter 2 of this thesis.

- [6] F.W. Altena and C.A. Smolders, *Macromolecules*, 15 (1982) 1491.
- [7] P.J. Flory, "Principles of Polymer Chemistry", Cornell University Press, Ithaca, 1953.
- [8] P.-G. de Gennes, "Scaling Concepts in Polymer Physics", Cornell University Press, Ithaca, 1979.
- [9] H.M. Tan, A. Moet, A. Hiltner and E. Baer, *Macromolecules*, 16 (1983) 28.
- [10] H.M. Tan, B.H. Chang, E. Baer and A. Hiltner, *Eur. Polym. J.*, 19 (1983) 1021.
- [11] P.T. van Emmerik and C.A. Smolders, *J. Polym. Sci. C*, 38 (1972) 73.
- [12] J.G. Wijmans and C.A. Smolders, appendix to this chapter, *Eur. Polym. J.*, 19 (1983) 1143.
- [13] M.H.V. Mulder, A.C.M. Franken and C.A. Smolders, *J. Membrane Sci.*, in press.
- [14] M.H.V. Mulder, J. Oude Hendrikman, J.G. Wijmans and C.A. Smolders, submitted to *J. Appl. Polym. Sci.*
- [15] D.A. Blackadder, H. Ghavamikia and A.H. Windle, *Polymer*, 20 (1979) 781.

**REMOVAL OF A LOW MOLECULAR WEIGHT, CRYSTALLIZABLE
POLYMER FRACTION FROM SOLUTIONS OF POLYSULFONE**

J.G. Wijmans and C.A. Smolders

SUMMARY

The oligomer fraction of poly[oxy-1,4-phenylenesulphonyl-1,4-phenyleneoxy-1,4-phenylene(1-methylethylidene)-1,4-phenylene](Polysulphone) with molecular weight between 450 and 900 daltons is responsible for the precipitation in concentrated solutions of polysulphone in N,N-dimethylformamide and other solvents. The precipitate is of a crystalline nature and consists mainly of the oligomers. These oligomers differ from the higher molecular weight molecules not only in crystallization properties. In a liquid-liquid phase separated system consisting of polysulphone, N,N-dimethylacetamide and water, the oligomers accumulate exclusively in the polysulphone-poor, dilute phase. The solubility parameter concept is used to illustrate the origin of this difference in behaviour. The removal of the oligomers from the dissolved polysulphone can be achieved by a crystallization process.

This appendix has been published in Eur. Polym. J., 13 (1983) 1143.

INTRODUCTION

Concentrated solutions of polysulphone (PSf) in various solvents tend to become turbid and produce a white solid mass upon sedimentation. The deposit is believed to be of a crystalline nature [1-3] and also the existence of crystalline entities in PSf films has been reported; the only evidence presented is that of microscopic observation.

In our laboratory, research on the mechanism of formation of synthetic membranes is carried out and therefore we are interested in the properties of casting solutions in relation to membrane structure and performance. PSf asymmetric ultrafiltration membranes, prepared from identical solutions, may show a wide variation of flux and rejection properties [4]; this effect could be connected with the fact that the casting solution itself is thermodynamically unstable. Therefore an investigation into the precipitation phenomenon has been made and a method to eliminate it has been sought.

EXPERIMENTAL

Polysulphone: P3500, Union Carbide, characterized by $\bar{M}_n = 14,000$, $\bar{M}_w = 46,000$ and $\bar{M}_z = 75,000$ (determined with HPLC). Referred to as PSf a.r. (as received).

The polysulphone precipitate (PSf precipitate) was kindly supplied by Dr. H.C.W.M. Buys (TNO Research Institute, Utrecht, The Netherlands) and was prepared in the following way. A 15% solution by weight of polysulphone P3500 in N,N-dimethylformamide (DMF) was allowed to stand for 3 months. The solution became turbid and slowly separated into two phases, viz. a clear solution above a white solid deposit. The deposit was filtered off and washed with DMF and petroleum ether 60/80 successively,

and was dried at room temperature. The yield was about 1 g of precipitate from 150 g of PSf.

N,N-dimethylformamide (DMF): p.a., ex. Fluka AG.

N,N-dimethylacetamide (DMAc): "analyzed reagent", ex. J.T. Baker.

Water: demineralized and ultrafiltrated.

Molecular weight distributions (MWD) were determined by means of a Waters High Performance Liquid Chromatograph. The eluent was tetrahydrofuran (THF).

Crystallinity was examined with a Philips 1310 Röntgen Diffractometer. For the diffraction experiment, where a powder was needed, the PSf a.r. granules were treated as follows. A solution of 3 g PSf a.r. in 100 g DMAc was added to a well stirred ethanol bath of 1.5 l. The precipitated PSf was filtered off and washed three times with isomeric hexane. The residue was dried *in vacuo* at 110°C. The MWD of this PSf powder showed that the low molecular weight fraction up to 900 daltons had disappeared during this procedure.

Infrared spectra were obtained with a Perkin-Elmer 257 apparatus. The spectrum of the PSf precipitate was taken from a KBr platelet containing the precipitate. The spectrum of the PSf a.r. was obtained from a thin PSf film, which was made by casting a solution of PSf a.r. in DMAc on a glass plate and evaporation of the DMAc in a N₂ atmosphere.

Differential Scanning Calorimetry was performed with a Perkin-Elmer DSC 2B apparatus.

Mass spectrometry was performed with a Varian Mat 311A apparatus.

RESULTS AND DISCUSSION

The nature of the precipitate

The molecular weight distribution (MWD) of the poly-

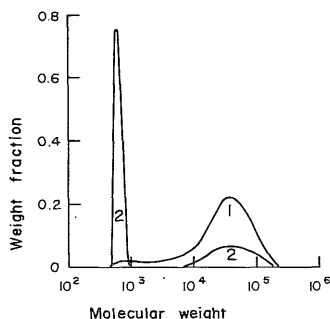


FIGURE 1. Molecular weight distributions of polysulphone: 1. The polymer as received; 2. The PSf precipitate.

sulphone (PSf) as received from Union Carbide shows that a certain amount of low molecular weight material is present (Fig. 1). According to Allison [1] these oligomers are responsible for the PSf precipitate, but no experimental evidence was given.

The PSf precipitate is insoluble at room temperature in the liquids that are good solvents for the PSf a.r., but it can partly be dissolved at elevated temperatures. A solution of the precipitate in THF was made in an autoclave. The MWD of the dissolved fraction of the precipitate is bimodal (see Fig. 1); this MWD shows that most of the material has a molecular weight between 450 and 900 daltons. In Fig. 2 the linear oligomers with molecular weights in that range are given. The insoluble part of the PSf precipitate was isolated by filtration and was dried *in vacuo* at 110°C. The yield was about 10 mg from 2 g PSf precipitate. From this insoluble fraction, a mass spectrum has been obtained and the spectrum shows a parent peak at 884 daltons. This value corresponds with the molecular weight of a cyclic PSf oligomer, i.e. the oligomer D of which the end-groups have joined, leading to a cyclic structure. Since this insoluble component is not present in the PSf a.r., we conclude that this cyclic PSf oligomer has been formed during the precipitation and

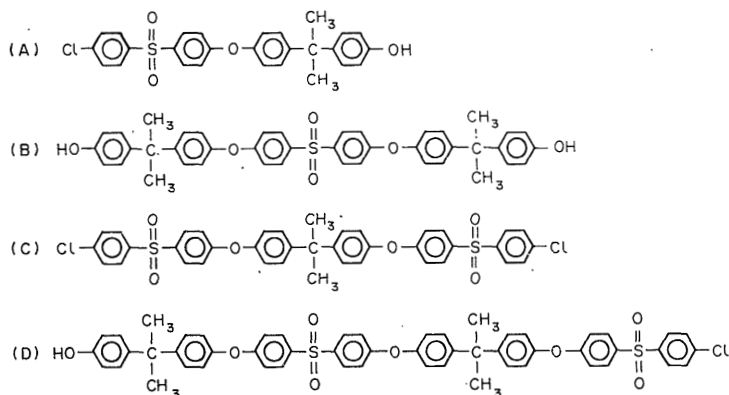


FIGURE 2. Oligomers of polysulphone. Polysulphone is the polycondensation product of 2,2,bis(4-hydroxyphenyl)propane and 4,4,dichlorodiphenylsulphoxide. The molecular weights are 478.5 (A), 670.0 (B), 729.0 (C) and 920.5 daltons (D).

sedimentation step which produced the PSf precipitate.

The X-ray diffraction pattern of the PSf precipitate demonstrates the presence of crystalline material (see Fig. 3, graph II). Since it was impossible to perform diffraction experiments on the PSf a.r. granules, the granules were converted into powder as described in the Experimental Section. The diffraction pattern of this powder shows amorphous scattering only (see Fig. 3, graph I). It should be noted that the oligomer fraction up to 900 daltons has disappeared during the coagulation. We tried several ways to grind or pulverize the granules and thus preserve the oligomers in the powder, but we were not successful. The PSf granules have too high elastic-mechanical strength, even if cooled to liquid N_2 temperature.

An i.r.-spectrum was taken to prove that the precipitate is indeed a polysulphone fraction. From Fig. 4 it can be seen that the precipitate has an additional absorption at 6μ compared to the spectrum of the PSf a.r. Upon heating the precipitate for 2 hr at $110^\circ C$ *in vacuo*, this particular absorption disappears, whereas the

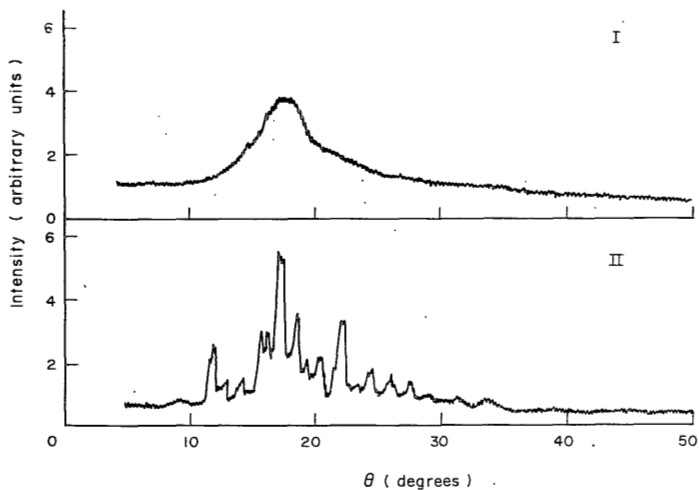


FIGURE 3. Diffraction patterns of polysulphone. I. PSF; II. PSf precipitate, fresh and after heating *in vacuo* at 110°.

crystallinity of the sample is not affected (see Fig. 3) Since DMF, in which solvent the precipitation has taken place, has a C=O stretch absorption at $6\ \mu$, we conclude that DMF was present in the precipitate and that the precipitate itself is a fraction of the polysulphone sample.

The precipitate was heated from 60 to 430°C in a Differential Scanning Calorimeter (DSC) in order to determine the melting temperature. Surprisingly, no endotherm was observed but there was an exotherm between 280 and 340°C. The heat effect amounts to about 20 J/g. After cooling to 60°C, no heat effects are observed upon reheating to 430°C. Inspection of the sample showed that the precipitate changed from a powder into a hard platelet with some mechanical strength. According to the i.r.-spectrum, no structural changes occurred during the DSC run. It seems that the exotherm is the result of a sintering process, i.e. a decrease of the total crystalline

surface. Recrystallization, another phenomenon producing an exotherm, is not considered here since in that case an endotherm should be expected shortly after the exotherm.

It is concluded that the phase separation found in concentrated solutions of PSf in DMF is a crystallization process, in which mainly the oligomers of the PSf take part. The same explanation is expected to hold for the precipitation phenomena in solutions of PSf in other solvents such as *N,N*-dimethylacetamide (DMAc) and dichloromethane. It should be noted here that the precipitation process shows a different time-scale in different solvents.

Solubility properties of the precipitate

The reason why the oligomers have a specific tendency to crystallize is not clear. From the standpoint of equilibrium thermodynamics, crystallization is more favourable for larger molecules in a homologous series. On the other hand, crystallization will be faster for smaller molecules.

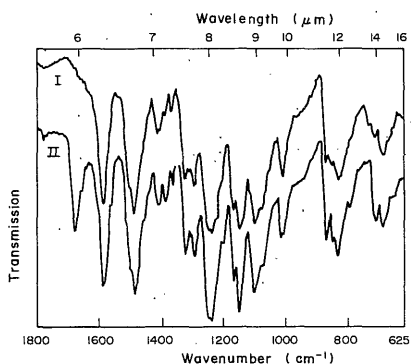


FIGURE 4. i.r. Spectra of polysulphone. I. PSf a.r. and PSf precipitate after heating *in vacuo* at 100°C for 2 hr. II. PSf precipitate, fresh.

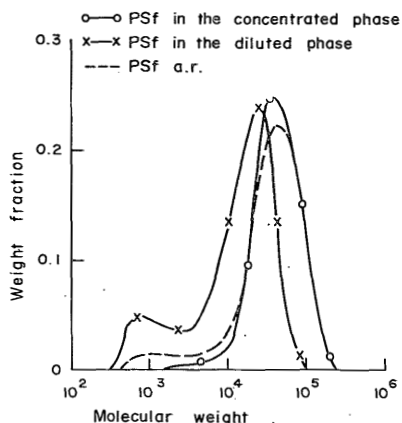


FIGURE 5. Molecular weight distributions of polysulphone, a liquid-liquid phase separated system, consisting of PSf, DMAc and H_2O . The PSf was isolated from the phases by a rapid distillation method described by Patat [5]. The volume ratio of the two equilibrium phases was about 1.

There is evidence that the oligomers of PSf do not have the same thermodynamic properties as the higher molecular weight molecules. Figure 5 shows the MWD of PSf in the two phases of a liquid-liquid phase separated system consisting of PSf, DMAc and water. The oligomers have accumulated in the phase with the high water and low polymer content. Although fractionation during liquid-liquid phase separation is not uncommon, the complete disappearance of the oligomers from the concentrated phase is remarkable and in our opinion this reflects a higher affinity of the oligomers for water in comparison with the high molecular weight molecules.

The hydroxy and the chloride end-groups influence the solubility properties of PSf and this influence will be larger for the oligomers than for the higher molecular weight molecules. Table 1 gives the solubility parameters of the PSf molecules with different molecular weights. The parameters have been calculated with the aid of the molar attraction constants of characteristic groups as listed by van Krevelen [6]. The molar attraction con-

TABLE 1. Solubility parameters of components in the system
PSF-DMAc-water or ethanol

	δ_d (cal/cm ³) ^{1/2}	δ_p (cal/cm ³) ^{1/2}	$\delta_h = \delta_{chem}$ (cal/cm ³) ^{1/2}	δ_{phys} (cal/cm ³) ^{1/2}
1. Polysulphone	9.0	2,3	2.7	9.3
2. Oligomer A*	9.0	2.1	4.2	9.2
3. Oligomer B*	9.3	1.8	4.7	9.5
4. Oligomer C*	8.7	2,5	2.7	9.1
5. Oligomer D*	9.0	2.1	3.5	9.2
6. DMac ⁺	8.2	5.6	5.0	9.9
7. Ethanol ⁺	7.3	4.3	9.5	8.5
8. Water ⁺	6.0	15.3	16.7	16.4
Water ⁺⁺	7.6	7.8	20.7	10.9

* See Fig. 2. ⁺ Taken from Ref. [8]. ⁺⁺ Taken from Ref. [10].

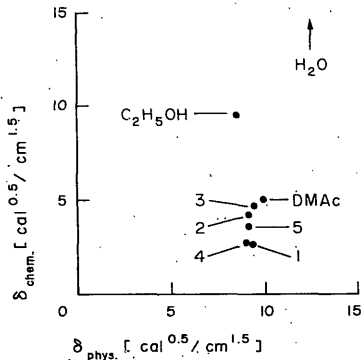


FIGURE 6. Solubility parameters for PSf (polymer and oligomers), DMac, ethanol and H₂O. The numbers indicated correlate with those in Table 1.

stants of the sulphone group, which are not included by van Krevelen, are calculated from the solubility parameters of dimethylsulphone [7]. In Fig. 6 the solubility parameters of PSf, DMac, ethanol and water are represented, using a two dimensional solubility parameter plot follow-

ing Bagley [8]:

$$\delta_{\text{phys.}} = (\delta_{\text{d}}^2 + \delta_{\text{p}}^2)^{\frac{1}{2}}$$

$$\delta_{\text{chem.}} = \delta_{\text{h}} \quad (1)$$

where δ_{d} = solubility parameter, due to dispersion forces, δ_{p} = solubility parameter due to dipole forces, δ_{h} = solubility parameter due to hydrogen bonding, $\delta_{\text{phys.}}$ = solubility parameter due to physical forces and $\delta_{\text{chem.}}$ = solubility parameter due to chemical interactions.

From Fig. 6 it can be concluded that the oligomers A, B and D differ from the PSf polymer mainly in their capability to form hydrogen bonds (i.e. the sulphone and hydroxy groups). This indicates indeed a higher affinity of the oligomers for water and ethanol compared to the PSf polymer.

Removal of the oligomer fraction

In order to prevent precipitation in solutions of polysulphone, Allison [1] proposed a process, involving two coagulation steps, to remove the oligomers. This method is laborious and consumes large quantities of chemicals if carried out on a scale larger than laboratory experiments. A better procedure to obtain an oligomer free solution is the following.

As has been stated above, a concentrated PSf solution produces after a sufficiently long sedimentation period a clear solution above a white precipitate. The resulting solution remains homogeneous for months if the precipitate is removed. The same observations have been made by Buys [10]. The concentration of the solution is scarcely affected by the precipitation.

We did not elaborate on an optimization of the process

by studying the crystallization kinetics. Once the kinetics are known, one could investigate the feasibility of an improved sedimentation step (e.g. by centrifugation) after a certain crystallization period and thus accelerate the process.

ACKNOWLEDGEMENTS

Thanks are due to G. van de Ridder, who performed the HPLC experiments, and to J. Boeysma, who performed the X-ray experiments.

REFERENCES

- [1] R. Allison, TRW Inc. Los Angeles, *Patent Ger. Offen.* 2,415,444, 23 Oct. 1975
- [2] B.J. MacNulty, *J. Mater.Sci.* 4, 841 (1969)
- [3] B.J. MacNulty, *J. Mater.Sci.* 8, 1495 (1973)
- [4] J.E. Cadotte, R.S. King and N.A. Newkumet, NTIS-Report, PB 80-127574, Sept, 1979
- [5] F. Patat and G. Träxler, *Makromolek. Chem.* 33, 113 (1959)
- [6] D.W. van Krevelen, *Properties of Polymers*, Elsevier, Amsterdam (1972)
- [7] C.M. Hansen and A. Beerbower, *Encyclopedia of Chemical Technology*, Supplement Vol. 889, Wiley, New York (1971)
- [8] E.B. Bagley, T.P. Nelson and J.M. Scigliano, *J. Paint Technol.* 43, 35 (1971)
- [9] A.F.M. Barton, *Chem. Rev.* 75, 6, 731 (1975)
- [10] H.C.W.M. Buys, Private communication.

PHASE SEPARATION PHENOMENA IN SOLUTIONS OF
POLY (2,6-DIMETHYL-1,4-PHENYLENEOXIDE) IN
MIXTURES OF TRICHLOROETHYLENE, 1-OCTANOL AND
METHANOL: RELATIONSHIP WITH MEMBRANE FORMATION*

J.G. Wijmans, H.J.J. Rutten and C.A. Smolders

SUMMARY

The phase boundaries in the quaternary system consisting of the polymer poly(2,6-dimethyl-1,4-phenyleneoxide) (PPO**), the solvent trichloroethylene (TCE) and the nonsolvents 1-octanol (1-oC₈H₁₇OH) and methanol (MeOH) are determined. The kinetics of crystallization are investigated by Pulse Induced Critical Scattering. The formation and properties of PPO membranes are discussed in relation to the phase separation phenomena.

INTRODUCTION

Polymeric synthetic membranes are usually made by the phase inversion process. The typical feature of this process is the induction of phase separation in a polymer solution through a change in the composition of the solution. The interplay of the phase separation phenomena and the rate of change in composition determines the membrane structure. In most cases an asymmetric structure is obtained; a very thin (0.1 to 0.5 μm) and dense top layer is supported by a porous

*A part of this work was presented at the First Europe-Japan Congress on Membranes and Membrane Processes, Stresa, Italy, June 18-22, 1984.

**PPO is a registered trademark of the General Electric Company.

sublayer of 0.1 to 0.2 mm thickness. The relationship between the preparation procedure and the ultimate membrane structure has been investigated by a number of research groups, and the approach adopted in our laboratory was extensively discussed in two reviews [1,2]. This mechanism of formation will be recapitulated in short here in the theory section.

In the past a study was carried out by Broens *et al.* [3] to prepare ultrafiltration membranes from the polymer poly-(2,6-dimethyl-1,4-phenyleneoxide) (PPO). The polymer PPO was selected since it has good chemical and physical properties. It appeared that membranes with promising ultrafiltration properties are obtained if a casting solution of 10% PPO in a 78%/22% mixture of trichloroethylene (TCE) and 1-octanol (OcoH) is immersed in a coagulation bath containing methanol (MeOH). The concentrations are expressed as % by weight. The addition of OcoH to the casting solution is essential to obtain membranes with an acceptable water permeability. If the TCE/OcoH mixture contains less than 18% OcoH, the membrane is not permeable to water. It was suggested [3] that the addition of OcoH increases the ability of the PPO molecules to crystallize and thus leads to a more grainy structure in the top layer and that the water permeation during ultrafiltration occurs through the voids of the densely packed crystalline nodules.

In this paper we will determine phase equilibria of the quaternary system consisting of PPO, TCE, OcoH and MeOH, and the kinetics of the PPO crystallization in this system. These data will be discussed in relation to the formation and properties of PPO membranes.

THEORY

Mechanism of membrane formation [1,2]

Two different types of phase separation are thought to be responsible for the asymmetry of the membranes:

- gelation (possibly induced by crystallization) for the formation of the skin, and
- liquid-liquid demixing followed by gelation of the polymer rich phase, for the formation of the porous substructure.

The two different types of phase separation are the result of different changes in composition characteristic for each layer. In Figure 1 a schematic ternary phase diagram is presented and the changes in composition are visualized by so-called coagulation paths.

If gelation occurs by formation of crystalline cross links, the solution/gel transition is a true thermodynamic equilibrium and in combination with liquid-liquid demixing it will create a three-phase region in the phase diagram as shown in Figure 2. Within the three-phase region all compositions will split up in the three compositions which form the corners of the three-phase triangle, that is if the equilibrium state is reached. The entry of the three-phase region is a dynamic process, i.e. a change in temperature or in composition, and the kinetics of both gelation and liquid-liquid demixing will be important. Except for high polymer concentrations, liquid-liquid demixing will in general be faster than gelation.

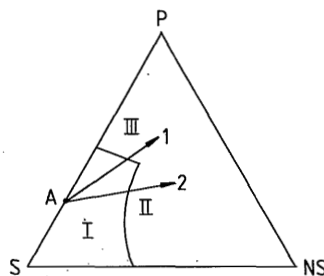


FIGURE 1. Ternary phase diagram.
 I: homogeneous solution; II: liquid-liquid demixing; III: gel area.
 The arrows 1 and 2 are possible coagulation paths characteristic for respectively the top layer and the porous substructure.

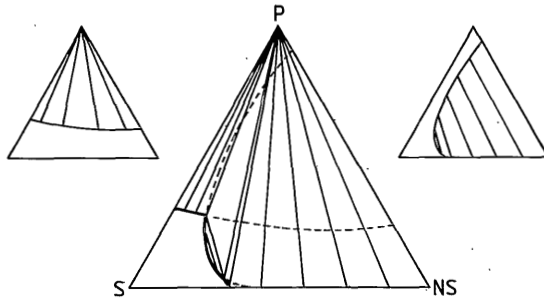


FIGURE 2. Phase diagram of a ternary system with a solubility gap in the liquid phase and a crystalline component P. The solubility gap (diagram on the right) intersects the melting curve (diagram on the left) and a three-phase region is formed.

Kinetics of crystallization

Crystallization takes place by formation of stable nuclei and subsequent growth of these nuclei: the so-called nucleation and growth mechanism. An equation widely used to describe the kinetics of isothermal growth is the Avrami equation [4]:

$$X = 1 - \exp(-a \cdot t^n) \quad (1)$$

where X is the degree of conversion, a is the growth constant, t is the time and n is the Avrami exponent. In the early stage of crystallization when the degree of conversion is small we can write:

$$X = a \cdot t^n \quad \text{or} \quad (2a)$$

$$V_n = b \cdot t^n \quad (2b)$$

where V_n is the volume of a nucleus which was formed at time $t=0$ and b is the growth constant of the nucleus. If all nuclei are formed at $t=0$ and if their number remains constant during the growth period, the value of the Avrami exponent is determined by the mechanism of growth and the shape of the nuclei. In the case of spherical nuclei, n has a value of $3/2$ for diffusion controlled growth and a value of 3 for interfacially controlled growth [5]. Generation of nuclei during the growth period will shift the apparent value of n in equation (2a) to higher values.

If crystallization is induced by a change in the stability conditions at time $t=0$, the number of nuclei at that moment will be zero. There is a transient period in which the steady state nucleus concentration is reached. A relation proposed to describe the nucleation frequency in this period is [6]

$$F_t = F \cdot \exp(-\tau/t) \quad (3)$$

where F_t is the nucleation frequency at time $t=t$ ($F_t = F$ at $t=\infty$) and τ is the time constant characteristic for the transient period. The time constant is related to the driving force for crystallization in the following way [5]:

$$\tau \propto \Delta G_v^{-4} \quad (4a)$$

or

$$\tau \propto (\ln(C_0/C_e))^{-4} \quad (4b)$$

where ΔG_v is the standard free energy of crystallization, C_0 is the solution concentration of the crystallizing component and C_e is the equilibrium or saturation concentration. Equation (4b) is derived from equation (4a) with the assumption that the activity coefficient is independent of the concentration. The driving force ΔG_v can also be expressed as the degree of undercooling:

$$\Delta G_V \propto (T_e - T) \quad \text{or} \quad \tau \propto (T_e - T)^{-4} \quad (5)$$

where T is the actual crystallization temperature and T_e is the equilibrium or melting temperature. In equation (5) the effect of the temperature on the diffusion, which plays a role in the nucleation frequency, is ignored. This implies that equation (5) will hold for limited temperature ranges only.

A simplification of the F_t -function of equation (3) is a step function in which the nucleation frequency jumps from zero to F at time $t=t'$. The volume of each nucleus at time t in that case is given by:

$$V_n = b \cdot (t-t')^n \quad (6)$$

It is obvious that the so-called induction time t' is related with the time constant τ . Equation (3) describes the transient period with a dimensionless time scale t/τ . We will therefore assume that t' is proportional to τ and thus that:

$$t' \propto (\ln(C_0/C_e))^{-4} \quad (7a)$$

or

$$t' \propto (T_e - T)^{-4} \quad (7b)$$

Light scattering

The light scattering of nuclei with diameters small compared to the wavelength of the light is given by the equation of Rayleigh [7]:

$$I_\theta = \text{constant} \cdot I_0 \cdot \left(\frac{n_n^2 - n_o^2}{n_o^2} \right)^2 \cdot V_n^2 \cdot N_n \cdot (1 + \cos^2 \theta) \quad (8)$$

where I_θ is the intensity of the light scattered at an angle θ , I_0 is the intensity of the incident light, n_n and n_o are the refractive index of respectively the nucleus and the surrounding medium, and N_n is the number of nuclei per unit volume.

If we restrict the analysis to the early stage of crystallization, i.e. the nuclei are assumed to be small and to exhibit Rayleigh scattering, combination of the equations (6) and (8) gives:

$$I_\theta = K \cdot (t-t')^{2 \cdot n} \quad (9)$$

where K is the growth or rate constant. The intensity versus time curves are in this way characterized by the exponent n (the mechanism of growth), the induction time t' (formation of stable nuclei) and the growth constant K (determined by the growth rate and the number of nuclei):

EXPERIMENTS

Materials

PPO was kindly supplied by General Electric Plastics, Bergen op Zoom, The Netherlands. The sample is characterized by $M_n = 21,000$ and $M_w = 44,000$ (measured by High Performance Liquid Chromatography). The solvents and non-solvents used are of reagent grade and were used without further purification.

Cloud points

Cloud points were measured using a method described earlier [8]. The location of the demixing gap was determined

at a temperature of 25 °C in pseudo-ternary systems with fixed ratios of OcoH and MeOH.

Differential Scanning Calorimetry

Appropriate amounts of PPO and of the nonsolvent/solvent mixture were weighed in aluminium sample pans and the pans were sealed. The solutions were homogenized at a temperature of 90 °C for at least two days. Only sample pans which showed no loss of weight during that period were used in the experiments. The DSC employed is a Perkin Elmer DSC 2 apparatus.

Pulse Induced Critical Scattering

This method has been developed by Gordon and coworkers [9,10] to investigate spinodal or critical demixing in polymer solutions. The experimental setup is also suited to investigate crystallization kinetics in its early stage after a sudden change in temperature, as was demonstrated by Koenhen [11]. The experiments are carried out in the following way.

A polymer mixture is brought into a very thin capillary glass tube with an inner and outer diameter of respectively 1.0 and 1.5 mm. The tube is sealed and its content is homogenized at an elevated temperature (90 °C normally). The tube is brought into a thermostate bath (25 °C normally) by means of a stepper motor and is thereby positioned exactly in a laser beam, see Figure 3. The formation of crystalline entities in the polymer solution causes scattering of the laser light and the scattering intensity at an angle of 30° is measured in time. Temperature control, the initiation of the stepper motor, the storage and the analysis of the

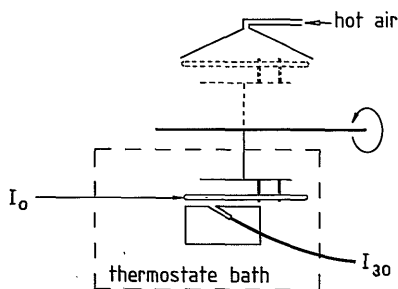


FIGURE 3. PICS apparatus.

The capillary tube is attached to a stepper motor axis and is moved at time $t=0$ from the 'up' position (hot air heating) to the 'down' position (thermostat bath). The scattered light is guided through an optical fiber to a light sensitive diode outside the bath.

intensity data are performed with the help of a microcomputer.

Membranes

Membranes were prepared by casting a solution on a glass plate and then by immersing this film in a coagulation bath containing methanol. The top surface of the membranes (the bath/film interface) is examined with a Jeol JSM 35CF scanning electron microscope after washing with water and air drying of the membranes.

RESULTS AND DISCUSSION

Crystallinity of PPO as received

Figure 4 displays the DSC thermogram upon heating of the PPO polymer as received (run I) and the DSC thermogram

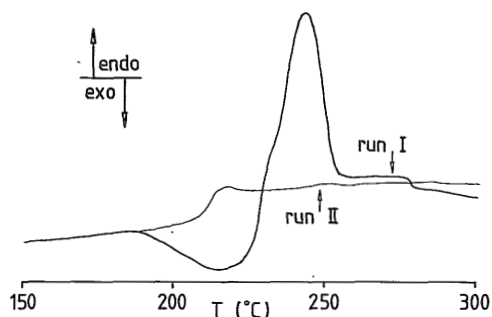


FIGURE 4. DSC thermogram of the PPO as received (run I) and upon reheating (run II). Heating range: 20 °C per minute.

upon reheating (run II). Run I shows a broad melting peak with a maximum at 245 °C, which is preceded by an exotherm at 220 °C. The exotherm is believed to be a recrystallization phenomenon. The sample is cooled rapidly from 300 °C to 50 °C and is then reheated again. Run II exhibits no endotherm or exotherm, but only a glass transition at 220 °C. This implies that this time the sample is completely amorphous and the same observation is made if the cooling rate is slow. These results are in agreement with the findings of Karasz and O'Reilly [12], although they did not detect such a pronounced recrystallization effect. From these experiments we conclude that PPO a.r. is partly crystalline but does not crystallize easily from the melt.

Phase diagram

The cloud point compositions at a temperature of 25 °C have been determined for five different ratios of OcoH and MeOH, see Figure 5. The rate of cooling in the turbidity experiments was 1 °C per 10 minutes. It is clear that MeOH

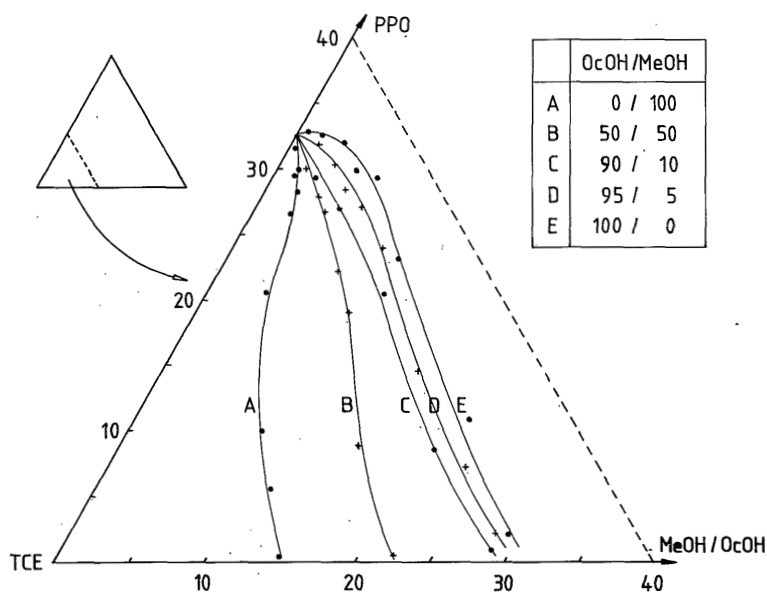


FIGURE 5. Cloud point compositions at 25 °C for five pseudo-ternary systems.

is a stronger nonsolvent for PPO than OcOH. Cloud point measurements usually yield the location of the liquid-liquid demixing gap in the phase diagram. However, in the binary PPO/TCE system no liquid-liquid demixing but crystallization takes place, so the phase boundaries displayed in Figure 5 are of a miscellaneous nature. It is expected that crystallization is responsible for the boundaries at high PPO concentrations and liquid-liquid demixing for the boundaries at high nonsolvent concentrations. The exact determination of the two regions is not possible as liquid-liquid demixing in this system is immediately followed by crystallization in the concentrated phase. This implies that *i*) all cloud point compositions display a crystallization exotherm upon cooling in DSC experiments, and that *ii*) separation of demixed systems into two liquid equilibrium

phases (a proof of liquid-liquid phase separation) is not possible.

To illustrate that at least at lower PPO concentrations liquid-liquid demixing occurs, the following experiment was conducted. Ternary solutions of PPO, TCE and OcOH were prepared and were cast on a glass plate and subsequently evaporated in a nitrogen atmosphere containing OcOH vapour. If it is assumed that in the first stage of evaporation only the TCE leaves the film (boiling points of TCE and OcOH being respectively 74°C and 194°C), we can evaluate the change in composition for each solution as is shown in Figure 6. After one day the films are completely dried in a vacuum stove and the structure of the surfaces is examined with the electron microscope, see Figure 7 for the micro-

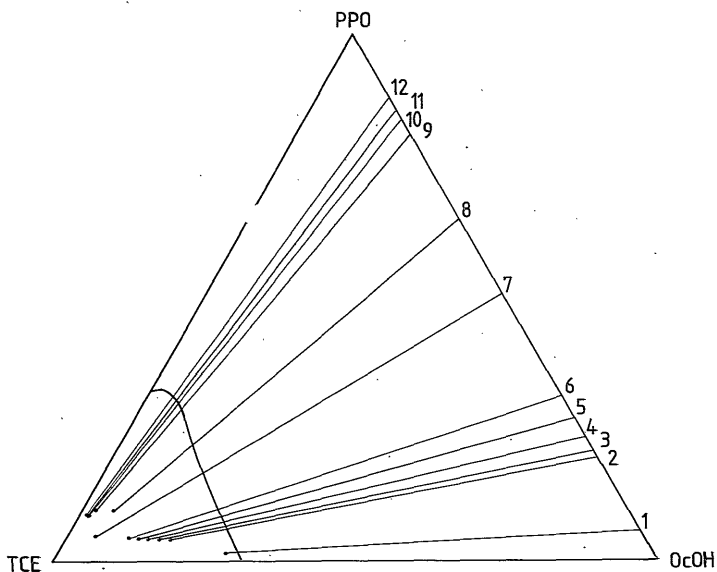


FIGURE 6. Initial compositions (●) of ternary casting solutions. The straight lines represent the change in composition if only TCE evaporates. The experiments are numbered 1 to 12, see also the text.

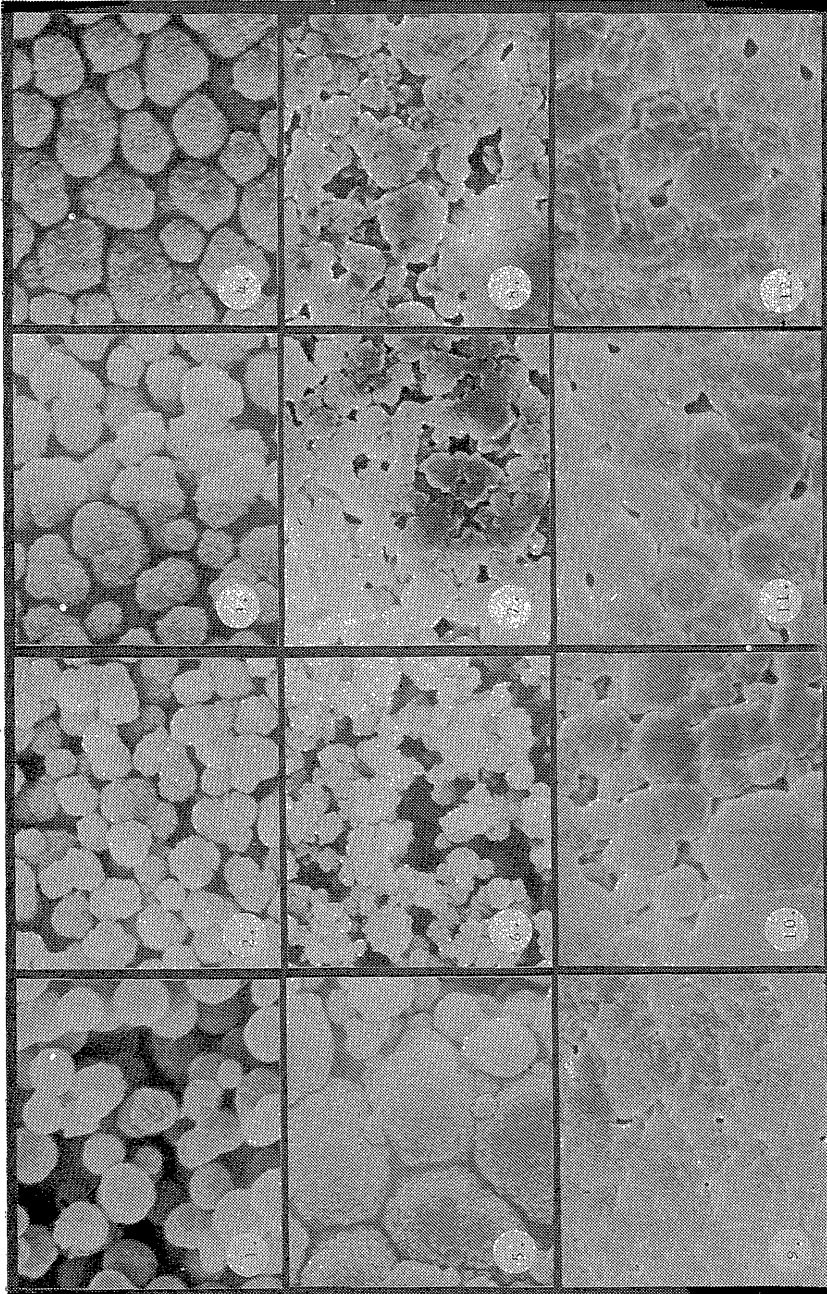


FIGURE 7. Micrographs of the top surface of PPO films. See for the preparation procedure the text. The numbers correlate with those of Figure 6.

graphs. Going from experiment no. 1 to no. 12 the PPO concentration at the moment the phase boundary is crossed, increases. We see that in the first four experiments liquid-liquid phase separation at the polymer poor side of the critical point has taken place (i.e. more or less densely packed solidified nuclei of the concentrated polymer phase). In experiment no. 6 the demixing has taken place on the polymer rich phase of the critical point, i.e. solidification of the concentrated polymer phase surrounding the nucleated dilute phase. Going from experiment no 6 to 12 the structure becomes denser although there is some variation. This result suggests that the critical point in this ternary system is at a PPO concentration of about 10%.

Kinetics of crystallization

The kinetics of crystallization at 25 °C has been investigated for eight different ratios of TCE, OcOH and MeOH, with PPO concentrations varying from 30% to 40%, see Table 1. The OcOH and MeOH content is kept low in order to avoid the possibility of liquid-liquid demixing in the samples. An example of a light scattering curve is given in Figure 8. The

TABLE 1

Compositions of TCE/OcOH/MeOH mixtures used in the PICS experiments. PPO concentrations vary from 30% to 40%.

	100/0/0	99/0/1	98/0/2
		98/1/1	
% OcOH ↓	98/2/0	97/2/1	96/2/2
	95/5/0		
	→ % MeOH		

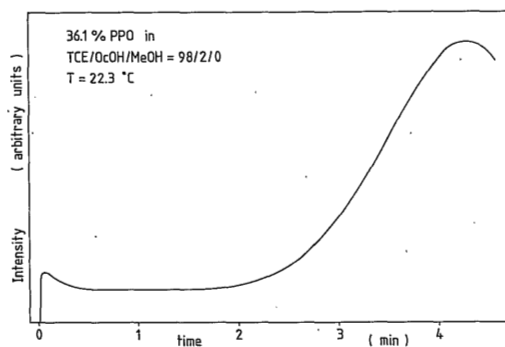


FIGURE 8. Intensity of scattered laser light (30° angle) as followed in time in a PICS experiment.

graph displays a distinct induction time before scattering is observed. The maximum in the curve is probably due to a change in the mode of scattering as the crystallization proceeds. The scattering intensity may decrease with increasing particle diameter if the diameter is large compared with the wave length of the light. If one uses equation (9) in the analysis of the scattering curves, one must be sure that the degree of conversion is low and that Rayleigh scattering occurs. To ascertain this, the point of inflexion in the I versus time curve is identified, and equation (9) is applied to the first part of the curve where I is less than one third of the intensity at the point of inflexion [11].

All intensity versus time plots were analyzed to obtain values for K , t' and n . The value of n is close to $3/2$ for all experiments, so the growth of the nuclei is diffusion controlled. The same observation was made by Koenhen [11] for crystallization in the system consisting of PPO and toluene. Setting n equal to $3/2$, the value of K and t' is computed using a least squares method. In each homologous series the growth constant increases and the induction

time decreases with increasing PPO concentration. This is expected as the driving force for crystallization increases with increasing PPO concentration. Using equation (7a) the induction time data yield information on the equilibrium (saturation) PPO concentration in each system at 25 °C. An example of a $t'^{-0.25}$ versus $\ln(C_0)$ plot is given in Figure 9 and the obtained values for C_e are listed in Table 2. The

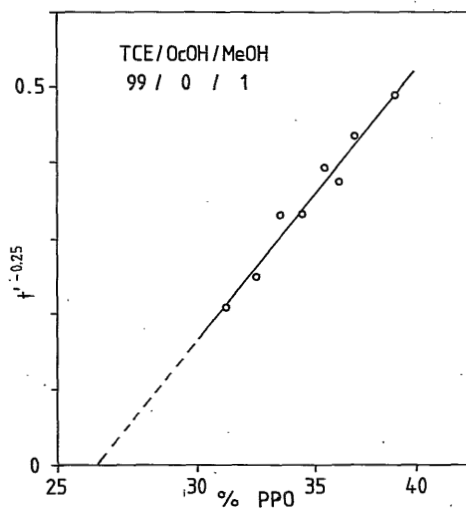


FIGURE 9. Induction time, t' (in seconds), as a function of the PPO concentration. $T = 25$ °C.

TABLE 2.

PPO saturation concentrations obtained from induction times (eq. (7a))

TCE/OcOH/MeOH	C_e (% PPO)	TCE/OcOH/MeOH	C_e (% PPO)
100/0/0	28.0 ± 2	95/5/0	26.5 ± 1.5
99/0/1	26.3 ± 0.3	98/1/1	26.0 ± 1
98/0/2	23.3 ± 0.5	97/2/1	25.3 ± 0.5
98/2/0	28.0 ± 2	96/2/2	22.4 ± 0.5

saturation concentrations are 4 to 5 percent lower than the cloud point compositions if the rate of cooling is 1 °C per 10 minutes. Agreement between C_e and the cloud point composition is reasonably well if the cooling rate is decreased to 1 °C per 24 hours.

In figures 10 and 11 the growth constant K and the induction time t' are plotted as a function of the percentage supersaturation, i.e. the actual PPO concentration minus C_e . In this way we correct for the change in equilibrium concentration and we are able to evaluate the effect of OcoH and MeOH on the kinetics of the PPO crystallization. The data are considerably scattered in the Figures 10 and 11, but it seems that no solvent/nonsolvent system deviates systematically from the others. Consequently it is concluded that no systematic effect of OcoH and/or MeOH on the nucleation and growth process of PPO crystallization is observed. The

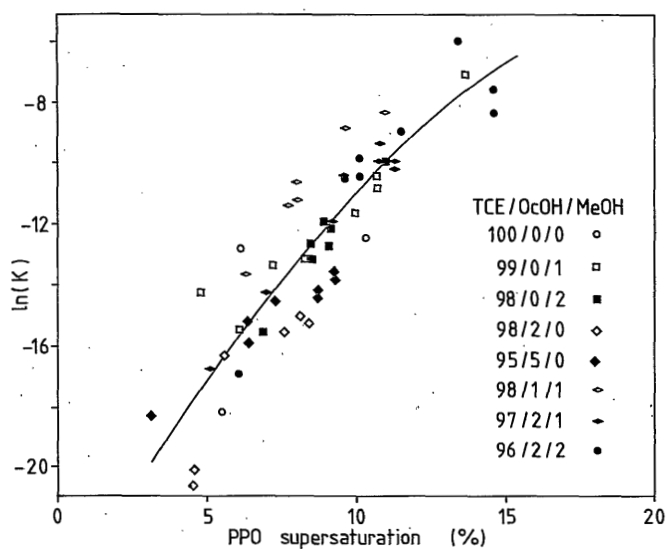


FIGURE 10. Growth constant, K (in arbitrary units), as a function of the PPO supersaturation, $(C_0 - C_e)$. $T = 25$ °C.

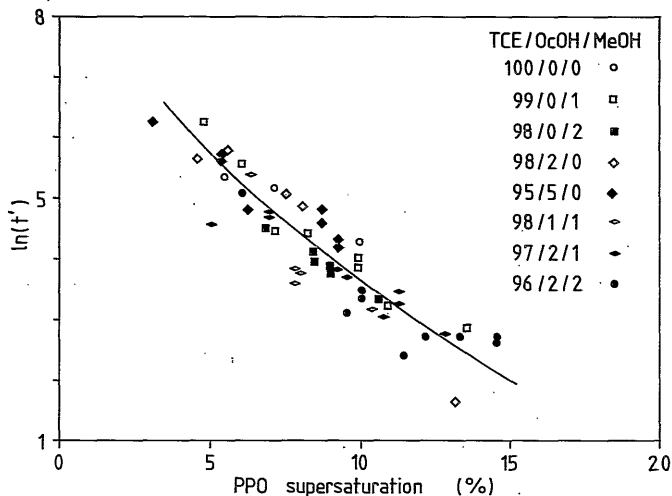


FIGURE 11. Induction time, t' (in seconds), as a function of the PPO supersaturation, $(C_0 - C_e)$. $T = 25^\circ\text{C}$.

growth constant K is determined by the rate of growth of the nuclei and the number of nuclei present per unit volume, see equations (8) and (9). To be able to distinguish these two quantities, one needs an independent method to determine the number of nuclei. Preliminary experiments with an optical microscope were not successful in this respect.

For two compositions the crystallization kinetics have been studied as a function of temperature. An increase in temperature will decrease the driving force for crystallization and thus will decrease K and increase t' . On the other hand the diffusion coefficient increases with increasing temperature and this favours both the nucleation and growth of the nuclei. The data displayed in Figure 12 show that the effect on the driving force is dominant: K and t' respectively decrease and increase with increasing temperature. The straight lines in the $t'^{-0.25}$ versus T plot are drawn according to equation (7b). Analysis of

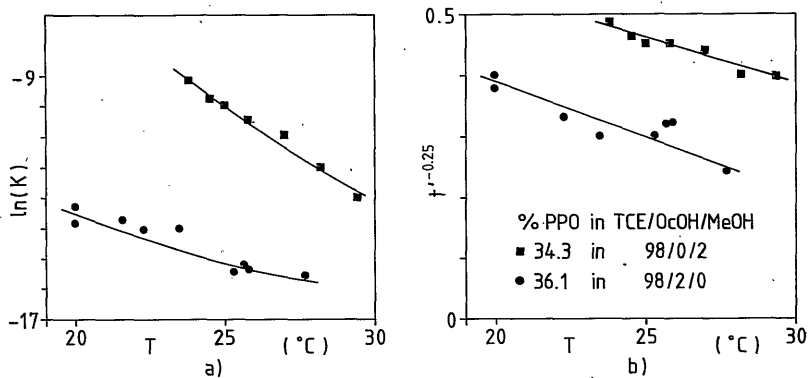


FIGURE 12. Growth constant K (a) and induction time t' (b) as a function of the crystallization temperature. t' is expressed in seconds.

data published previously by Koenhen [11] shows that the dependence of t' on T is very well described by equation (7b) (crystallization in PPO-toluene solutions).

PPO membranes

In previous work PPO membranes have been prepared by Broens *et al.* [3] and by Buys *et al.* [13] by immersing a PPO/TCE/OcOH film in a MeOH coagulation bath. At a constant polymer concentration of 10% the amount of OcOH in the casting solution is varied and the resulting membranes are examined on their ultrafiltration [3] and gas separation [13] properties. In the next section these results are discussed.

In addition to the experiments of Broens and Buys, we prepared membranes from casting solutions with a constant TCE/OcOH ratio of 78/22 and with varying PPO concentrations: 6, 8, 9 and 10%. The micrographs of the top surface of the membranes are shown in Figure 13. It is clear that

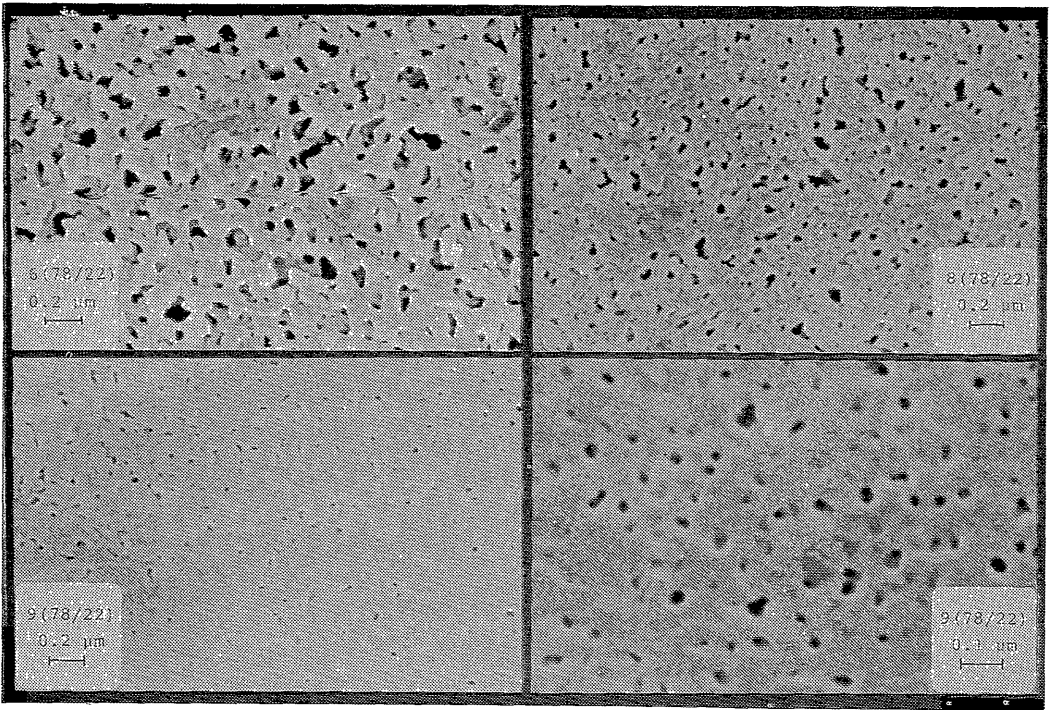


FIGURE 13. Micrographs of the top surface of PPO membranes. Code reveals composition of casting solution: %PPO(%TCE/%COH). Coagulation bath: MeOH.

the porosity of the top layer decreases if the PPO concentration increases and that the porous structure is the result of liquid-liquid demixing. At a PPO concentration of 10% no pores could be detected at a magnification of 100,000 times, indicating that the pore radius is smaller than 50 Angstroms.

PREPARATION AND PROPERTIES OF PPO MEMBRANES

The permeability data of the PPO membranes prepared by Broens [3] and by Buys [13] are summarized in Table 3. It

TABLE 3.

Permeation characteristics of PPO membranes. Casting solution: 10% PPO in OcoH/TCE. Coagulation bath: MeOH

% OcoH/%TCE	J_w^a (cm/hr)	$10^{+12} \cdot P_{O_2}^b$ (m^3/s)/($m^2 \cdot N/m^2$)	α_{O_2/N_2}^c
0/100	0		
5/95	0	10	4.0
10/90	0	20	2.9
15/85	0	270	1.8
18/82	< 0.5	> 10000	1.0
20/80	1-2		
22/78	5-25		

^a Steady state, pure water flux at a pressure difference of 3 atmospheres. Source: reference 3.

^b Oxygen permeability. Source: reference 13.

^c Selectivity for oxygen in oxygen/nitrogen separation. Source: reference 13.

is clear that an increase in initial OcoH content of the casting solution leads to membranes with a more open structure. For OcoH/TCE ratios lower than 18/82 the membranes have gas separation properties and no water flux is obtained under ultrafiltration conditions. The ideal or highest attainable O_2/N_2 separation factor with PPO membranes is about 5.0 [14], so the gas separation membranes are not completely tight: convective transport takes place through defects or very small pores. At a OcoH/TCE ratio equal to 18/82 the membrane becomes permeable to water and shows no selectivity in O_2/N_2 separation. Upon increasing the OcoH/TCE ratio to 22/78 the water permeability increases and since PPO is a hydrophobic polymer the transport of water must take place through distinct pores.

Broens [3] formulated a hypothesis in which the addition of OcoH favours the crystallization of the PPO and leads to a more open structure of gelled PPO layers. However, the results of the PICS experiments do not show a significant effect of OcoH on the crystallization kinetics. This

poses the question whether another mechanism can explain the drastic influence of OcOH on the membrane properties.

In Figure 14 the locations of the casting solution compositions are drawn in the ternary PPO/TCE/OcOH phase diagram. The points at the line of constant PPO concentration (10%) represent the casting solutions employed by Broens and Buys. An increase in OcOH content brings the composition nearer to the liquid-liquid demixing gap. In fact, a casting solution with OcOH/TCE ratio equal to 22/78 is thermodynamically unstable at 22 °C and this may account for the large variation in waterpermeability as reported by Broens [3] for the resulting membranes (cast at 'room temperature').

Upon immersing a casting solution in the MeOH bath, TCE and OcOH diffuse into the bath and the PPO concentration increases. The penetration of the MeOH into the film moves the liquid-liquid demixing boundary to the left in the phase diagram, as can be seen from Figure 5. As we deal with a quaternary system it is very difficult to visualize the coagulation by coagulation paths, but we think it is plausible that an increase in initial OcOH content favours

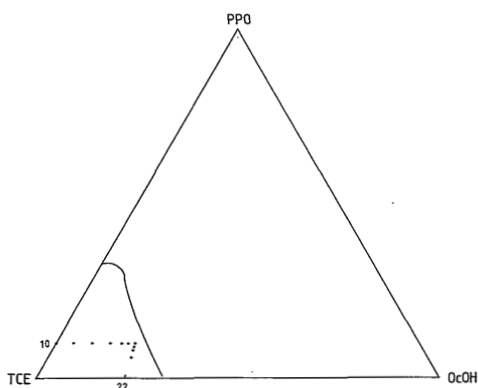


FIGURE 14. Composition of casting solutions drawn in the ternary PPO/TCE/OcOH phase diagram, see text.

the occurrence of liquid-liquid demixing in the film. Evaluating the permeability data of Table 3, we suggest that for initial OcoH/TCE ratios upto 18/82 the top layer is a dense gelled layer of which the thickness decreases with increasing OcoH concentration. If the OcoH/TCE ratio is 18/82 or higher small pores are present in the top layer due to liquid-liquid demixing and the pore radius probably increases with increasing OcoH concentration. The micrographs of Figure 13 support the hypothesis of liquid-liquid demixing in the top layer if the OcoH concentration is high.

A question not yet addressed is whether crystallization plays a role in the formation of PPO membranes. It is clear that gelation in PPO systems is accompanied and probably induced by crystallization. However, the increase in PPO concentration in especially the top layer is so rapid that the crystalline entities are probably not larger than the size of a stable nucleus: a dried PPO ultrafiltration membrane shows no or a very small melting peak upon heating in a DSC experiment. In the case of homogeneous PPO membranes the interplay of precipitation rate and crystallization kinetics determined the mechanical stability of the film. A solution of 10% PPO in TCE cast with a thickness of 0.1 mm yields upon evaporation of the TCE a film with excellent mechanical properties: flexible and strong. If the evaporation rate is slowed down or if the casting thickness is increased the film becomes stiff and brittle due to a higher degree of crystallinity.

REFERENCES

- [1] C.A. Smolders, in "Ultrafiltration Membranes and Applications", A.R. Cooper. ed., Plenum Press, New York, 1980.
- [2] J.G. Wijmans and C.A. Smolders, Chapter 2 of this

thesis.

- [3] L. Broens, D.M. Koenhen and C.A. Smolders, *Desalination*, 22 (1977) 205.
- [4] M. Avrami, *J. Chem. Phys.*, 7 (1939) 1103; 8 (1940) 212; 9 (1941) 177.
- [5] D. Turnbull, *Solid State Physics*, Vol. 3, Academic Press, New York, 1956.
- [6] J.B. Zeldovich, *Acta Physicochem. USSR*, 1 (1943) 1.
- [7] G. Oster, *J. Colloid Sci.*, B9 (1974) 435.
- [8] J.G. Wijmans, J. Kant and C.A. Smolders, Chapter 3 of this thesis.
- [9] M. Gordon, J. Goldsbrough and J.W. Kennedy, *J. Polym. Sci. Polym. Symp.*, 61 (1977) 199.
- [10] K. Derham, J. Goldsbrough and M. Gordon, *Pure Appl. Chem.*, 38 (1974) 97.
- [11] D.M. Koenhen, C.A. Smolders and M. Gordon, *J. Polym. Sci. Polym. Symp.*, 93 (1978) 61.
- [12] F.E. Karasz and J.M. O'Reilly, *Polym. Lett.*, 3 (1965) 561.
- [13] H.C.W.M. Buys, A.E. Jansen, H.F. van Wijk, D. Bargeman and C.A. Smolders, paper presented at the Third Symposium on Synthetic Membranes in Science and Industry, Tübingen, 1981.
- [14] W. Pusch and A. Walch, *Angew. Chem.*, 21 (1982) 660.

THE MECHANISM OF FORMATION OF MICROPOROUS OR SKINNED MEMBRANES PRODUCED BY THE IMMERSION PRECIPITATION PROCESS

J.G. Wijmans, J.P.B. Baaij and C.A. Smolders

SUMMARY

Cellulose acetate and polysulfone casting solutions were coagulated in water/solvent mixtures with differing solvent content. Precipitation in pure water yielded skinned membranes. Precipitation in water/solvent mixtures with solvent concentration exceeding a certain minimum value (which is different for different systems) resulted in microporous membranes. This phenomenon has been explained in terms of the model description for the formation of asymmetric membranes as adopted in our laboratory. In this model, the skin formation is related to gelation and the formation of the porous substructure to liquid-liquid phase separation.

It is made plausible that the addition of solvent to the coagulation bath favours nonsolvent inflow and hence liquid-liquid demixing in the precipitating film.

This chapter has been published in *J. Membrane Sci.*, 14 (1983) 263.

INTRODUCTION

The majority of commercially available synthetic membranes are produced by the so-called phase inversion process. In this process, a homogeneous polymer solution is brought to phase separation by means of a penetrating nonsolvent and/or a solvent outflow.

The concept "phase inversion process" covers a range of different techniques, each leading to a specific membrane structure. The two techniques that will be discussed in this paper are (i) precipitation from the vapour phase, and (ii) immersion precipitation. Precipitation from the vapour phase yields symmetric microporous membranes whereas the immersion precipitation process usually results in asymmetric ultra- or hyperfiltration membranes. These membranes are called asymmetric since their cross-section reveals an asymmetric structure: a very dense and thin skin supported by a porous sublayer.

Recently it was discovered in our laboratory [1] that with immersion precipitation it is also possible to obtain microporous membranes; to achieve this, solvent was added to the coagulation bath. This is a very interesting phenomenon since knowledge about ways to avoid the formation of a skin may lead to a better understanding of skin formation.

Examples of this type of membrane formation for various polymers will be given and discussed in terms of the formation mechanism, especially considering how the addition of solvent to the coagulation bath prevents skin formation.

THEORY

Phase separation

Several authors have tried to explain the formation of asymmetric membranes in terms of phase separation phenomena in polymer solutions [2-9]. In recent years, experimental evidence was gathered in our laboratory [6,7,10, 11] that two different types of phase separation phenomena are responsible for the asymmetric structure of the membranes.

In a system consisting of a polymer, a solvent and a nonsolvent, the demixing types that can be distinguished are (see Fig. 1):

(i) Liquid-liquid phase separation:

The solution lowers its free enthalpy by separating into two liquid equilibrium phases. There are two ways for this demixing to occur: by nucleation and growth of droplets of the second phase and by instantaneous spinodal demixing. The spinodal demixing gap is surrounded by the composition area where phase separation by nucleation and growth takes place; since this latter phenomenon is a relatively fast process, spinodal demixing is not very probable in polymer solutions.

(ii) Crystallization or gelation:

The polymer molecules decrease the free enthalpy of the solution by forming ordered structures. At low polymer concentrations single crystals will be formed, but at higher concentrations the usually very small crystalline regions can act as physical crosslinks between the polymer molecules and the result is a thermoreversible gel.

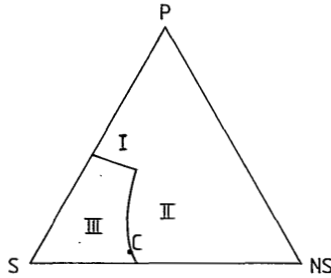


Fig. 1. Ternary phase diagram; P: polymer; S: solvent; NS: nonsolvent; C: critical point; I: gelation; II: liquid-liquid phase separation; III: homogeneous solution.

Mechanism of formation

In the immersion precipitation process a polymer solution, cast on a support, is immersed in a bath containing a nonsolvent. As was first suggested by Koenhen [6], we assume that the skin is formed by gelation and that the porous sublayer is the result of liquid-liquid phase separation by nucleation and growth. The factor determining the type of phase separation at any point in the cast film is the local polymer concentration at the moment of precipitation. In the first split second after immersion there is a rapid depletion of solvent from the film and a relatively small penetration of nonsolvent. This means that the polymer concentration at the film/bath interface increases and that the gel boundary is crossed (transition III to I in Fig. 1). The thin and dense gel-layer that is formed in this way, the skin, will act as a resistance to solvent outdiffusion, and at positions beneath the toplayer, demixing will occur at lower polymer and higher nonsolvent concentrations. So here the type of demixing will be liquid-liquid phase separation (transition III to II in Fig. 1). The demixing gap is entered at the polymer-rich side of the critical point, so the nuclei consist of the polymer-poor phase, and the result is a

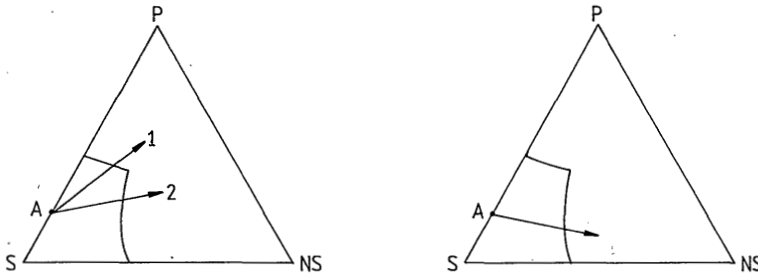


Fig. 2. Schematic course of composition for skinlayer (1) and bottom-layer (2) of a polymer film with initial composition A upon immersing into a nonsolvent bath.

Fig. 3. Coagulation path of a polymer film with initial composition A when brought in contact with a nonsolvent vapour phase saturated with solvent.

porous structure, the pores of which are filled with the dilute solvent/nonsolvent phase.

The approximate changes of composition for the toplayer and the substructure, the so-called "coagulation paths", are given in Fig. 2. A more detailed description of the concentration profiles in a precipitating casting solution can be found in the paper by Bokhorst et al. [9].

In the case of precipitation from the vapour phase, the cast polymer solution is in contact with a nonsolvent vapour phase, saturated with the solvent used. In this process there is no solvent outflow but only a nonsolvent inflow. The change of composition in the film is illustrated in Fig. 3: the only possible demixing mechanism is liquid-liquid phase separation and the result is a microporous membrane without a skin.

From the model description presented here, we can infer that the direction of the coagulation path and thus the ratio of the nonsolvent inflow and solvent outflow is of the utmost importance for the resulting membrane structure.

EXPERIMENTAL

For membrane preparation the polymer solutions were handcast (0.15 mm) on a glass plate and immersed in a non-solvent bath containing different amounts of solvent. The temperature of the coagulation bath was about 23°C. After 30 minutes in this first bath, the membranes were transferred to a pure water bath. The structure of the membranes was studied with aid of a Jeol JSM U3 electron microscope. Micrographs were taken from the topside, the bottomside and the cross-section of the membrane. The top-layers of the membranes were examined for the presence of pores. The membranes were considered to be microporous if, at a magnification of 3000 times, pores could be detected in the toplayer (i.e. pore radius > 0.1 μm).

The membranes were made from a variety of polymer/solvent/nonsolvent systems. The nonsolvent used was water in all cases (demineralized and ultrafiltrated). The polymer-solvent pairs are listed in Table 1. The solvents were of reagent grade and were used without further purification; the cellulose acetate (CA) was obtained from Eastman Kodak (E 398-3) and the polysulfone (PSf) was the P 3500 type from Union Carbide. The polyvinylpyrrolidone (PVP), used as an additive to the PSf solutions, had a molecular weight of 360,000 dalton and was purchased from Fluka AG.

TABLE 1

Polymer-solvent pairs used in the experiments

Polymer	Solvent	Polymer	Solvent
CA	DMSO	PSf	DMAc
CA	DMAc	PSf	NMP
CA	dioxane		
CA	acetone		

RESULTS AND DISCUSSION

Microporous membranes obtained by immersion precipitation

The addition of solvent to the coagulation bath slows down the rate of precipitation: it takes more time before the cast film becomes turbid. The same observations have been made by Strathmann [12]. At too high solvent concentrations, precipitation does not take place and the polymer slowly dissolves in the coagulation bath.

In all cases which we studied, see Table 1, it appears that it is possible to produce microporous membranes by adding solvent to the coagulation bath, each system having its own minimum solvent concentration (see Table 2) required for a porous toplayer. In Fig. 4 micrographs of porous structures in the toplayer are given.

It seems that this method to obtain microporous membranes can be applied to every membrane-forming ternary system. For instance, we also know from preliminary experiments in our laboratory that the systems polyvinylidene-fluoride/*N*-methylpyrrolidone/water and poly-2,6-dimethyl-1,4-phenyleneoxide/trichloroethylene/methanol yield a microporous structure if sufficient solvent is added to the coagulation bath. Further, it is interesting to focus the attention on the paper published by Strathmann [12]; on the Nomex/DMAc/water system, and to look at the micrographs on p.199 and the figure that displays the 'time to turbidity' as a function of the DMAc content of the coagulation bath on p. 191. In our opinion the membrane precipitated in a bath containing 75% DMAc could very well be a microporous one.

TABLE 2

Minimum solvent concentrations (% by wt.) in the coagulation bath, if microporous toplayers are desired.

Casting solution			Minimum solvent content (%) in coagulation bath	% Nonsolvent at liquid-liquid boundary in phase diagram ^a
Polymer	Solvent	Pol.(%)		
PSf	DMAc	15	80	4
PSf	NMP	15	65	9
CA	DMSO	15	60	13
CA	DMAc	20	55	15
CA	dioxane	20	40	30
CA	acetone	20	30	28

^aObtained from turbidity measurements

Figure 4 shows the effect of an increasing solvent concentration on the toplayer of the membranes made from a casting solution of CA in dioxane. The radius of the pores gradually increases from 0.2 μm to 1 μm when the solvent content increases from 30 to 50% by weight.

A well known method to increase the pore radii in the porous substructure of a polysulfone asymmetric membrane is to add a high molecular weight component to the casting solution [13]. Figure 5 shows the topsurface and the bottomsurface of a membrane precipitated from a PSf/PVP/DMAc casting solution in a mixture of 11% by weight of water in DMAc. Upon increasing the water content to 16%, the pores in both the topsurface and bottomsurface become smaller, especially in the toplayer. From these micrographs it can be seen (Table 3) that the microporous membranes have a gradient in pore radius: the pores in the toplayer are smaller than the pores in the bottomlayer.

Furthermore, it appears that changing the solvent concentration in the bath has a greater influence on the pore size in the toplayer compared to the bottomlayer. This means that with aid of two variables, i.e. the solvent

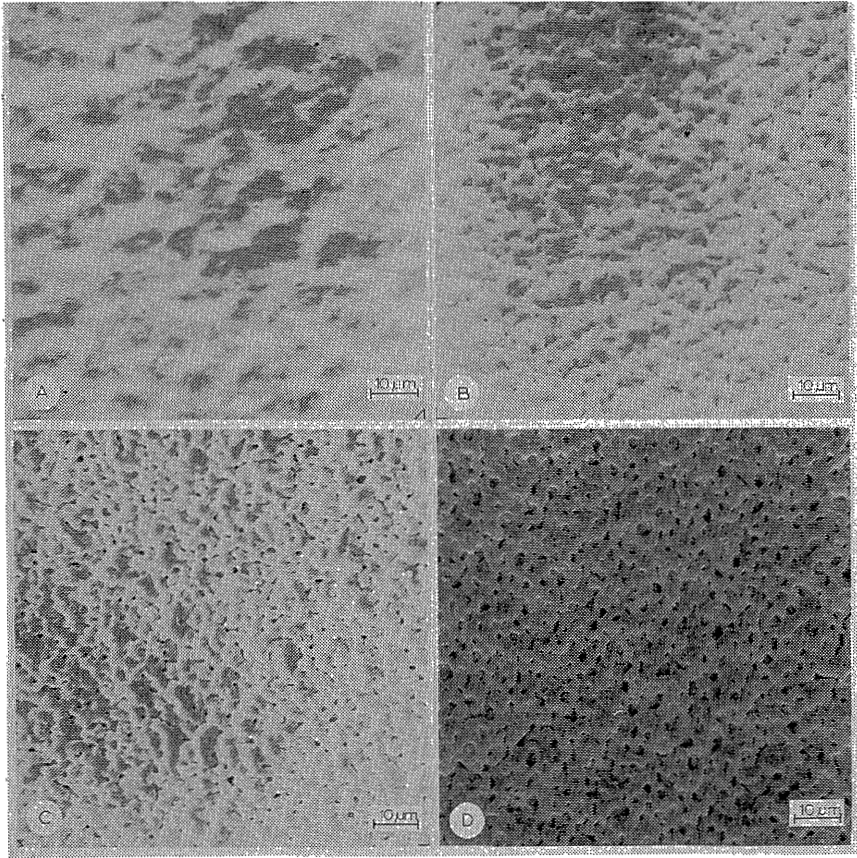


Fig. 4. Micrographs of topsurface of membranes precipitated from a casting solution of 20% by wt. CA in dioxane in a water/dioxane coagulation bath, containing (a): 30%, (b): 40%, (c): 45%, and (d): 50% dioxane.

TABLE 3

Pore radii of microporous PSf membranes (see micrographs, Fig. 5)

Water' (% by wt.) in water/DMAc coagulation bath	Topsurface (μm)	Bottomsurface (μm)
11	8	10
16	0.1	6

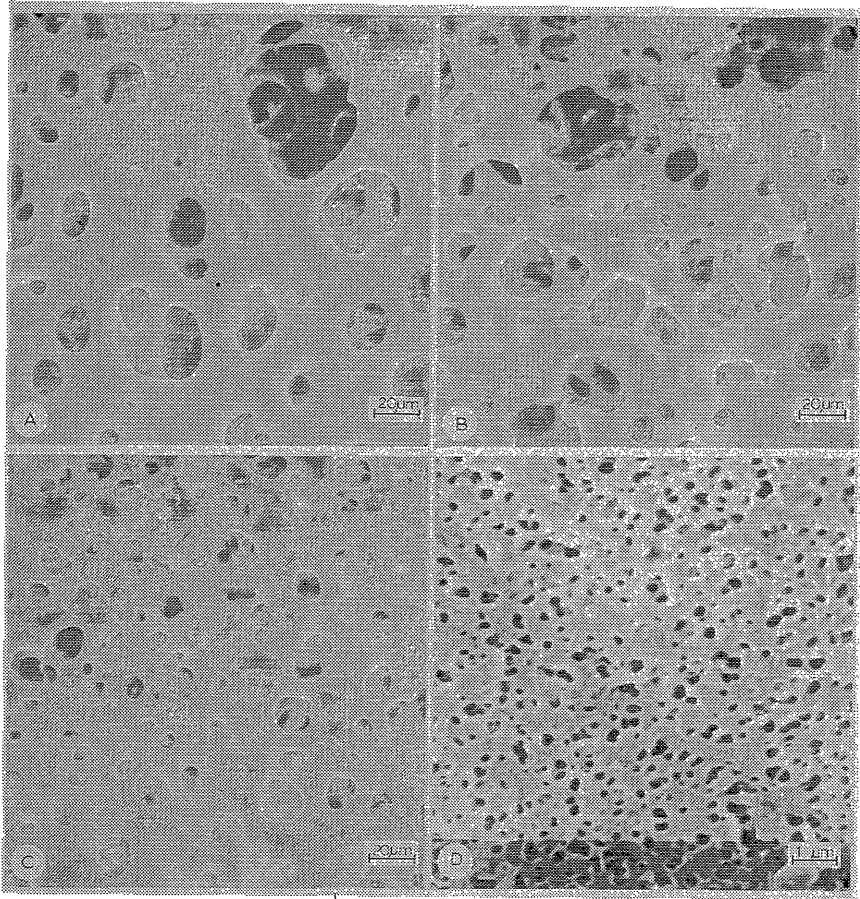


Fig. 5. Micrographs of membranes precipitated from a PSf/PVP/DMAc casting solution (13/12/75% by wt.) in a water/DMAc coagulation bath containing 11% (a + b) and 16% (c + d) water. a + c: bottom surface (glass side). b + d: topsurface (bath side).

concentration of the bath and the composition of the casting solution, microporous membranes with almost every combination of average pore radius and pore radius gradient can be obtained.

In this way it should be possible to make microporous films that can be used in microfiltration and in biomedical applications.

The mechanism of formation

The interesting question is how the addition of solvent to the coagulation bath prevents the formation of a skin. To answer this, we will restrict ourselves to the ternary system.

As appeared from the model for the mechanism of formation given in the theoretical section, the ratio of solvent outflow to nonsolvent inflow is important for skin formation. We calculated the difference of chemical potential at the film/bath interface for solvent and nonsolvent as a function of solvent content in the coagulation bath (see Fig. 6). For the chemical potentials, the Flory-Huggins [14] expressions for a ternary system were used:

$$\begin{aligned} \frac{\Delta\mu_1}{RT} &= \ln v_1 + v_2 \left(1 - \frac{v_1}{v_2}\right) + g_{12}v_2^2 - v_2^2v_1g'_{12} - \left[\ln \phi_1 - \frac{v_1}{v_2} \phi_2 \right. \\ &\quad \left. - \frac{v_1}{v_3} \phi_3 + (1 - \phi_1) (1 + g_{12}\phi_2 + g_{13}\phi_3) - \frac{v_1}{v_2} g_{23}\phi_2\phi_3 - \phi_1 u_2^2 g'_{12} \right] \\ \frac{\Delta\mu_2}{RT} &= \ln v_2 + v_1 \left(1 - \frac{v_2}{v_1}\right) + \frac{v_2}{v_1} g_{12}v_1^2 + v_1^2v_2g'_{12} - \left[\ln \phi_2 - \frac{v_2}{v_1} \phi_1 \right. \\ &\quad \left. - \frac{v_2}{v_3} \phi_3 + (1 - \phi_2) \left(1 + \frac{v_2}{v_1} g_{12}\phi_2 + g_{23}\phi_3\right) - \frac{v_2}{v_1} \phi_1\phi_3g_{13} + \frac{v_2}{v_1} \phi_1 u_1 u_2 g'_{12} \right] \\ g'_{12} &= \frac{\partial g_{12}}{\partial u_2} = \frac{\partial g_{12}}{\partial u_2} \\ u_2 &= \phi_2 / (\phi_1 + \phi_2) \\ u_1 &= \phi_1 / (\phi_1 + \phi_2) \end{aligned} \quad (1)$$

The subscripts refer to the nonsolvent (1), the solvent (2) and the polymer (3). $\Delta\mu_i$, ϕ_i , v_i , and v_i are the chemical potential difference over the interface, the volume frac-

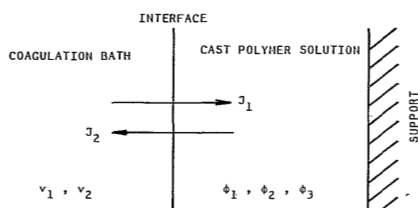


Fig. 6. Fluxes of nonsolvent (J_1) and solvent (J_2), respectively, at the interface of coagulation bath and cast polymer film.

tion in the casting solution, the volume fraction in the coagulation bath and the molar volume of component i respectively. R is the gas constant and T is the temperature in Kelvin. The g_{ij} parameter is the interaction parameter between components i and j ; g_{12} is assumed to be a function of $u_2 = \phi_2 / (\phi_1 + \phi_2)$ in the notation of Zivny and Pouchly [15]. Only binary interaction parameters are considered.

The interaction parameters, characteristic for the three ternary systems for which calculations have been made, are listed in Table 4 and are taken from Altena [16].

TABLE 4

Interaction parameters

Non-solvent (1)	Solvent (2)	Polymer (3)	g_{13}	g_{23}	g_{12}	$= \frac{atbu_2 + cu_2^2 + du_2^3 + eu_2^4}{a \quad b \quad c \quad d \quad e}$				
						a	b	c	d	e
water	dioxane	CA	1.4	0.4	0.92	-0.69	7.15	-12.91	8.17	
water	DMF	CA	1.4	0.4	0.50	0.04	0.8	-1.2	0.82	
water	DMF	PSf	3.7	0.4	0.50	0.04	0.8	-1.2	0.82	

From Fig. 7 it appears that the ratio of chemical po-

tential difference of the nonsolvent and the solvent increases upon increasing the solvent concentration in the bath. The composition taken for the casting solution is 20% by weight of polymer, 79.99% of solvent and 0.01% of nonsolvent. We have to assume that some nonsolvent is present in the casting solution, otherwise the calculated chemical potential difference will become infinite (see eqn. (1)). Since the nonsolvent concentration is very small, the calculated ratio is characteristic for the first moment of the coagulation process, i.e. the formation of the toplayer. The absolute values of $\Delta\mu_i$ in the various systems differ, but the ratio of $\Delta\mu_1/\Delta\mu_2$ appears to be the same. The chemical potential difference $\Delta\mu_i$, is the driving force for the mass transport through the film/bath interface J_i , as can be seen from the simplified phenomenological relation (cross terms neglected):

$$J_i = L_i(\phi_i, v_i)\Delta\mu_i \quad (2)$$

where L_i is the permeability coefficient of component i , which may be a function of ϕ_i and v_i . If we disregard the influence of L_i (on which no data are available), then the outcome of the calculation on $\Delta\mu_1/\Delta\mu_2$ (see Fig. 7) indicates that the nonsolvent inflow increases relatively to the solvent outflow if the solvent content of the bath is increased. Or, in other words, the nonsolvent inflow decreases less rapidly compared to the decreasing solvent outflow, as it is obvious that mass transfer is reduced by adding solvent to the bath.

In our opinion this means that conditions are created such that demixing in the toplayer will take place at lower polymer concentrations and at higher nonsolvent concentrations. As a consequence, at a certain solvent concentration in the bath, liquid-liquid phase separation will be possible in the toplayer, and the result is a toplayer with pores.

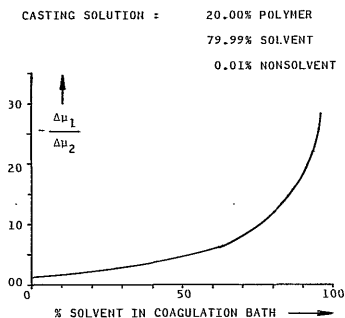


Fig. 7. The ratio $-\Delta\mu_1/\Delta\mu_2$ as a function of solvent concentration by weight in the coagulation bath; calculated for the systems CA/dioxane/water, CA/DMF/water and PSF/DMF/water.

In Table 2, experimental data on some microporous membranes are gathered. In the last column, the ternary systems are characterized by the approximate water concentrations needed for liquid-liquid phase separation. It appears that systems for which a small amount of water is enough to bring about liquid-liquid phase separation need a high solvent concentration in the bath (see column 4 of Table 2) if microporous membranes are desired. At first sight this result may seem strange since it should be easy in such systems to reach the liquid-liquid demixing gap, as is illustrated in Fig. 8. However, it is known that the systems which are sensitive to water show a rapid coagulation with a high solvent outflow [17]. Apparently a high solvent concentration in the bath is needed in those cases to decrease the solvent outflow to a sufficiently low value in order to prevent skin formation.

To give a quantitative explanation, one needs data on solvent outflow and nonsolvent inflow during coagulation for the different systems. Research on this subject is being carried out in our laboratory; the results will be pub-

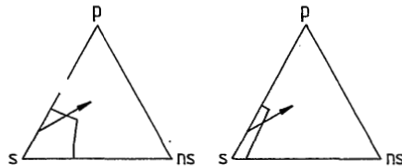


Fig. 8. Influence of the position of the liquid-liquid demixing gap on the type of phase separation at a fixed coagulation path.

lished in the future.

CONCLUSIONS

Casting solutions, which immersed in pure nonsolvent give asymmetric ultra- or hyperfiltration membranes, will yield microporous membranes if sufficient solvent is added to the coagulation bath.

This phenomenon can be explained with the aid of the mechanism of formation of asymmetric membranes which has been put forward in our laboratory. This model predicts that the relative magnitude of nonsolvent inflow and solvent outflow during the coagulation process has a strong influence on the ultimate membrane structure.

ACKNOWLEDGEMENT

The authors thank F.W. Altena for the enlightening discussions on the subject.

A part of this work was made possible by a grant from the Ministerie van Economische Zaken of The Netherlands to a co-operative research project in which Wafilin B.V. and the Twente University of Technology participated. The authors wish to thank Wafilin B.V. for their permis-

sion to publish these results.

REFERENCES

- [1] J.P.B. Baaij, patent applied for by Wafilin B.V., Hardenberg, The Netherlands (1981).
- [2] M.A. Frommer, I. Feiner, O. Kedem and R. Bloch, The mechanism for formation of "skinned" membranes, II. Equilibrium properties and osmotic flows determining membrane structure, *Desalination*, 7 (1970) 393.
- [3] H. Strathmann, P. Scheible and R.W. Baker, A rationale for the preparation of Loeb-Sourirajan cellulose acetate membranes, *J. Appl. Polym. Sci.*, 15 (1971) 811.
- [4] H. Strathmann and K. Kock, The formation mechanism of phase-inversion membranes, *Desalination*, 21 (1977) 241.
- [5] M. Guillotin, C. Lemoyne, C. Noel and L. Monnerie, Physicochemical processes occurring during the formation of cellulose diacetate membranes. Research of criteria for optimizing membrane performance. IV. Cellulose diacetate-acetone organic additive casting solutions, *Desalination*, 21 (1977) 165.
- [6] D.M. Koenhen, M.H.V. Mulder and C.A. Smolders, Phase separation phenomena during the formation of asymmetric membranes, *J. Appl. Polym. Sci.*, 21 (1977) 199.
- [7] L. Broens, D.M. Koenhen and C.A. Smolders, On the formation mechanism of asymmetric ultra- and hyper-filtration membranes, *Desalination*, 22 (1977) 205.
- [8] C. Cohen, G.B. Tanny and S. Prager, Diffusion-controlled formation of porous structures in ternary polymer systems, *J. Polym. Sci.*, A-2, 17 (1979) 477.
- [9] H. Bokhorst, F.W. Altena and C.A. Smolders, Formation of asymmetric cellulose acetate membranes,

- Desalination, 38 (1981) 349.
- [10] L. Broens, F.W. Altena, C.A. Smolders and D.M. Koehem, Asymmetric membrane structure as a result of phase separation, *Desalination*, 32 (1980) 33.
- [11] F.W. Altena and C.A. Smolders, Phase separation phenomena in solutions of cellulose acetate, I. Scanning calorimetry of cellulose acetate in mixtures of dioxane and water, *J. Polym. Sci. Polym. Symp.*, 69 (1981) 1.
- [12] H. Strathmann, K. Kock, P. Amar and R.W. Baker, The formation mechanism of asymmetric membranes, *Desalination*, 16 (1975) 179.
- [13] I. Cabasso, E. Klein and J.K. Smith, Polysulfone hollow fibers. II. Morphology, *J. Appl. Polym. Sci.*, 21 (1977) 165.
- [14] P.J. Flory, Principles of Polymer Chemistry, Cornell Univ. Press, New York, 1953.
- [15] A. Živný and J. Pouchlý, Theoretical analysis of sorption of a binary solvent in a polymer phase. I. Occurrence and character of inversion in preferential sorption, *J. Polym. Sci.*, A-2, 10 (1972) 1467.
- [16] F.W. Altena and C.A. Smolders, Calculation of liquid-liquid phase separation in a ternary system of a polymer in a mixture of a solvent and a nonsolvent, *Macromolecules*, 15 (1982) 1491.
- [17] M.A. Frommer and D. Lancet, The mechanism of membrane formation: Membrane structures and their relation to preparation conditions, in: H.K. Lonsdale and H.E. Podall (Eds.), *Reverse Osmosis Membrane Research*, Plenum Press, New York, 1972.

THE FORMATION OF MEMBRANES FROM TERNARY SYSTEMS: VARIATION OF PREPARATION PARAMETERS

J.G. Wijmans, R.J. Johanns and C.A. Smolders

SUMMARY

Within ternary membrane forming systems three variables are used to change the structure of the top layer of the membrane: *i*) the polymer concentration and *ii*) the nonsolvent concentration, both in the casting solution, and *iii*) the solvent concentration in the coagulation bath. These variables do not influence the phase equilibria in the ternary system, so the observed effects are discussed in relation to the exchange of solvent and nonsolvent. A model is proposed to give a qualitative description of the solvent/nonsolvent exchange at the first instance of coagulation.

INTRODUCTION

Synthetic polymer membranes are usually made by casting a polymer solution as a film on a suitable support and then immersing this film in a coagulation bath containing a nonsolvent. The exchange of solvent and nonsolvent, which must be miscible, causes precipitation of the polymer film and a membrane with a specific structure is formed. The structure depends on the compounds used and the exact preparation procedure. In many cases the structure is asymmetric: a thin and dense top layer, formed at the film/bath interface, is

supported by a porous substructure. There are two distinct factors that determine the membrane structure; *i*) the material transfer between the film and the bath, i.e. the exchange of the low molecular weight components, since the polymer is assumed not to leave the film, and *ii*) the thermodynamic properties of the multicomponent (at least ternary) system, i.e. the phase equilibria and the kinetics of phase separation.

In the investigation described in this paper we restrict ourselves to ternary membrane forming systems consisting of a polymer, a solvent and a nonsolvent. Within such a ternary system there are several parameters which can be varied in order to change the membrane structure:

- the polymer concentration in the casting solution;
 - the solvent concentration in the coagulation bath;
 - the nonsolvent concentration in the casting solution,
- and
- the temperature of the casting solution and the coagulation bath.

In a previous publication [1] it was shown that the presence of solvent in the coagulation bath strongly influences the membrane structure. Casting solutions, which when immersed in pure nonsolvent produce asymmetric ultra- or hyperfiltration membranes, yield membranes with a microporous top layer if sufficient solvent is added to the coagulation bath. In the present study we will extend the previous work [1] to the variation of the polymer concentration and the nonsolvent concentration in the casting solution. Although the temperature is known to affect the membrane structure, the temperature is not used as a parameter in this study. The objective is to vary only those parameters which do not change the phase equilibria in the membrane forming system. In this way the changes in the membrane structure can be ascribed to changes in the magnitude of the exchange of solvent and nonsolvent.

THEORY

The analysis of the formation of membranes in terms of phase separation phenomena and rates of precipitation started in the early seventies with work by Strathmann [2,3] and Frommer [4]. Koenhen, Mulder and Smolders [5] took the same approach and formulated a mechanism of formation of asymmetric membranes in which the formation of the top layer is related to gelation and the formation of the porous substructure to liquid-liquid phase separation followed by gelation of the concentrated phase. This mechanism has proven to be a fruitful basis for the interpretation of membrane preparation procedures of which a recent review has been given by Wijmans and Smolders [6]. The mechanism is a working hypothesis as no direct proof of its correctness hitherto has been presented. The role of liquid-liquid demixing in the formation of the porous substructure is generally accepted, but the formation of the skin by gelation and the existence of different coagulation paths for different layers of the membrane are not.

In the formulation of Koenhen *et al.* the local polymer concentration at the moment of precipitation is different for the top layer and for the substructure. It is assumed that the ratio of solvent outflow and nonsolvent inflow is large for the top layer, leading to a local composition which is concentrated in polymer and where gelation takes place. The exchange ratio is smaller for the substructure, so the local polymer concentration remains lower than in the top layer, and the phase boundary reached is the liquid-liquid demixing boundary. In Figure 1 a very schematic picture of this process is given. In the ternary phase diagram the approximate changes in composition, the so-called coagulation paths, are given for the top layer (arrow 1) and the substructure (arrow 2). Originally it was suggested that both the top layer of an ultrafiltration membrane and the top layer of a more dense membrane (hyperfiltration, pervaporation or gas separation) are formed by gelation.

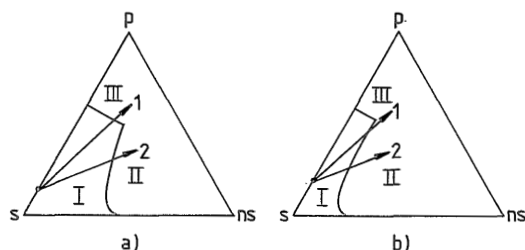


FIGURE 1. Schematic description of the coagulation process (immersion precipitation). I: homogeneous solution; II: liquid-liquid demixing gap; III: gel area; 1 and 2: coagulation paths, see text, a) formation of hyperfiltration membranes, b) formation of ultrafiltration membranes.

The apparently more open structure of the ultrafiltration membranes was believed to be due to local ordering accompanying the gelation process: crystallization and the formation of nodules. Recent investigations into the formation of polysulfone [7] and polyphenyleneoxide [8] ultrafiltration membranes lead us to the conclusion that the very small (and probably scarce) pores in the top layer of an ultrafiltration membrane are the result of liquid-liquid demixing. In this case the coagulation path responsible for the formation of the top layer intersects the liquid-liquid demixing gap in the vicinity of the gel/solution boundary, see Figure 1b.

From the description given above it is clear that the direction of the coagulation path, i.e. the ratio of solvent outflow and nonsolvent inflow, plays an important role in the realization of the membrane structure. In a previous publication [1] we used the ratio $\Delta\mu_1/\Delta\mu_2$ as an indication for the ratio J_1/J_2 . The quantity J_1/J_2 is the ratio of the inflow of nonsolvent (subscript 1) and the outflow of sol-

vent (subscript 2) characteristic for the top layer; $\Delta\mu_i$ is defined as the difference in chemical potential of species i between the coagulation bath and the original composition of the casting solution, hence as the driving force for transport of species i at the first moment of coagulation. Neglecting the influence of the transport coefficients it was assumed that a change in the initial ratio $\Delta\mu_1/\Delta\mu_2$ is reflected in a corresponding change in J_1/J_2 . Addition of the solvent to the coagulation bath increases the absolute value of $\Delta\mu_1/\Delta\mu_2$ and thus favours the inflow of nonsolvent. In this way it was explained why microporous membranes are formed if sufficient solvent is present in the coagulation bath [1] .

The ratio $\Delta\mu_1/\Delta\mu_2$ is now calculated as a function of the polymer concentration and the nonsolvent concentration in the casting solution. The relations used for the chemical potentials and the values of the interaction parameters can be found in the preceding paper [1]. The results are given in Figure 2. Figure 2a shows the ratio $-\Delta\mu_1/\Delta\mu_2$ as a function of the nonsolvent concentration in the casting solution for five different bath compositions. The ratio $-\Delta\mu_1/\Delta\mu_2$ decreases as the nonsolvent concentration increases, so the outflow of solvent is favoured. A larger solvent outflow or a steeper coagulation path would lead to smaller pores in a microporous top layer if the starting point of the path is unchanged. However, the addition of nonsolvent to the casting solution brings the initial composition nearer to the liquid-liquid demixing gap, and this favours the formation of larger pores. Thus, the addition of nonsolvent to the film has two consequences which are counteractive and a prediction of its overall effect on the membrane structure is not possible.

The decrease in $-\Delta\mu_1/\Delta\mu_2$ with increasing nonsolvent content in the casting solution is more rapid if more solvent is present in the coagulation bath. The reason for this is that the nonsolvent concentration in the film for which the chemical potential difference over the film/bath interface,

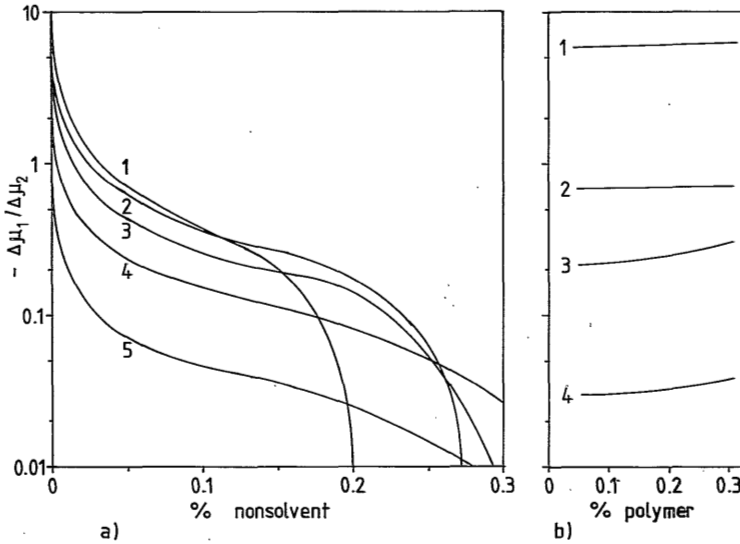


FIGURE 2. Ratio $-\Delta\mu_1/\Delta\mu_2$ as a function of nonsolvent concentration (a) and polymer concentration (b) in the casting solution.
 (a) Nonsolvent/solvent composition in the coagulation bath: 25/75 (1), 50/50 (2), 75/25 (3), 95/5 (4) and 99.99/0.01 (5);
 (b) Nonsolvent/solvent composition in the coagulation bath: 50/50 (1 and 3) and 100/0 (2 and 4). Nonsolvent/solvent composition in the casting solution: 0/100 (1 and 2) and 20/80 (3 and 4).

$\Delta\mu_1$, is zero, is lower if the nonsolvent concentration in the bath is smaller.

In Figure 2b the influence of the polymer concentration in the casting solution on $-\Delta\mu_1/\Delta\mu_2$ is presented. It is clear that the polymer concentration has a much smaller effect compared to the solvent and nonsolvent concentration in the coagulation bath and the casting solution respectively. Thus, if the direction of the coagulation path is practically unchanged, an increase in initial polymer concentration will result in smaller pores in a microporous top layer or in a thicker skin layer.

Figures 2a and b show the results calculated for the system cellulose acetate/dioxane/water. For other ternary systems the results are almost the same [1].

EXPERIMENTAL

The polymers used were Polysulfone P3500, PSf (Union Carbide), and Cellulose Acetate E 398-3, CA (Eastman Kodak). The solvents and nonsolvents were of reagent grade and were used without further purification. The water was demineralized and ultrafiltrated.

The casting solutions were hand cast (0.2 mm) on a glass plate and immersed in a coagulation bath containing a mixture of solvent and nonsolvent. After thirty minutes the glass plate together with the film was transferred to a pure nonsolvent bath and was kept there for at least a day.

Electron micrographs were taken with a Jeol JSM 35 CF scanning electron microscope, after air drying of the membranes.

Abbreviations:

cellulose acetate: CA	N,N-dimethylacetamide : DMAC
polysulfone : PSf	N,N-dimethylsulfoxide : DMSO
isopropanol : iPrOH	N-methylpyrrolidone : NMP

RESULTS AND DISCUSSION

Solvent concentration in the coagulation bath

The results published previously showed that the pore radii in a microporous top layer increased if the solvent concentration in the coagulation bath was increased [1]. This is in accordance with a change in the direction of the coagulation path as shown in Figure 3a. In an analogous way one expects that the thickness of a skin layer decreases if the solvent concentration in the bath increases. To verify this, membranes were made from the ternary system PSf/DMAC/iPrOH which is known to yield membranes with a thick skin (visible with electron microscopy) if the polymer concentration in the casting solution is high [9].

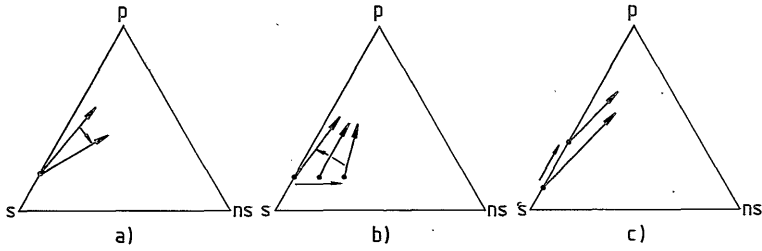


FIGURE 3. Change in direction and/or starting point of the coagulation path responsible for the top layer formation upon increasing the solvent concentration in the coagulation bath (a); upon increasing the nonsolvent concentration in the casting solution (b); and upon increasing the polymer concentration in the casting solution (c).

In Figure 4 the skin thickness, as measured by electron microscopy, is plotted as a function of the DMAc concentration in the coagulation bath. Four of the corresponding micrographs of the cross section of the membranes are represented in Figure 5. Figure 4 and 5 confirm that an increase

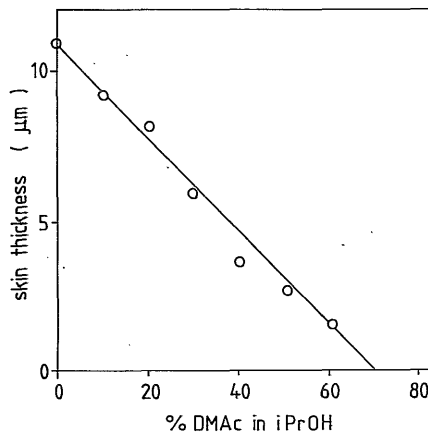


FIGURE 4. Thickness of the skin of polysulfone membranes as a function of the DMAc concentration in the DMAc/iPrOH coagulation bath, see also Figure 5. Casting solution: 30% PSf in DMAc.

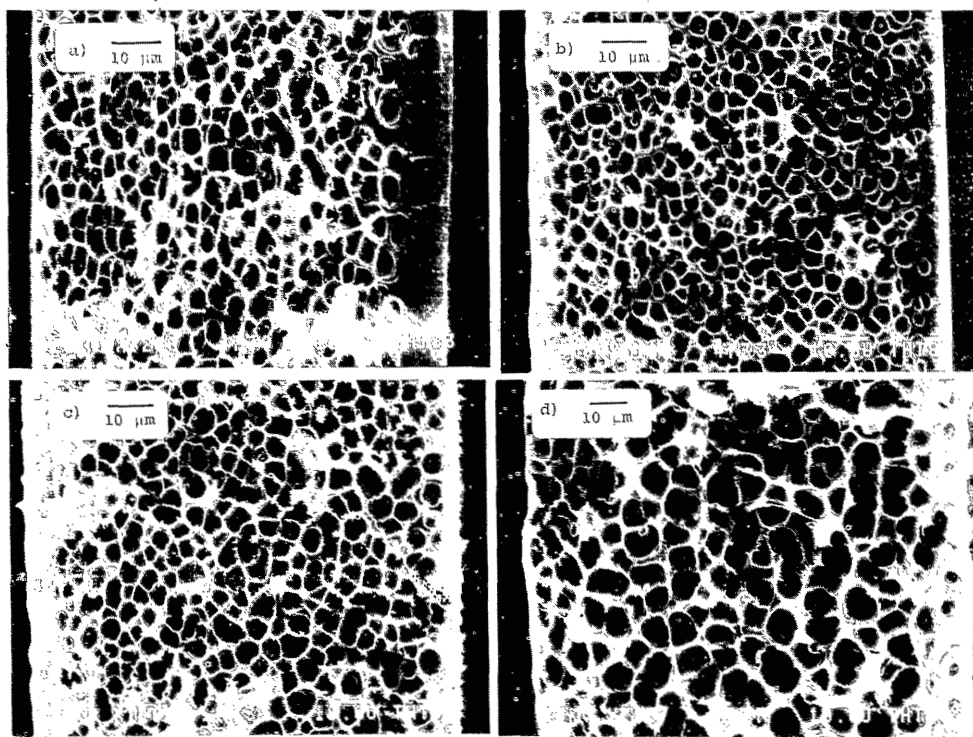


FIGURE 5. Micrographs of cross sections of Polysulfone membranes. See also Figure 4. Casting solution: 30% PSf in DMAc. Composition of DMAc/iPrOH coagulation bath: 0/100 (a), 30/70 (b), 50/50 (c) and 70/30 (d).

in the solvent concentration in the bath decreases the skin thickness. This is a strong support both for the model description presented in the previous paper [1] as for the hypothesis on the formation of the skin. That gelation is responsible for the formation of the skin of these membranes is in our opinion evident from the micrograph of Figure 5a and from the observation that the displayed membrane has pervaporation properties [9].

Nonsolvent concentration in the casting solution

The water (nonsolvent) concentration in the solvent/nonsolvent mixture of the casting solution has been varied for four different ternary membrane forming systems. The composition of the coagulation bath has been chosen such that the top layer of the membranes formed from the binary casting solutions (no water present) is microporous. The effect of the water concentration on the pore diameter is shown in Figure 6.

The CA/Dioxane/water system yields membranes with a very uniform pore structure in the top layer, of which the average diameter can be determined accurately. The water content of the casting solution has a marked influence on the pore diameter: at first the diameter decreases with increasing water concentration, then it passes through a minimum and increases. This can be explained by the twofold effect of the nonsolvent concentration in the casting solution as discussed in the theory section and displayed in Figure 3b. At low water concentrations the change in the direction of the coagulation path apparently dominates over the change in the starting point of the path, at higher water concentrations the situation seems to be reversed.

The other three systems studied show a behaviour similar to that of the CA/Dioxane/water system. For the system CA/DMSO/water the initial decrease in pore diameter upon adding water is very pronounced: no pores could be detected at a magnification of 100,000 times if the water concentration in the casting solution is in between 3% and 11%.

Polymer concentration in the casting solution

Binary casting solutions with varying polymer concentrations are immersed in a solvent/nonsolvent coagulation bath. The dependence of the mean pore diameter in the top layer

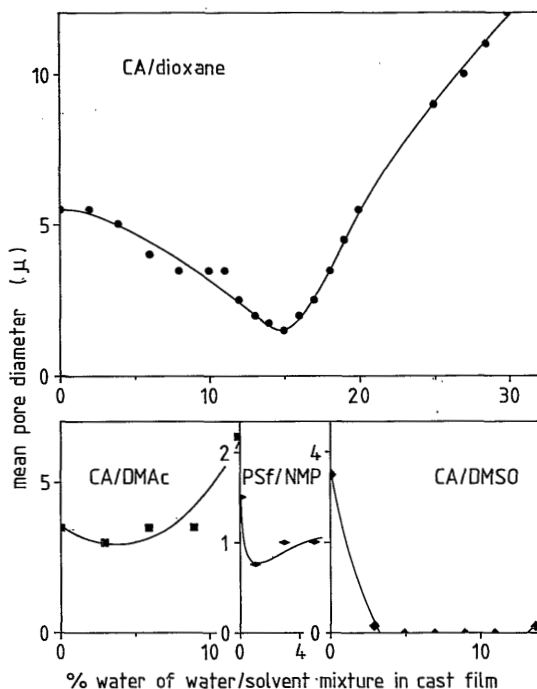


FIGURE 6. Mean pore diameter in the top surface of membranes as a function of the water (nonsolvent) concentration in the solvent/nonsolvent mixture in the casting solution.

CA/Dioxane/water system:

Casting solution: 15% CA in dioxane/water as indicated

Coagulation bath: 50%/50% Dioxane/water

CA/DMAc/water system:

Casting solution: 15% CA in DMAc/water as indicated

Coagulation bath: 70%/30% DMAc/water

CA/DMSO/water system:

Casting solution: 15% CA in DMSO/water as indicated

Coagulation bath: 70%/30% DMSO/water

PSf/NMP/water system:

Casting solution: 20% PSf in NMP/water as indicated

Coagulation bath: 80%/20% NMP/water.

on the polymer concentration is represented in Figure 7. The CA/DMSO/water system shows a continuous decrease of the pore size with increasing polymer concentration. This

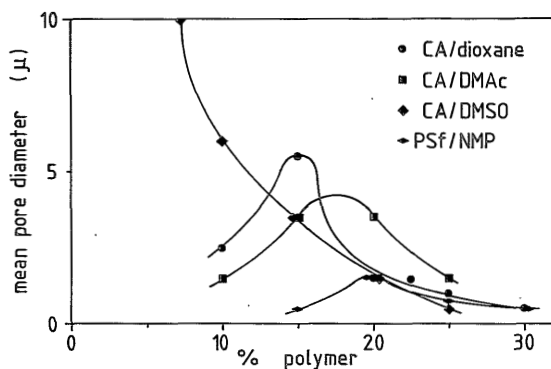


FIGURE 7. Mean pore diameter in the top surface of membranes as a function of the polymer concentration in the binary (no water present) casting solution. See Figure 6 for the compositions of the various solvent/nonsolvent coagulation baths.

is in agreement with the effect of the change in the starting point of the coagulation path as illustrated by Figure 3c. An analogous result was obtained by Mulder *et al.* [9], who showed that the thickness of the skin of membranes made from the system PSf/DMAc/iPrOH clearly increases with increasing polymer concentration in the casting solution.

The maximum in the pore diameter versus polymer concentration plot of Figure 7 displayed by the systems CA/Dioxane/water, CA/DMAc/water and PSf/NMP/water is not in accordance with the trend of Figure 3c. Apparently the use of the ratio $-\Delta\mu_1/\Delta\mu_2$ as an indication for J_1/J_2 is an oversimplification in these cases. It seems very likely that the transport coefficients, which connect the flows J_i to the driving forces $\Delta\mu_i$, depend on the polymer concentration. In fact, it has already been shown that the solvent outflow from the cast film increases as the polymer concentration decreases [10]. This may be the reason for a smaller ratio J_1/J_2 at low polymer concentrations, leading to less porous top layer structures. At high polymer concentrations the effect of the change in the starting point as shown in Figure 3c dominates

and the pore diameter decreases with increasing polymer concentration.

CONCLUSIONS

The nonsolvent concentration and polymer concentration of the casting solution have a considerable influence on the porosity of the top layer of microporous membranes. The general trend observed is in accordance with the predictions of the model description presented previously [1].

REFERENCES

- [1] J.G. Wijmans, J.P.B. Baaij and C.A. Smolders, *J. Membrane Sci.*, 14 (1983) 263, chapter 5 of this thesis.
- [2] H. Strathmann, P. Scheible and R.W. Baker, *J. Appl. Polym. Sci.*, 15 (1971) 811.
- [3] H. Strathmann, K. Kock, P. Amar and R.W. Baker, *Desalination*, 16 (1975) 179.
- [4] M.A. Frommer and D. Lancet, in *Reverse Osmosis Membrane Research*, H.K. Lonsdale and H.E. Podall, eds., Plenum Press, New York, 1972.
- [5] D.M. Koenhen, M.H.V. Mulder and C.A. Smolders, *J. Appl. Polym. Sci.*, 21 (1977) 199.
- [6] J.G. Wijmans and C.A. Smolders, Chapter 2 of this thesis, to appear in the NATO ASI Series.
- [7] J.G. Wijmans, J. Kant, M.H.V. Mulder and C.A. Smolders, Chapter 3 of this thesis.
- [8] J.G. Wijmans, H.J.J. Rutten and C.A. Smolders, Chapter 4 of this thesis.
- [9] M.H.V. Mulder, J. Oude Hendrikman, J.G. Wijmans and C.A. Smolders, submitted to *J. Appl. Polym. Sci.*

[10] F.W. Altena, J. Smid, J.W.A. van den Berg, J.G.
Wijmans and C.A. Smolders, submitted to *Polymer*.

DIFFUSION DURING THE IMMERSION PRECIPITATION PROCESS

J.G. Wijmans, F.W. Altena and C.A. Smolders

INTRODUCTION

Polymer membranes can be obtained by the so-called immersion precipitation process in which a cast solution of a polymer in a solvent is immersed in a nonsolvent bath. The structure of the membranes produced in this manner is determined by two distinct factors: (i) the phase separation phenomena (equilibria and kinetics) in the ternary system, and (ii) the rate of diffusive solvent-nonsolvent exchange during the immersion.

Mechanisms of formation of synthetic membranes which incorporate these two factors have been proposed by several authors [1-8]. In this note we comment on the mathematical description of the diffusion problem as suggested by Cohen, Tanny, and Prager [6] in their paper "Diffusion-Controlled Formation of Porous Structures in Ternary Polymer Systems". This description includes a steady-state assumption which, in our point of view, is erroneous. Nevertheless, when this assumption is not applied, the paper of Cohen, Tanny, and Prager offers a valuable approach to the diffusion problem.

This appendix has been published in J. Polym. Sci. Polym. Phys. Ed., 22 (1984) 519.

THE MODEL

Cohen, Tanny, and Prager [6] propose a theory for the appearance of two-phase structures during the formation of polymer membranes from a casting solution immersed in a nonsolvent bath. This theory contains a series of assumptions, some concerning the phase separation phenomena and the others the diffusion phenomenon. Since this note deals with the diffusion problem, we summarize here the diffusion model.

(i) A schematic representation of the immersion process is given in Figure 1. At time $t = 0$ the casting solution possesses its original volume fractions ϕ_1^C , ϕ_2^C , and ϕ_3^C (1 denotes a nonsolvent, 2 a solvent and 3 a polymer). At time $t = t$ a diffusion layer has propagated to $z = z_d(t)$. The coordinate z is a position coordinate in a laboratory frame. The volume fractions at the film surface are ϕ_1^S , ϕ_2^S , and ϕ_3^S , which are considered to be at equilibrium with the coagulation bath. At time $t = t$ the film/bath interface has moved away from $z = 0$ as a result of the net volume outflow.

(ii) A position coordinate is introduced, measured in terms of the volume m of polymer per unit area of membrane between the interface and the point of observation [9]:

$$m(z) = \int_0^z \phi_3(z) \cdot dz$$

or

$$dm = \phi_3 \cdot dz \quad (1)$$

As a consequence, the film/bath interface is always at $m = 0$. The position of the film/support interface on the m axis, M_r , is also independent of time:

$$M = \int_0^Z \phi_3(z) \cdot dz \equiv \phi_3^C \cdot Z \quad (2)$$

(iii) The diffusion fluxes J_1 and J_2 through surfaces of fixed m are assumed to be linearly related to the driving forces:

$$J_1 = - \frac{D_1(\phi_1, \phi_2)}{RT} \cdot \phi_1 \cdot \frac{\partial \mu_1}{\partial m},$$

$$J_2 = - \frac{D_2(\phi_1, \phi_2)}{RT} \cdot \phi_2 \cdot \frac{\partial \mu_2}{\partial m} \quad (3)$$

D_1 and D_2 are the diffusion coefficients for nonsolvent and solvent in the polymer-fixed reference frame and μ_1 and μ_2 are the chemical potentials. Cross terms have been neglected, but nevertheless eqs. (3) are interrelated through the expressions for D_1 , D_2 , μ_1 , and μ_2 .

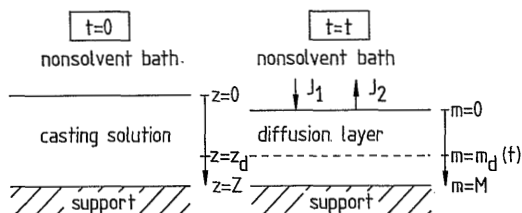


Fig. 1. Schematic representation of the immersion process at two different times. J_1 and J_2 are the nonsolvent and solvent volume flux, respectively. The coordinate z is fixed; the coordinate m is measured in terms of the polymer volume per unit area membrane between $z = 0$ and the point of observation.

(iv) Fick's law, applied in the "m" reference frame, gives (see Appendix A)

$$\frac{\partial(\phi_1/\phi_3)}{\partial t} = - \frac{\partial J_1}{\partial m},$$

$$\frac{\partial(\phi_2/\phi_3)}{\partial t} = - \frac{\partial J_2}{\partial m} \quad (4)$$

where $\phi_3 = 1 - \phi_1 - \phi_2$.

The initial and boundary conditions are:

$$t = 0: \phi_1(m, 0) = \phi_1^C, \phi_2(m, 0) = \phi_2^C \quad (5)$$

$$m = 0: \phi_1(0, t) = \phi_1^S, \phi_2(0, t) = \phi_2^S \quad (6)$$

$$m = M; J_1(M, t) = J_2(M, t) = 0 \quad (7)$$

(v) Cohen, Tanny, and Prager restrict themselves to the case in which the diffusion layer has not yet reached the support. Thus, eq. (7) is replaced by

$$m = m_d(t): \phi_1(m_d, t) = \phi_1^C, \phi_2(m_d, t) = \phi_2^C \quad (8)$$

(vi) Furthermore, they assume that the concentration distribution in the diffusion layer at every time is the steady-state distribution for a sheet of thickness $m_d(t)$ satisfying the boundary conditions (6) and (8). This implies that the fluxes J_1 and J_2 are independent of m :

$$\frac{\partial J_1}{\partial m} = \frac{\partial J_2}{\partial m} = 0 \quad (9)$$

It should be noted that, owing to the steady-state assumption, eq. (4) and the initial condition (5) no longer have a bearing on the solution of the diffusion problem.

(vii) The diffusion problem is now reduced to eqs. (3). The ratio of J_1 and J_2 can be written as

$$\frac{J_1}{J_2} = \sigma = \frac{\phi_1}{\phi_2} \cdot \frac{d\mu_1}{d\mu_2} \quad (10)$$

The assumption made here is that the ratio $D_1(\phi_1, \phi_2) / D_2(\phi_1, \phi_2)$ is constant and unity. The ratio σ normally has a negative value.

(viii) If the differentials of the chemical potentials are expressed as functions of the volume fractions, one finds

$$\frac{d\phi_2}{d\phi_1} = \frac{\sigma\phi_2(\partial\mu_2/\partial\phi_1) - \phi_1(\partial\mu_1/\partial\phi_1)}{\phi_2(\partial\mu_1/\partial\phi_2) - \sigma\phi_2(\partial\mu_2/\partial\phi_2)} \quad (11)$$

This first-order differential equation yields the relation between ϕ_1 and ϕ_2 in the diffusion layer as a function of the ratio σ and one of the boundary conditions.

With the aid of the Flory-Huggins expressions [10] for the chemical potentials together with eq. (11), Cohen, Tanny, and Prager calculated the composition paths within the ternary phase diagram and discussed them in relation to the formation of membranes.

CRITIQUE OF THE STEADY-STATE ASSUMPTION

Equation (11) has been derived using the steady-state condition (9). In our view this condition can not be applied to this diffusion problem. The use of it neglects the initial condition (5) and therefore does not satisfy the mass conservation law.

To make this point clear, the following example is considered. Equations (3) are rewritten as

$$\begin{aligned}
 J_1 &= - \frac{D_1}{RT} \cdot \phi_1 \cdot \left[\frac{\partial \mu_1}{\partial \phi_1} + \frac{\partial \mu_1}{\partial \phi_2} \cdot \frac{d\phi_2}{d\phi_1} \right] \cdot \frac{d\phi_1}{dm} \\
 J_2 &= - \frac{D_2}{RT} \cdot \phi_2 \cdot \left[\frac{\partial \mu_2}{\partial \phi_2} + \frac{\partial \mu_2}{\partial \phi_1} \cdot \frac{d\phi_1}{d\phi_2} \right] \cdot \frac{d\phi_2}{dm}
 \end{aligned}
 \tag{12}$$

Equation (12) together with the steady-state assumption and one of the boundary conditions yields the concentration profiles $\phi_1(m, t)$ and $\phi_2(m, t)$. Since there is no analytical solution for the coupled differential equation (12), we represent the solution as follows:

$$\begin{aligned}
 \phi_1(m, t) &= F_1(m, t, D_1, D_2, J_1, J_2, \mu_1, \mu_2) \\
 \phi_2(m, t) &= F_2(m, t, D_1, D_2, J_1, J_2, \mu_1, \mu_2)
 \end{aligned}
 \tag{13}$$

In this way ϕ_1 and ϕ_2 are expressed as functions of all these parameters. With respect to time $t = 0$ the change in nonsolvent and solvent content per unit area of membrane at time $t = t_1$ is, respectively,

$$\Delta V_1 = \int_0^{m_d(t_1)} \left[\frac{\phi_1(m, t_1)}{\phi_3(m, t_1)} - \frac{\phi_1^c}{\phi_3^c} \right] dm$$

and

$$\Delta V_2 = \int_0^{m_d(t_1)} \left[\frac{\phi_2(m, t_1)}{\phi_3(m, t_1)} - \frac{\phi_2^c}{\phi_3^c} \right] dm \quad (14)$$

$$\Delta V_1 / \Delta V_2 = F_3(m, t_1, D_1, D_2, J_1, J_2, \mu_1, \mu_2) \quad (15)$$

On the other hand, the concentration distribution as described by eqs. (13) is generated by the nonsolvent and solvent fluxes through the interface, so the quantities ΔV_1 and ΔV_2 must be equal to $-\int_0^{t_1} J_1(t) dt$ and $-\int_0^{t_1} J_2(t) dt$, respectively, where $J_1(t)/J_2(t) = \sigma$ at every time, and therefore

$$\frac{\Delta V_1}{\Delta V_2} = \int_0^{t_1} J_1(t) dt / \int_0^{t_1} J_2(t) dt = \sigma \quad (16)$$

Comparing eqs. (15) and (16), we see that this condition is not fulfilled. Equations (15) and (16) are identical only if the concentration profiles are computed under the restriction of eqs. (4) and (5). From Eqs. (12) and (15) it can be seen that in the Cohen, Tanny, and Prager description the ratio $\Delta V_1/\Delta V_2$ depends on the interaction parameters that appear in the Flory-Huggins expressions for the chemical potentials.

DISCUSSION

It has been pointed out above that the ϕ_1 vs ϕ_2 curve, calculated with the aid of eq. (11) and characteristic for a certain ratio σ (see Fig. 2), cannot give the correct concentration distribution in a film which is subject to a nonsolvent-solvent exchange with the same ratio σ . The consequence is that the composition paths drawn in the ternary phase diagrams by Cohen, Tanny, and Prager are not valid. This can be illustrated by two peculiar features of the composition paths shown in Figures 3-5 of their paper and also in our Figure 3. Figure 3 has been taken from the thesis of Altena [11], who used in Eq. (11) the following expressions for the chemical potentials [10]:

$$\begin{aligned}
 (\mu_1 - \mu_1^0)/RT &= \ln(\phi_1) - s \cdot \phi_2 - r \cdot \phi_3 \\
 &+ (1 + \chi_{12} \cdot \phi_2 + \chi_{13} \cdot \phi_3) \cdot (1 - \phi_1) - s \cdot \chi_{23} \cdot \phi_2 \cdot \phi_3, \\
 (\mu_2 - \mu_2^0)/RT &= s \cdot \ln(\phi_2) - \phi_1 - r \cdot \phi_3 \\
 &+ (s + \chi_{12} \cdot \phi_1 + s \cdot \chi_{23} \cdot \phi_3) \cdot (1 - \phi_2) - \chi_{13} \cdot \phi_1 \cdot \phi_3 \quad (17)
 \end{aligned}$$

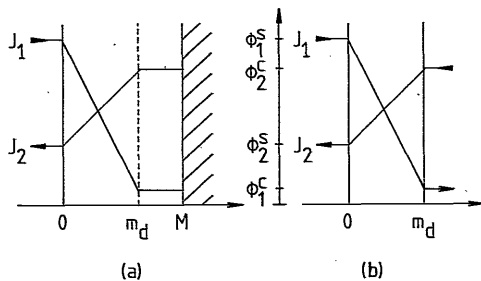


Fig. 2. Concentration profiles: (a) concentration distribution in a cast polymer film, when the diffusion boundary has reached m_d ; (b) steady-state concentration distribution in a sheet with thickness m_d .

The chemical potentials are expressed per mole of segments, one mole of segments having the same volume as one mole of species 1. The χ_{ij} parameters are the interaction parameters of components i and j ; s and r are v_1/v_2 and v_1/v_3 , the ratios of the molar volumes.

From Figure 3 it can be seen that (i) the location of the composition path at a constant ratio σ depends on the thermodynamic properties of the system and that (ii) the average polymer content does increase for $\sigma = -1$.

Although the interaction parameters will have some influence on the concentration distribution, it is clear that the average change in composition in the film should be solely determined by the fluxes J_1 and J_2 . Furthermore, it is obvious that if $\sigma = -1$, i.e., if the volume of solvent leaving is replaced by an equal volume of nonsolvent entering, the average polymer concentration should remain constant. In fact, the latter has been stated implicitly by Cohen, Tanny, and Prager themselves in deriving their eq. (10) [6]. This equation, the result of the mass balance in time, reads

$$\int_0^t (J_1 + J_2) \cdot dt = \int_0^{\text{md}} \left(\frac{1}{\phi_3^c} - \frac{1}{\phi_3} \right) \cdot dm \quad (18)$$

If the ratio σ has the value -1 , which means $J_1 + J_2 = 0$, this equation implies that $\bar{\phi}_3 = \phi_3^c$.

Since eq. (11) cannot be applied to our diffusion problem, we have to return to eqs. (3) and (4), which describe the diffusion phenomenon together with the conditions (5)-(7). The use of boundary condition (6) presumes equilibrium between the nonsolvent bath and the film surface. In case the bath is not well stirred, Cohen, Tanny, and Prager suggest the use of finite transfer coefficients within a boundary layer, which will influence the surface concentrations.

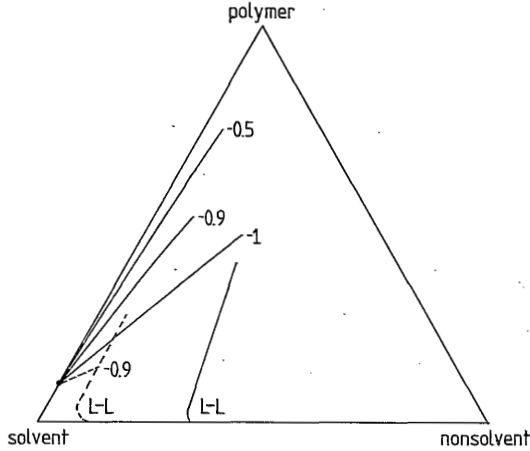


Fig. 3. Composition paths for various values of σ in the ternary polymer/solvent/nonsolvent system. Parameter values: $s = 0.2$; $r = 0.002$; $\chi_{13} = 1.5$, $\chi_{23} = 0.0$ and $\chi_{12} = 1.0$ (—) or $\chi_{12} = 0.0$ (---). The binodals for liquid-liquid phase separation have been calculated [11,12].

In our opinion, even if there is no concentration gradient in the bath, there will be another resistance to the mass transport, i.e., the resistance in the film/bath interface itself. Thus, eq. (6) is replaced by

$$m = 0: \frac{D_1 \cdot \phi_1}{RT} \cdot \frac{\partial \mu_1}{\partial m} = -J_1(0, t) = L_1 \cdot \Delta \mu_1$$

$$\frac{D_2 \cdot \phi_2}{RT} \cdot \frac{\partial \mu_2}{\partial m} = -J_2(0, t) = L_2 \cdot \Delta \mu_2 \quad (19)$$

L_1 and L_2 are the permeability coefficients for nonsolvent and solvent in the interface. The potential difference $\Delta \mu_i$ is the difference at the interface:

$$\Delta \mu_i = \mu_i, \text{ casting solution, } m = 0 \ (\phi_1, \phi_2)$$

$$- \mu_i, \text{ coagulation bath, } m = 0 \ (v_1, v_2) \quad (20)$$

The volume fractions of nonsolvent and solvent in the bath are v_1 and v_2 . We have used similar relations to describe the volume fluxes through the interface at the first instance of coagulation [13]. Equations (3)-(5), (7) and (19) together describe the diffusion during immersion precipitation and they can be solved numerically in order to yield the concentration profiles in the polymer film as a function of time (see Appendix B for a specific example). In this way it is possible to evaluate the influence of the transport parameters L_1 and D_1 ; this work is in progress. From eq. (19) it can already be deduced that the ratio $J_1(0,t)/J_2(0,t)$ in general is not independent of time. In our opinion this is very important with respect to the formation of asymmetric structures in the film [8,11].

APPENDIX A

The mass conservation law is applied to the differential volume element shown in Figure 4. For the accumulation of species i we write

$$\begin{aligned} A \cdot (\phi_i \cdot \Delta z)_{t+\Delta t} - A \cdot (\phi_i \cdot \Delta z)_t &= A \cdot \Delta m \cdot \left(\frac{\phi_i}{\phi_3}\right)_{t+\Delta t} - A \cdot \Delta m \cdot \left(\frac{\phi_i}{\phi_3}\right)_t \\ &= \frac{\partial (\phi_i / \phi_3)}{\partial t} \cdot \Delta m \cdot \Delta t \cdot A \end{aligned}$$

Flow of species i in minus flow of species i out can be expressed as

$$A \cdot \Delta t \cdot (J_i)_m - A \cdot \Delta t \cdot (J_i)_{m+\Delta m} = - \frac{\partial J_i}{\partial m} \cdot \Delta m \cdot \Delta t \cdot A$$

Thus

$$\frac{\partial (\phi_i/\phi_3)}{\partial t} = - \frac{\partial J_i}{\partial m} \quad (A1)$$

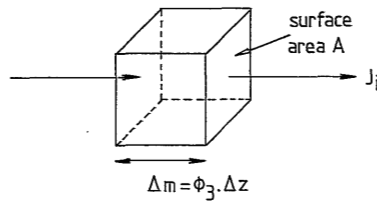


Fig. 4. Differential volume element.

APPENDIX B

The diffusion problem as described by eqs. (3)-(5), (7), and (19) has been solved for the case

$$J_1(0,t) = -J_2(0,t) = \text{constant} \quad (B1)$$

This boundary condition has been chosen to permit us to compare the computed concentration profile with the concentration path calculated with the aid of eq. (11) for $\sigma = -1$ (see Fig. 3). The numerical procedure used is the NAG library routine D03PGF [14] and the parameters in the equations had the following values:

$$J_1(0,t) = 2.10^{-5} \text{ m/s}$$

$$D_1 = 2.10^{-9} \text{ m}^2/\text{s}$$

$$J_2(0,t) = -2.10^{-5} \text{ m/s}$$

$$D_2 = 5.10^{-9} \text{ m}^2/\text{s}$$

$$\phi_1^C = 0.0001$$

$$\chi_{12} = 0.0$$

$$\phi_2^C = 0.7999$$

$$\chi_{13} = 1.5$$

$$\phi_3^C = 0.2000$$

$$\chi_{23} = 0.0$$

$$s = 0.2$$

$$r = 0.002$$

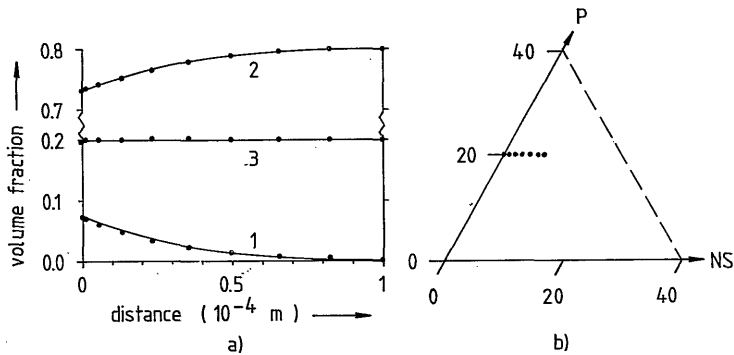


Fig. 5. Concentration profile (a) and concentration path (b) calculated with the aid of eqs. (3)-(5), (7), (19), and (BI).

The concentration profile and the concentration path at time $t = 0.1 \text{ s}$ are displayed in Figure 5.

From this figure it appears that the overall polymer concentration in the film has not changed in the case $\sigma = -1$, as would be expected.

REFERENCES

- [1] H. Strathmann, P. Scheible, and R.W. Baker, *J. Appl. Polym. Sci.*, 15, 811 (1971)
- [2] M.A. Frommer and D. Lancet, in *Reverse Osmosis Research*, H.K. Lonsdale and H.E. Podall, Eds., Plenum, New York, 1972.
- [3] M. Guillotin, C. Lemoyne, C. Noël, and L. Monnerie, *Desalination*, 21, 165 (1977),
- [4] H. Strathmann and K. Koch, *Desalination*, 21, 241 (1977).
- [5] D.M. Koenhen, M.H.V. Mulder, and C.A. Smolders, *J. Appl. Polym. Sci.*, 21, 199 (1977).
- [6] C. Cohen, G.B. Tanny, and S. Prager, *J. Polym. Sci. Polym. Phys. Ed.*, 17, 477 (1979).
- [7] C.A. Smolders, in *Ultrafiltration Membranes and Applications*, A.R. Cooper, Ed., Plenum, New York, 1980.
- [8] H. Bokhorst, F.W. Altena, and C.A. Smolders, *Desalination*, 38, 349 (1981).
- [9] G.S. Hartley and J. Crank, *Trans. Faraday Soc.*, 45, 801 (1949).
- [10] P.J. Flory, *Principles of Polymer Chemistry*, Cornell University, Ithaca, NY, 1953.
- [11] F.W. Altena, Thesis, Twente University of Technology, 1982, Chap. 7.
- [12] F.W. Altena and C.A. Smolders, in F.W. Altena's thesis, Twente University of Technology, Enschede, 1982 Chap. 5 [*Macromolecules*, 15, 1491 (1982)].
- [13] J.G. Wijmans, J.P.B. Baaij, and C.A. Smolders, *J. Membr. Sci.*, 14, 263 (1983).
- [14] P.M. Dew and J.E. Walsh, Numerical Analysis Report No. 49, University of Manchester, 1980.

PART II

**THE CONCENTRATION POLARIZATION PHENOMENON IN
ULTRAFILTRATION**

FLUX LIMITATION IN ULTRAFILTRATION: OSMOTIC PRESSURE MODEL AND GEL LAYER MODEL

J.G. Wijmans, S. Nakao* and C.A. Smolders

SUMMARY

The characteristic permeate flux behaviour in ultrafiltration, i.e. the existence of a limiting flux which is independent of applied pressure and membrane resistance and a linear plot of the limiting flux versus the logarithm of the feed concentration, is explained by the osmotic pressure model. In the mathematical description presented here, a quantity $\Delta\Pi.n/(R_m.k)$ is introduced which is the ratio of the resistance caused by the osmotic pressure and the resistance of the membrane itself. For high values of this quantity (>19) the flux is practically limited by the osmotic pressure.

Factors leading to high values of the quantity $\Delta\Pi.n/(R_m.k)$ are discussed and it is concluded that in the ultrafiltration of medium molecular weight solutes (10,000 to 100,000 Daltons) osmotic pressure limitation is more likely than gel layer limitation.

*Present address: Institute of Industrial Science, University of Tokyo, 7-22-1 Roppongi, Minatoku, Tokyo 106, Japan.

This chapter has been published in J. Membrane Sci., 20 (1984) 115

INTRODUCTION

Ultrafiltration is a pressure driven membrane process by which macromolecular solutes are separated from the solvent. In actual applications the permeate flux increases less than linearly with the pressure difference over the membrane, and it is always smaller than the pure solvent flux. At higher pressure differences the permeate flux is no longer significantly affected by the pressure difference: it levels off to almost constant values. This constant flux is called 'limiting flux' and it is independent of membrane resistance. Under unchanged mass transfer conditions only the feed concentration is an important variable, and a linear relationship can be obtained in the plot of the limiting flux versus the logarithm of the feed concentration.

These characteristic phenomena have been explained by the gel layer model [1,2]. In addition to this model another mechanism for flux limitation, the so-called osmotic pressure model, has been proposed [3,4]. Since the osmotic pressure model has received more and more attention recently [5,6] it is very interesting to investigate whether this model is capable of predicting the complete flux behaviour. This is the aim of the present work.

THE GEL LAYER MODEL [1,2]

The concentration of the solute at the membrane surface, c_m , is much higher than that in the bulk solution due to concentration polarization. Assuming a rejection of 100% and neglecting the influence of concentration profile and permeate flux on the mass transfer coefficient, k , the following relation for c_m is obtained [2]

$$c_m = c_b \cdot \exp(J/k) \quad (1)$$

where c_b is the bulk concentration and J is the permeate flux. The concentration c_m increases rapidly with the permeate flux reaching a concentration c_g , where the solution is not fluid anymore. The thus formed gel layer at the membrane surface has a hydraulic resistance which reduces the permeate flux to such an extent that:

$$J_{\infty} = k \cdot \ln(c_g/c_b) \quad (2)$$

where J_{∞} is the limiting flux in ultrafiltration. Since the gel concentration is assumed to be constant, eq. (2) predicts a linear plot for J_{∞} versus $\ln(c_b)$ with a slope equal to $-k$; extrapolation to $J_{\infty} = 0$ will yield the $\ln(c_g)$ value. It also predicts that J_{∞} is not a function of the membrane resistance as long as the rejection value is constant.

In practice it appears that eq. (2) is very useful in correlating experimental limiting fluxes [2,7], but it also has been shown that the information obtained on gel concentrations is not reliable. For identical solutions different authors find widely varying values for c_g [8] and these values sometimes are too low (solutions at that concentration being still fluid) or too high (c_g values found by extrapolation exceeding 100%).

THE OSMOTIC PRESSURE MODEL [3,4]

The concentration c_m is significantly higher than the bulk concentration and therefore the osmotic pressure of the solution at the membrane surface is no longer negligible. The permeate flux is governed in this case by:

$$J = \frac{\Delta P - \Delta \Pi}{R_m} \quad (3)$$

where ΔP is the hydraulic pressure difference, $\Delta \Pi$ is the osmotic pressure difference and R_m is the membrane resistance. Again a rejection of 100% is assumed and in that case the osmotic pressure difference is determined by the concentration at the membrane surface, c_m .

When the applied pressure is increased the permeate flux will at first increase. This results in a higher value for c_m and thus in a larger osmotic pressure. In this way the pressure increase is partly canceled by the osmotic pressure increase. If $\Delta \Pi$ increases rapidly with the permeate flux, the increase in ΔP may lead to only a small increase in the permeate flux.

MATHEMATICAL DESCRIPTION OF THE OSMOTIC PRESSURE MODEL

In this section the mathematical expressions which show the characteristic flux behaviour are derived. The osmotic pressure difference of macromolecular solutions relative to the pure solvent increases much more than linearly with concentration which can be represented as follows:

$$\Delta \Pi = a \cdot c^n \quad (4)$$

where a is a constant and n an exponent larger than 1. Des Gennes [9] has shown that for semidilute macromolecular solutions n will have a value of about two. For more concentrated solutions the exponent is even larger than two [10].

The osmotic pressure difference $\Delta \Pi$ strongly depends on the permeate flux J since the latter determines the concentration c_m , as is shown by eq. (1). Thus eq. (3) can be rewritten as:

$$J = \frac{\Delta P - a \cdot c_D^n \cdot \exp(n \cdot J/k)}{R_m} \quad (5)$$

From eq. (5) it is clear that J will not increase linearly with ΔP . For the derivative $\partial J/\partial \Delta P$ we find:

$$\begin{aligned} \frac{\partial J}{\partial \Delta P} &= (R_m + a \cdot c_b^n \cdot \frac{n}{k} \cdot \exp(n \cdot J/k))^{-1} \\ &= (R_m + \frac{n}{k} \cdot \Delta \Pi)^{-1} \\ &= \frac{1}{R_m} \cdot (1 + \frac{\Delta \Pi \cdot n}{R_m \cdot k})^{-1} \end{aligned} \quad (6)$$

and we see that for high effective osmotic pressures the increase in J with ΔP is almost zero.

In Figure 1 the quantity $R_m \cdot \partial J/\partial \Delta P$ is represented as a function of the quantity $\Delta \Pi \cdot n/(R_m \cdot k)$. The physical meaning of these two dimensionless numbers is illustrated by the following equations which both can be derived from eq. (5):

$$R_m \cdot \frac{\partial J}{\partial \Delta P} = \frac{\partial J}{\partial \Delta P} / \left(\frac{\partial J}{\partial \Delta P} \right)_{\text{pure solvent}} \quad (7)$$

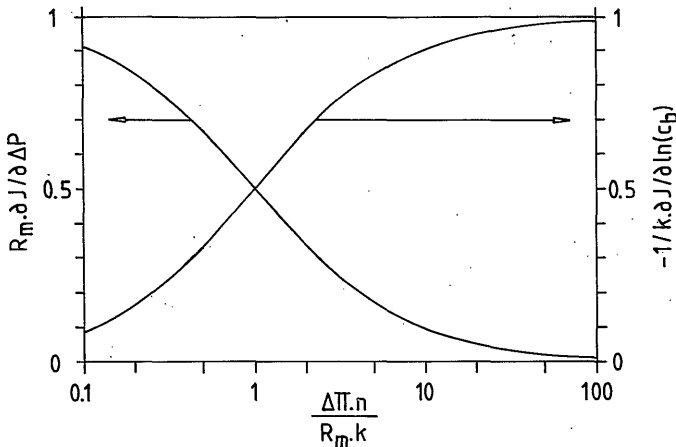


FIGURE 1. Effectiveness of pressure increase, $R_m \cdot \partial J/\partial \Delta P$ versus the ratio of osmotic resistance and membrane resistance, $\Delta \Pi \cdot n/(R_m \cdot k)$. Derivative of permeate flux with respect to the logarithm of bulk concentration, $-1/k \cdot \partial J/\partial \ln(c_b)$ versus the ratio $\Delta \Pi \cdot n/(R_m \cdot k)$.

$$\frac{\Delta\Pi \cdot n}{R_m \cdot k} = \frac{\partial\Delta\Pi}{\partial J} / R_m \quad (8)$$

Thus $R_m \cdot \partial J / \partial \Delta P$ is the ratio of the slope of the actual J versus ΔP curve and that of the pure solvent flux J_{ps} versus ΔP curve. The latter slope is the maximum slope which can be achieved, so $R_m \cdot \partial J / \partial \Delta P$ is a measure for the effectiveness of a pressure increase. $\Delta\Pi \cdot n / (R_m \cdot k)$ appears to be the ratio of the resistance caused by the osmotic pressure and the resistance of the membrane itself. The sum of these two resistances constitutes the actual total resistance, as is deduced from eq. (3):

$$\frac{\partial \Delta P}{\partial J} = R_m + \frac{\partial \Delta \Pi}{\partial J} \quad (9)$$

Figure 1 shows that the build up of an osmotic pressure gradually leads to a limiting flux. The effectiveness of a pressure increase becomes less and one can define more or less arbitrarily a 'limiting flux region'. If the permeate flux is supposed to be a limiting flux when $\partial J / \partial \Delta P$ is 5% or less of the pure solvent permeability, then the condition for flux limitation is read from Figure 1 to be:

$$\frac{\Delta\Pi \cdot n}{R_m \cdot k} > 19 \quad (10)$$

The second important feature, i.e. the permeate flux as a function of bulk concentration, can also be described by a derivative. After rearranging and differentiating eq. (5), one obtains:

$$\begin{aligned} \frac{\partial J}{\partial \ln(c_b)} &= - \left(\frac{1}{k} + \frac{1/n}{\Delta P / R_m - J} \right)^{-1} \\ &= -k \cdot \left(1 + \frac{1/n}{P\bar{c} \cdot (J_{ps}/J - 1)} \right)^{-1} \\ &= -k \cdot \left(1 + \frac{R_m \cdot k}{\Delta\Pi \cdot n} \right)^{-1} \end{aligned} \quad (11)$$

where $P\delta = J/k$ is the boundary layer Péclet number and $J_{ps} = \Delta P/R_m$ is the pure solvent flux. Eq. (11) shows that a plot of J versus $\ln(c_b)$ will yield a straight line with a slope equal to $-k$ when J_{ps}/J is large and/or when the Péclet number is large. These two conditions can be combined into one: $\Delta\Pi.n/(R_m.k) \gg 1$. In Figure 1 the quantity $\partial J/\partial \ln(c_b)$ divided by $-k$ is given as a function of $\Delta\Pi.n/(R_m.k)$. In the 'limiting flux region' the slope of a J versus $\ln(c_b)$ plot is equal to $-k$ within 5%. It must be noted that the absolute value of the actual slope is always smaller than k .

At high values of the ratio $\Delta\Pi.n/(R_m.k)$ the permeate flux depends only slightly on the membrane resistance R_m . This can be inferred from eq. (5), presented here in a different way:

$$J.R_m + a.c_b^n \exp(n.J/k) = \Delta P \quad (5')$$

When $\Delta\Pi.n/(R_m.k)$ is large, the term $J.R_m$ is small compared to $\Delta\Pi$ and ΔP . In that case the permeate flux is given by:

$$J = \frac{k}{n} \cdot \ln(\Delta P / (a.c_b^n)) \quad (12)$$

which upon differentiating with respect to $\ln(c_b)$ yields a slope exactly equal to $-k$. Eq. (12) is also obtained for the highly hypothetical case of a membrane with no hydrodynamic resistance and with a perfect solute rejection.

CALCULATED EXAMPLE OF OSMOTIC PRESSURE EFFECT

In Figures 2 and 3 the results of a model calculation, using eq. (5), are given. The parameters are chosen to be characteristic for a typical ultrafiltration experiment:

$n = 2$; a macromolecular solute with $\bar{M}_n = 70,000$
 $a = 100 \text{ atm}$; $\Delta\Pi = 1 \text{ atm}$ at weight fraction = 0.1
 $R_m = 5.10^5 \text{ atm.s/m}$; a membrane having a molecular weight cut-off of about 40,000
 $k = 2.10^{-6} \text{ m/s}$; turbulent flow ($Re = 5,000$), diffusion coefficient of solute = $5.10^{-11} \text{ m}^2/\text{s}$

$\Delta P = 0 \text{ to } 10 \text{ atm}$

$c_b = 0.0001 \text{ to } 0.1 \text{ weight fraction}$

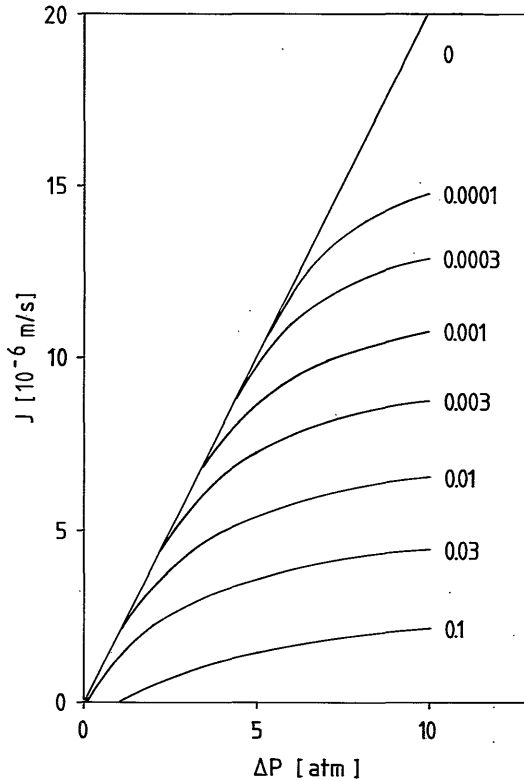


FIGURE 2. Calculated permeate flux as a function of applied pressure. Numbers identifying each curve indicate bulk concentration c_b .

As is expected the effectiveness of pressure increase becomes gradually less for higher applied pressures and higher bulk concentrations, and the permeate fluxes decrease with increasing bulk concentrations, see Figure 2. Most commercial ultrafiltration membranes possess a membrane resistance which is smaller than the value of $5 \cdot 10^5$ atm.s/m used in our calculation. As will be clear from the analysis given above, smaller values for R_m lead to a more pronounced osmotic pressure effect, i.e. flux limitation at lower applied pressures.

In Figure 3 the permeate flux is plotted as a function of c_b for two different applied pressures. It is clear that for high bulk concentrations, that is for high values of $\Delta\Pi \cdot n / (R_m \cdot k)$, the slope $\partial J / \partial \ln(c_b)$ approaches $-k$ (see broken lines in Figure 3). For low bulk concentrations J approaches the pure solvent flux. The intercept at the $J=0$

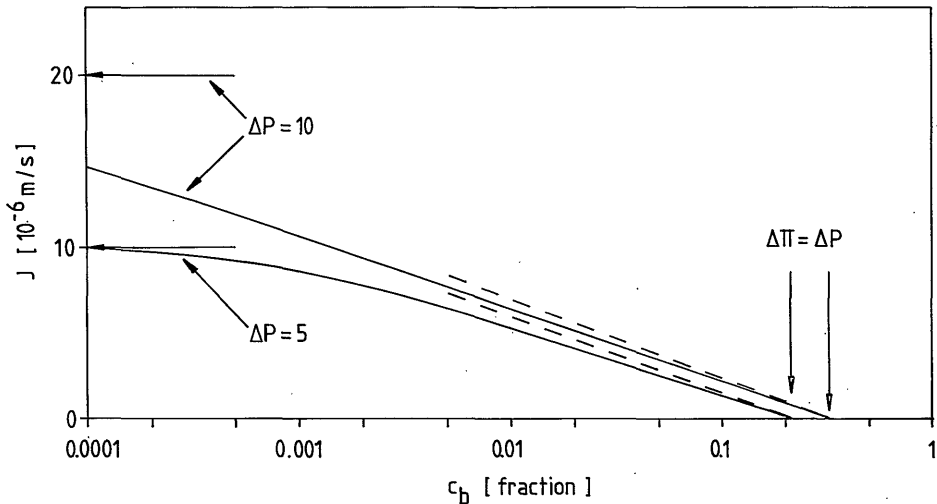


FIGURE 3. Permeate flux J as a function of bulk concentration for two pressures: $\Delta P = 5$ and $\Delta P = 10$ atm.

- ← : pure solvent flux
- : ultrafiltration flux
- - - : slope = $-k$

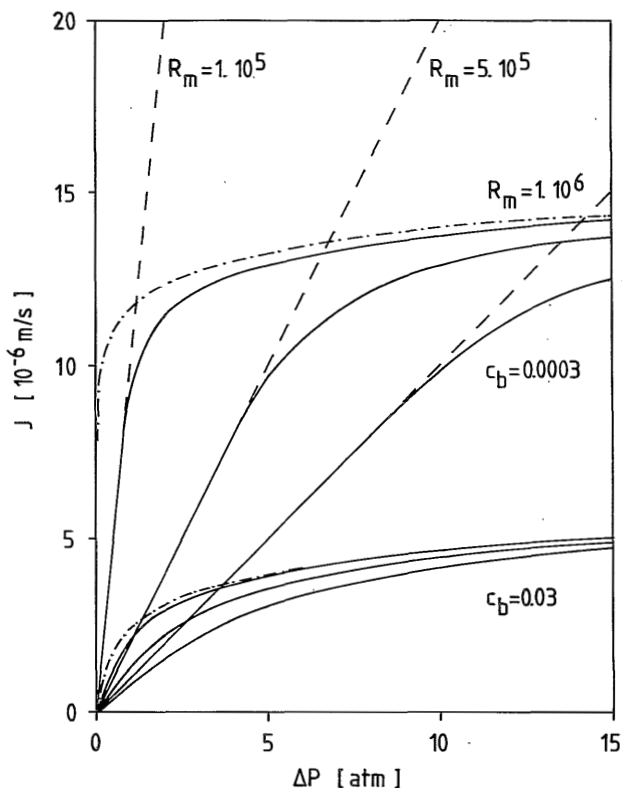


FIGURE 4. Permeate flux J as a function of applied pressure ΔP for two different feed concentrations and three different membrane permeabilities. $n = 2$; $a = 100$ atm; $k = 2.10^{-6}$ m/s.

- : pure solvent flux
- : ultrafiltration permeate flux
- .-.-.-.- : permeate flux calculated with eq. (12)

axis gives the bulk concentration for which $\Delta\Pi = \Delta P$. In this respect the osmotic pressure model deviates from the gel layer model which predicts an intercept not depending on ΔP .

Figure 4 illustrates the diminishing importance of the membrane resistance R_m as the osmotic pressure increases. For high osmotic pressures, the actual permeate flux approaches the permeate flux of the 'ideal' membrane as described by eq. (12).

DISCUSSION AND CONCLUSIONS

It has been shown that the osmotic pressure model is capable of explaining the most important features of the permeate flux behaviour in ultrafiltration. This is confirmed with the model calculation and it can be illustrated by experimental data [4,11]. Goldsmith [4] showed that under circumstances where no gel layer is expected, i.e. a low molecular weight polyethylene glycol ($\bar{M}_n = 15,500$ Daltons) as the solute and the concentration c_m smaller than 10% by weight, an almost limiting flux can be obtained in which case the J versus $\ln(c_b)$ plot is linear for a given pressure ΔP . Vilker *et al.* [11] concluded from osmotic pressure measurements and ultrafiltration experiments that the permeate flux in the ultrafiltration of bovine serum albumine is limited by the osmotic pressure.

The predictions of the osmotic pressure model are practically equivalent to those of the gel layer model. Two differences are: *i*) the osmotic pressure model does not predict a fully limiting flux and *ii*) contrary to the gel layer model, the osmotic pressure model explains the deviation of the permeate flux from the pure solvent flux at low pressures. At high pressure differences, the dependency of the permeate flux on the pressure difference decreases gradually. Eventually this dependency becomes so small that it is hidden within the experimental error.

The analogous result obtained from both models makes it very difficult to conclude from experimental data which mechanism is actually in operation. A possible answer may come from analyzing the intercept at the $J = 0$ axis in the J versus $\ln(c_b)$ plot. According to the two mechanisms discussed, there are two possibilities: *i*) the concentration thus found has an osmotic pressure nearly equal to the applied pressure difference or *ii*) it is reasonable on physical grounds to designate this concentration as the gel concentration.

It is also possible to examine the probability of os-

otic pressure limitation by evaluating the value of the ratio $\Delta\Pi.n/(R_m.k)$. In that case data on mass transfer coefficient and osmotic pressure must be available. See Table 1 for values of $\Delta\Pi.n/(R_m.k)$ in the model calculation displayed in Figure 4.

TABLE 1

Ratio of osmotic resistance and membrane resistance, $\Delta\Pi.n/(R_m.k)$, calculated at $\Delta P = 10$ atm for the model calculation displayed in Figure 4. Reduction of the flux by osmotic pressure is the most severe for high flux membranes

R_m (10^5 atm.s/m)	$\Delta\Pi.n/(R_m.k)$	
	$c_b = 0.0003$	$c_b = 0.03$
0	∞	∞
1	86.22	95.30
5	7.12	15.54
10	0.17	5.83

We will summarize here the factors which lead to a high value of this ratio:

- a high permeate flux, i.e. a high applied pressure or a low membrane resistance;
- a high feed concentration;
- a low mass transfer coefficients, i.e. a low degree of mixing near the membrane surface or a small diffusion coefficient of the solute;
- a high exponent n , i.e. a macromolecular solute;
- a high value of the constant a , i.e. a low molecular weight of the solute (which will be counteractive through the diffusion coefficient and the exponent n).

From these factors it can be concluded that in ultrafiltration using solutes with molecular weights in medium (10,000 to 100,000 Daltons) and high (> 100,000 Daltons)

ranges the permeate flux may be limited by osmotic pressure. There are two additional considerations: *i*) the concentration c_m of a high molecular weight solute must be very high to give effective osmotic pressures and *ii*) the gel concentration of a high molecular weight solute will be low. These considerations make gel layer limitation more likely in ultrafiltration using high molecular weight solutes, whereas osmotic pressure limitation is expected in ultrafiltration using medium molecular weight solutes.

ACKNOWLEDGEMENT

The authors are indebted to M.J. van der Waal for stimulating discussions during the preparation of the manuscript.

SYMBOLS

a	constant defined by eq. (4) (atm)
c	solute concentration (weight fraction)
c_b	solute concentration in bulk of feed (weight fraction)
c_g	gel concentration of solute (weight fraction)
c_m	solute concentration at membrane surface (weight fraction)
J	ultrafiltration permeate flux (m/s)
J_{ps}	pure solvent flux (m/s)
k	mass transfer coefficient (m/s)
\bar{M}_n	number averaged molecular weight (Dalton)
n	exponent defined by eq. (4)
Pe	Péclet number
Re	Reynolds number
R_m	membrane resistance (atm.s/m)

- ΔP hydraulic pressure difference (atm)
 $\Delta \Pi$ osmotic pressure difference (atm)

REFERENCES

- [1] H.J. Bixler, L.M. Nelsen and L.W. Bluemle, Jr.,
Trans. Amer. Soc. Artif. Int. Organs, 14 (1968) 99.
- [2] W.F. Blatt, A. Dravid, A.S. Micheals and L.M. Nelsen,
in: *Membrane Science and Technology*, J.E. Flinn, ed.,
Plenum Press, New York, 1970.
- [3] A.A. Kozinski and E.N. Lightfoot, *AIChE Journal*, 17
(1971) 81.
- [4] R.L. Goldsmith, *Ind. Eng. Chem. Fundam.*, 10 (1971)
113.
- [5] P. Aptel and M. Clifton, *Ultrafiltration*, lecture
presented at the NATO Advanced Studies Institute on
Synthetic Membranes, Alcabideche, Portugal, 1983.
- [6] G. Jonsson, *Ultrafiltration of highly viscous solu-
tions*, lecture presented at the 4th Symposium on
Synthetic Membranes in Science and Industry,
Tübingen, Germany, 1983.
- [7] M.C. Porter, *Ind. Eng. Chem. Prod. Res. Develop.*,
11 (1972) 234.
- [8] P. Dejmek, *PhD Thesis*, Lund Institute of Technology,
Sweden, 1975.
- [9] P. G. des Gennes, *Scaling Concepts in Polymer Physics*,
Cornell University Press, Ithaca, 1979.
- [10] P.J. Flory, *Principles of Polymer Chemistry*, Cornell
University Press, Ithaca, 1953.
- [11] V.L. Vilker, C.K. Colton, K.A. Smith and D.L. Green,
J. Membrane Sci., in press.

HYDRODYNAMIC RESISTANCE OF CONCENTRATION POLARIZATION BOUNDARY LAYERS IN ULTRAFILTRATION

J.G. Wijmans, S. Nakao*, J.W.A. van den Berg, F.R.
Troelstra and C.A. Smolders

SUMMARY

The influence of concentration polarization on the permeate flux in the ultrafiltration of aqueous Dextran T70 solutions can be described by *i)* the osmotic pressure model and *ii)* the boundary layer resistance model. In the latter model the hydrodynamic resistance of the non-gelled boundary layer is computed using permeability data of the Dextran molecules obtained by sedimentation experiments. It is shown both in theory and in experiment that the two models are equivalent.

INTRODUCTION

In membrane filtration processes the permeate fluxes are smaller than the pure solvent fluxes in practically all cases. A number of phenomena has been suggested to account for this flux reduction: *i)* a decrease of the hydraulic driving force by an osmotic pressure, *ii)* the resistance of

*Present address: Institute of Industrial Science, University of Tokyo, 7-22-1 Roppongi, Minatoku, Tokyo 106, Japan.

the concentration polarization boundary layer, *iii*) the resistance of a gel layer, *iv*) an increase in membrane resistance by plugging of the pores and *v*) the resistance of an adsorption layer. When the membrane shows a perfect or almost perfect rejection of the solute(s) plugging of the pores will be negligible and for many nonprotein solutes adsorption at the membrane surface is practically absent. We will therefore concentrate in this paper on the first three of the phenomena mentioned above.

Theoretical considerations will show that in most ultrafiltration separation processes the phenomena (*i*) (osmotic pressure) and (*ii*) (resistance of concentration polarization boundary layer) are equivalent. This is checked by ultrafiltration experiments with Dextran T70 solutions. The resistance of the concentration polarization boundary layer (called boundary layer from now on) is calculated with the help of the solvent permeability of the Dextran molecules. Following Mijnlief and Jaspers [1] this permeability is determined by sedimentation experiments.

THEORY

Mass balance in the boundary layer

Due to the rejection of the solute at the membrane surface the solute concentration near that surface will increase. As a result of the concentration gradient so generated, solute molecules will diffuse away from the membrane surface. In a cross flow membrane filtration process a steady state is reached when the convection of solute molecules towards the membrane is equal to the diffusion of solute molecules back to the bulk of the solution, see Figure 1. When the rejection of the solute is 100% the solute molecules have a velocity relative to the membrane equal to zero. In a solute fixed or membrane fixed frame

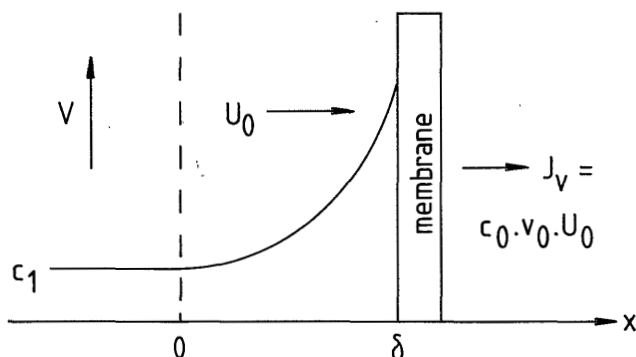


FIGURE 1. Schematic representation of the polarization phenomenon in a cross flow system. V is the axial bulk velocity and δ is the boundary layer thickness.

of reference the diffusion equation for the solvent reads:

$$c_0 U_0 = -D^1 \cdot \frac{dc_0}{dx} \quad (1)$$

where c_0 is the solvent concentration in g/ml, U_0 is the solvent velocity relative to the membrane, D^1 is the mutual diffusion coefficient in the solute fixed frame and x is the coordinate perpendicular to the membrane surface. The subscript 0 refers to the solvent, whereas the subscript 1 will refer to the solute. The diffusion coefficient is generally defined and measured within a mean-volume-velocity fixed frame of reference. If we denote the latter diffusivity as D , then the following relation exists (2):

$$D^1 = \frac{D}{c_1 \cdot v_1} \quad (2)$$

Since $c_0 \cdot v_0 + c_1 \cdot v_1 = 1$, where v is the specific volume in ml/g we have:

$$dc_0 = - \frac{v_1}{v_0} \cdot dc_1 \quad (3)$$

and since the permeate flow $J_v = c_0 \cdot v_0 \cdot U_0$, we rewrite eq. (1) as:

$$c_1 \cdot J_v = D \cdot \frac{dc_1}{dx} \quad (4)$$

Equation (4) is the well-known concentration polarization equation and the derivation given above clearly shows that the diffusion coefficient to be used in this equation is the volume fixed coefficient D.

Application of the film model for the mass transfer near the membrane surface gives the boundary conditions for eq. (4):

$$\begin{aligned} x = 0 & \quad ; \quad c_1 = c_b \\ x = \delta & \quad ; \quad c_1 = c_m \end{aligned} \quad (5)$$

The boundary layer thickness δ is the quotient of D and the mass transfer coefficient k. The value of the diffusion coefficient depends on concentration and hence it will vary over the boundary layer thickness and an averaged value for D must be used. Integration of eq. (4) under the condition that J_v is constant (steady state) yields:

$$c_m = c_b \cdot \exp(J_v/k) \quad (6)$$

Force balance in the boundary layer

Up to here, we have evaluated the mass balance of the boundary layer. In the stationary boundary layer there is also a force balance: the net force acting on each particle is zero. The solute molecules in the boundary layer

are subject to a thermodynamic force directed to the bulk of the solution due to their gradient in chemical potential. The force balance implies that the drag force exerted by the solvent flow on the solute molecules per gram of solute, F_1 , is equal to

$$F_1 = \frac{d\mu_1}{dx} = \frac{d\mu_1^C}{dx} + v_1 \cdot \frac{dP}{dx} \quad (7)$$

where μ is the chemical potential per gram, μ^C is the concentration part of the chemical potential and P is the hydraulic pressure. In eq. (7) it is assumed that only concentration and pressure gradients are present in the boundary layer. The balance of the drag forces yields for the drag force exerted by the solute molecules on the solvent flow per gram solvent, F_0 :

$$c_0 \cdot F_0 + c_1 \cdot F_1 = 0 \quad (8)$$

This drag force, F_0 , is balanced in turn by the force due to the chemical potential gradient of the solvent, so:

$$F_0 = \frac{d\mu_0}{dx} = \frac{d\mu_0^C}{dx} + v_0 \cdot \frac{dP}{dx} \quad (9)$$

The Gibbs-Duhem relation reads:

$$c_0 \cdot d\mu_0^C + c_1 \cdot d\mu_1^C = 0 \quad (10)$$

and inserting eq. (7) and (9) in eq. (8) and applying eq. (10) we obtain:

$$c_0 \cdot v_0 \cdot \frac{dP}{dx} + c_1 \cdot v_1 \cdot \frac{dP}{dx} = 0 \quad (11)$$

From eq. (11) it is clear that

$$\frac{dP}{dx} = 0 \quad (12)$$

which means that in the boundary layer there is no pressure drop. The solvent flow is subject to a hydrodynamic boundary layer resistance but the energy dissipation in this layer is exactly compensated by the decrease in the chemical potential of the solvent due to its concentration gradient. Eqs. (8) and (12) are valid only if the complete boundary layer has the properties of a Newtonian fluid. Viscoelastic behaviour in the boundary layer or formation of a gel layer will give rise to a pressure drop outside the membrane.

Dejmek [3] was the first to analyze the force balance in a concentration polarization layer, but he did not reach the conclusion that the pressure drop in the boundary layer is zero. Wales [4] showed clearly that $dP/dx = 0$ using an approach somewhat different from the one given by us. Wales restricts his analysis to laminar boundary layers. In his opinion there is no assurance that $dP/dx = 0$ in turbulent boundary layers where next to molecular diffusion also eddy diffusion is operative. Contrary to this view, we think that also in turbulent flow systems the pressure drop in the boundary layer is zero. We have two arguments for this: *i)* in the analysis given above no diffusion coefficient was used, and *ii)* in the film theory for mass transfer the boundary layer is evaluated as a stagnant layer with a thickness δ , which is determined by both the molecular and the eddy diffusivity.

Hydrodynamic resistance of the boundary layer

The boundary layer in ultrafiltration can be seen as a stagnant, concentrated polymer solution through which the solvent permeates. For polymer concentrations exceeding the 'overlap' concentration, where the individual domains of

the polymer molecules touch each other, the solvent molecules have to flow through the polymer coils. In more dilute solutions the solvent flow takes place mainly around the polymer coils. According to Mijnlief and Jaspers [1] the permeability of such a stagnant polymer solution can be calculated from a totally different experimental situation: sedimentation in an analytical ultracentrifuge cell. This follows from their analysis of the flow equations for sedimentation and permeation and they have obtained:

$$p = \frac{\eta_0 \cdot s}{c_1 \cdot (1 - v_1/v_0)} \quad (13)$$

where s is the sedimentation coefficient of the polymeric solute and η_0 is the dynamic viscosity of the solvent. The permeability p has been defined by Darcy [5] and remembering that in the boundary layer the osmotic pressure gradient is the driving force for the solvent flow, see Figure 2, we have:

$$J_v = \frac{p}{\eta_0} \cdot \frac{d\Pi}{dx} \quad (14)$$

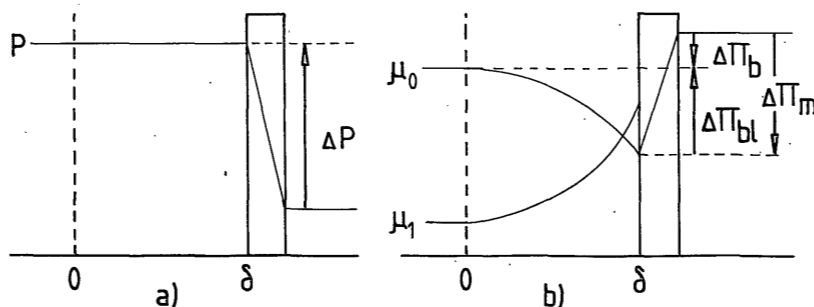


FIGURE 2. Gradients of pressure (a) and chemical potential (b) in and near the membrane in an ultrafiltration process.

Integration of eq. (14) over the thickness of the boundary layer yields:

$$J_v = \frac{\Delta \Pi_{bl}}{\eta_0 \int_0^{\delta} p^{-1} \cdot dx} \quad (15)$$

where $\Delta \Pi_{bl}$ is the osmotic pressure difference over the boundary layer. The permeability depends on the concentration and since there is a concentration profile in the boundary layer, the permeability will be a function of the coordinate x . Thus, the hydrodynamic resistance of the boundary layer, R_{bl} , is defined as:

$$R_{bl} = \int_0^{\delta} p(x)^{-1} \cdot dx \quad (16)$$

Expressions for the permeate flux

In the preceding sections we have shown that although the boundary layer is responsible for a hydrodynamic resistance, there is no drop in hydraulic pressure over the boundary layer. According to Figure 2 there are two different but equivalent ways to describe the permeate volume flux:

$$J_v = \frac{1}{\eta_0} \cdot \frac{\Delta P - \Delta \Pi_m}{R_m} \quad (17)$$

and

$$J_v = \frac{1}{\eta_0} \cdot \frac{\Delta P - \Delta \Pi_b}{R_m + R_{bl}} \quad (18)$$

ΔP is applied hydraulic pressure difference and R_m is the

membrane resistance. $\Delta\Pi_b$ and $\Delta\Pi_m$ are osmotic pressure differences due to differences in the chemical potential:

$$d\Pi = -\frac{1}{v_0} \cdot d\mu^c \quad \text{or} \quad \Delta\Pi = -\frac{1}{v_0} \cdot \Delta\mu_0^c \quad (19)$$

A relation that can be obtained from eqs. (17) and (18) is:

$$J_v = \frac{1}{\eta_0} \cdot \frac{\Delta\Pi_{b1}}{R_{b1}} \quad (20)$$

Eq. (20) is identical with eq. (15) and holds for every steady-state boundary layer. In contrast with the eqs. (17) and (18), eq. 20 is not suited for the calculation of the permeate flux since it is not an independent relation. We will return to this in the following section.

In most ultrafiltration applications the osmotic pressure difference between the bulk of the feed solution and the permeate will be very small, so

$$\Delta\Pi_b \ll \Delta\Pi_{b1} \quad \text{and} \quad \Delta\Pi_b \ll \Delta P \quad \text{and} \quad \Delta\Pi_m \approx \Delta\Pi_{b1} \quad (21)$$

According to eq. (21) we can rewrite eq. (18) as follows:

$$J_v \approx \frac{1}{\eta_0} \cdot \frac{\Delta P}{R_m + R_{b1}} \quad (22)$$

Eq. (22) represents the 'boundary layer resistance' model while eq. (17) is the representative of the 'osmotic pressure' model. They both hold for a non gel polarized situation. If gel formation does occur, the resistance of the gel layer must be added to the membrane resistance in the equations (17), (18) and (22). It is emphasized here that if one uses the osmotic pressure model, one implicitly assumes that $dP/dx = 0$ in the boundary layer.

Relationship between permeation, diffusion and osmotic pressure

Comparing eq. (4) with eq. (14) we see that there must exist a relationship between diffusivity, permeability and the dependency of the osmotic pressure on concentration. The relation between sedimentation and diffusion is given by the Svedberg equation (6):

$$D = \frac{s \cdot c_1}{(1-v_1 \cdot \rho)} \cdot \frac{d\mu_1^c}{dc_1} \quad (23)$$

Here, ρ is the density of the solution ($\rho = c_0 + c_1$). With the help of eqs. (10) and (19) and using

$$(1-v_1 \cdot \rho) = v_0 \cdot c_0 \cdot (1-v_1/v_0) \quad (24)$$

we obtain

$$D = \frac{s}{(1-v_1/v_0)} \cdot \frac{d\Pi}{dc_1} \quad (25)$$

Substitution of eq. (13) into eq. (25) yields:

$$D = \frac{c_1 \cdot P}{\eta_0} \cdot \frac{d\Pi}{dc_1} \quad (26)$$

This relation between diffusivity and permeability makes the equations (4) and (14) equivalent. Mijnlieff and Jaspers [1] previously pointed out that there is one basic phenomenological relation which describes permeation, sedimentation and diffusion, and equation (26) is the result of this connection. The interdependency of permeability and diffusion coefficient has also been investigated by McDonnell and Jamieson [7]. The expression obtained by them differs

from our equation (26) by a factor $\rho \cdot v_0$, which originates from the fact that they have used the diffusion equation of the mass fixed reference frame instead of the volume fixed reference frame.

EXPERIMENTS

Ultrafiltration

The ultrafiltration experiments were carried out in a thin channel cell using solutions of Dextran T70 (Pharmacia, $M_n = 36,200$ and $M_w = 70,300$) in water (ultrafiltered, demineralized) as the feed. The cell has an effective membrane width of 60 mm and a channel height of 5.9 mm. The membrane area length is 100 mm and the length of the entrance region is 250 mm. The membranes used are Kalle Polysulfone membranes of the Nadir type. The experimental setup is shown in Figure 3 and the experimental procedure is as follows:

- 1) The membrane is compacted at $\Delta P = 600$ kPa for at least 50 hours in order to obtain a time independent water flux;
- 2) The pure water flux is measured at three different pressures and at three different bulk velocities;
- 3) A certain amount of concentrated Dextran T70 solution is added to the system, after which the system is given 60 minutes to mix;
- 4) The permeate flux is measured at three different pressures (lowest pressure difference first) 15 minutes after the pressure has been set;
- 5) Step 4 is carried out for three different axial bulk velocities (highest velocity first);
- 6) The sequence of steps 3-5 is repeated twice, so the permeate flux is measured at three different bulk concentrations (lowest concentration first).

The solute concentration in the feed and the permeate

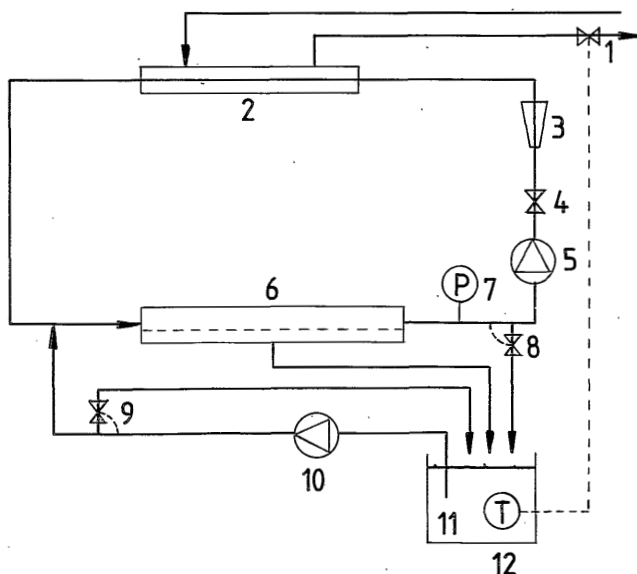


FIGURE 3. Schematic representation of the ultrafiltration device. 1: valve cooling water; 2: heat exchanger; 3: flow meter; 4: valve; 5: recirculation pump; 6: filtration cell; 7: manometer; 8: back pressure valve; 9: back pressure valve; 10: injection pump; 11: feed stock solution; 12: thermistor.

were measured by a Beckman model 915A Total Organic Carbon Analyzer. The temperature was maintained at 25 °C in all experiments.

Osmotic pressure

Although the ultrafiltration experiments were carried out using Dextran T70 as the solute, the investigations into the properties of Dextran solutions were performed using both Dextran T70 and Dextran T500 (Pharmacia, $M_n = 119,500$ and $M_w = 465,000$). In all cases the experiments with T70 were performed at 25 °C and those with T500 at 20 °C. The osmotic pressure of the Dextran solutions relative to pure

water was measured with a high pressure osmometer (8). The membranes used in the osmometer were Sartorius 'allerfeinst'.

Sedimentation coefficient

Sedimentation experiments were performed with a Beckman-Spinco model E Analytical Ultracentrifuge. The sedimentation coefficients were determined at different concentrations from the displacement of the maximum of the concentration gradient curve.

In order to calculate the permeability from the sedimentation coefficient, the specific volume of the Dextran in water has to be known. This quantity was calculated from the slope of the solution density versus concentration plot. Densities were measured with a Paar Digital Precision Density Meter model DMA 50.

Diffusion coefficient

The diffusion coefficients were determined by the boundary layer broadening method using a synthetic boundary cell of the ultracentrifuge mentioned above. The concentration difference at the boundary at the beginning of each experiment was maximally 0.026 g/ml and smaller than 0.01 g/ml in most cases. The concentrations mentioned further on are the mean concentrations. The diffusion coefficients obtained with this kind of experiment are the volume fixed diffusion coefficients.

RESULTS AND DISCUSSION

Osmotic pressure

The osmotic pressure data for both Dextran T70 and T500

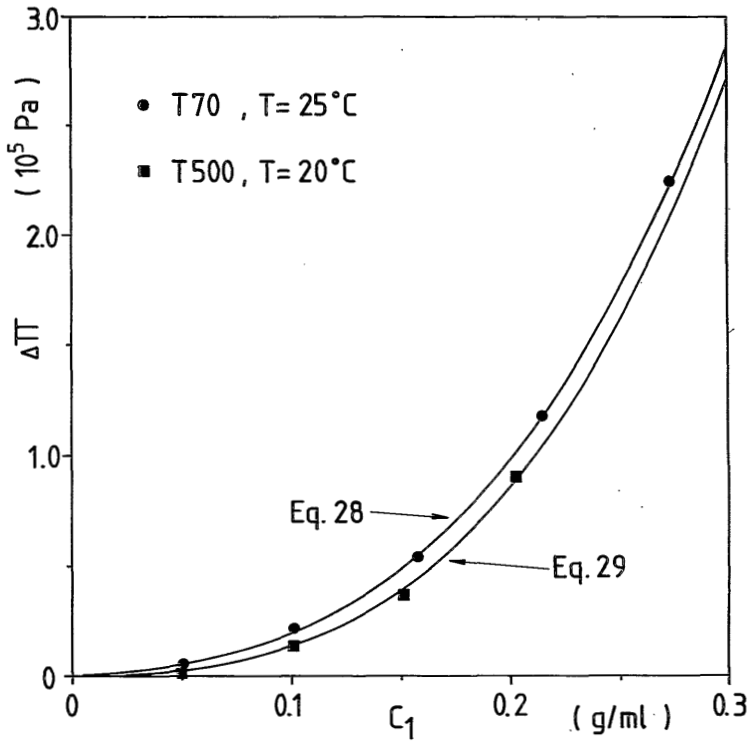


FIGURE 4. Osmotic pressure of Dextran solutions relative to pure water.

are given in Figure 4. The osmotic pressure in a broad concentration range is conveniently represented by the general form [9]:

$$\Delta\Pi = A_1 \cdot c_1 + A_2 \cdot c_1^2 + A_3 \cdot c_1^3 \quad (27)$$

A least squares fit to the experimental data of Figure 4 gives:

$$\text{T70 : } \Delta\Pi = 0.375 c_1 + 7.52 c_1^2 + 76.4 c_1^3 \quad (10^5 \text{ Pa}) \quad (28)$$

$$\text{T500: } \Delta\Pi = 0.0867 c_1 + 2.98 c_1^2 + 89.8 c_1^3 \quad (10^5 \text{ Pa}) \quad (29)$$

According to van 't Hoff's law the coefficient A_1 of eq. (27) must be equal to $R.T/M_n$. The value of $R.T/M_n$ is 0.684 and 0.204 (10^5 Pa.ml/g) for T70 and T500 respectively, so there is a substantial deviation. The origin for this deviation is probably that the osmotic experiments were carried out with concentrations larger than 0.05 g/ml. Eq. (27) reduces to the van 't Hoff law in very dilute solutions only. Since we are interested in the osmotic pressure of more concentrated solutions, the equations (28) and (29) are used to express the concentration dependence of $\Delta\Pi$. From Figure 4 it is clear that the influence of M_n on the osmotic pressure is relatively small for concentrated solutions.

Sedimentation coefficient

The sedimentation coefficients for T70 are plotted in Figure 5 together with literature data on T70 [10] and T500 [11]. The experiment with T70 at a temperature of 20 °C indicates that the sedimentation coefficient only slightly depends on the temperature. Consistent with this observation is the fact that the sedimentation coefficients of T70 and T500, measured at 25 °C and 20 °C respectively, are identical for concentrations larger than 0.04 g/ml. The latter concentration is the overlap concentration of the Dextran T70 in water. The data of Brown *et al.* [10] were measured with a Dextran T70 fraction with $M_n = 44,000$ and $M_w = 64,000$ and they agree very well with our experiments.

The concentration dependence of the sedimentation coefficient is usually expressed as:

$$\frac{1}{s} = \frac{1}{s_0} \cdot (1 + K_1 \cdot c_1 + K_2 \cdot c_1^2) \quad (30)$$

The coefficients s_0 and K_1 have been determined as a function of the molecular weight M_w of Dextran fractions

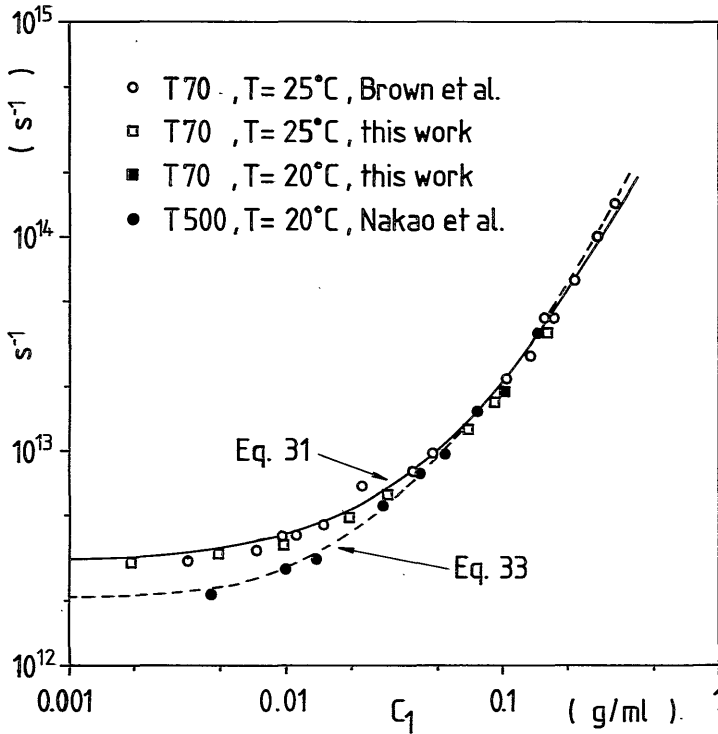


FIGURE 5. Sedimentation coefficients of Dextran in water.

by a number of authors [12-14]. Using these values, a least squares fit to the experimental data gives the value for the coefficient K_2 :

$$T70 : \frac{1}{s} = \frac{1}{3.3 \cdot 10^{-13}} \cdot (1 + 32.0 c_1 + 258.0 c_1^2) \quad (s^{-1}) \quad (31)$$

$$T500 : \frac{1}{s} = \frac{1}{8.5 \cdot 10^{-13}} \cdot (1 + 106.0 c_1 + 617.0 c_1^2) \quad (s^{-1}) \quad (32)$$

In the fitting procedure the data obtained at concentrations larger than 0.04 g/ml have been used for both Dextran fractions. Eq. (31) is quite satisfactory as appears from Figure 5. Eq. (32) agrees well with the experimental data

for concentrations larger than 0.02 g/ml. However, at lower concentrations there is a significant difference and therefore the least squares method was applied to obtain values for all three coefficients:

$$T500: \frac{1}{s} = \frac{1}{5.06 \cdot 10^{-13}} \cdot (1 + 43.2 c_1 + 500.8 c_1^2) \quad (s^{-1}) \quad (33)$$

The partial specific volume of T70 and T500 in water appears to be concentration independent in the experimental concentration range (up to 0.3 g/ml) and has a value of 0.644 ml/g ($T = 25^\circ\text{C}$) and 0.625 ml/g ($T = 20^\circ\text{C}$) respectively.

Diffusion coefficient

The diffusion coefficient of T70 and T500 is given in Figure 6. For Dextran T70 data obtained by Clifton [15] are included. Clifton used the following relation to express his data:

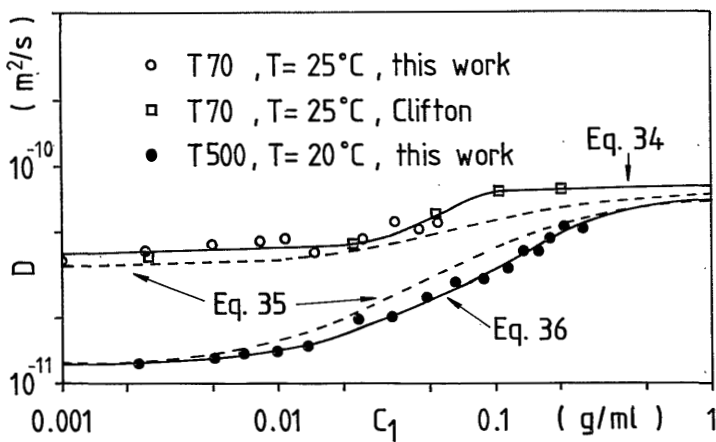


FIGURE 6. Mutual diffusion coefficients of Dextran and water.

$$T70: D = 5.96 \cdot 10^{-11} + 2.12 \cdot 10^{-11} \cdot \tanh(28.4 c_1 - 1.491) \quad (\text{m}^2/\text{s}) \quad (34)$$

and eq. (34) agrees well with our results.

Since we performed osmotic and sedimentation experiments we are able to calculate diffusion coefficients through the Svedberg equation. Combining eqs. (25), (27) and (30) we obtain:

$$D = \frac{s_0 \cdot (A_1 + 2 \cdot A_2 \cdot c_1 + 3 \cdot A_3 \cdot c_1^2)}{(1 - v_1/v_0) \cdot (1 + K_1 \cdot c_1 + K_2 \cdot c_1^2)} \quad (35)$$

The broken lines in Figure 6 are calculated with eq. (35). Although the calculated and experimental values do not match exactly, we think the agreement is remarkable. Eq. (35) predicts the right order of magnitude of the diffusion coefficient and fairly well represents its concentration dependence.

The diffusion data for the Dextran T500 cannot be described by a formula similar to eq. (34). A least squares fit to the data using a second order or a third order polynomial gives anomalous results for high concentrations: the diffusion coefficient decreases (second order) respectively increases (third order) very rapidly at concentrations exceeding 0.5 g/ml. In view of the results for Dextran T70 and of the curves drawn according to eq. (35), we think this is very improbable. Therefore we suggest the following relation to represent the diffusion data of the Dextran T500:

$$T500: D = 1.204 \cdot 10^{-11} + 2.614 \cdot 10^{-10} c_1 - 4.167 \cdot 10^{-10} c_1^2 + 2.132 \cdot 10^{-10} c_1^3 \quad (\text{m}^2/\text{s}) \quad (36)$$

Eq. (36) is obtained by a least squares fit to the experimental data extended with two points calculated by means of

eq. (35): $D = 6.5 \cdot 10^{-11} \text{ m}^2/\text{s}$ at $c_1 = 0.5 \text{ g/ml}$ and $D = 7.0 \cdot 10^{-11} \text{ m}^2/\text{s}$ at $c_1 = 1.0 \text{ g/ml}$.

Ultrafiltration

The permeate flux versus applied pressure data obtained with the ultrafiltration experiments are represented in Figure 7. The permeate flux increases with increasing pressure although the slope of the J_v versus ΔP curve decreases. The slope does not become zero ('limiting flux') under the circumstances studied. Furthermore, the permeate flux decreases with an increasing bulk concentration and with a decreasing axial bulk velocity. All this is in full accordance with the osmotic pressure model for ultrafiltration [16]. The rejection of the T70 molecules by the membrane decreased with increasing pressure, with an increasing bulk concentration and with a decreasing axial velocity. The

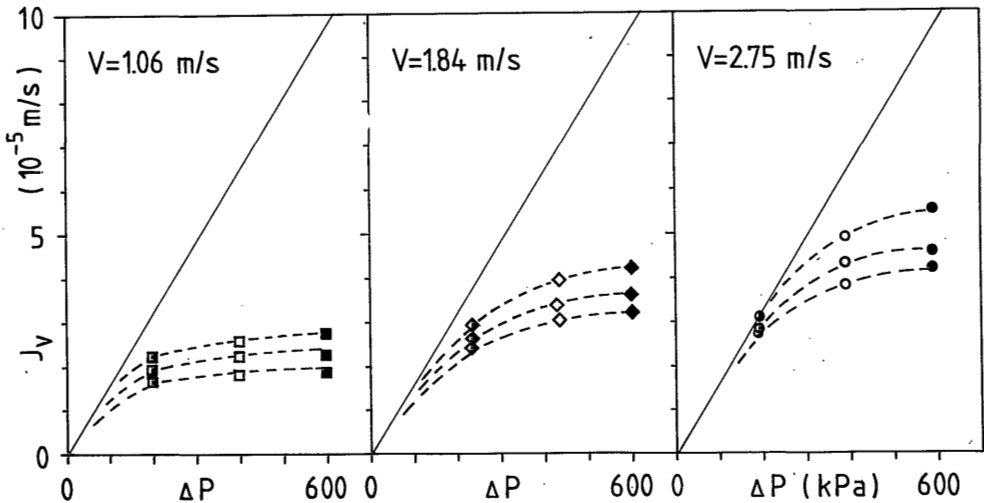


FIGURE 7. Ultrafiltration permeate fluxes as a function of applied pressure, axial bulk velocity and bulk concentration. The bulk concentrations are 0.000430, 0.000935 and 0.00142 g/ml. —: pure water flux.

lowest rejection value was 96% and the rejection was higher than 98% in all but three experiments.

The pure water flux increased linearly with ΔP and thus the membrane resistance was independent of the applied pressure and did not vary with the axial velocity. This indicates that fouling of the membrane by the ultrafiltered water did not occur and that R_m has a constant value of $6.94 \cdot 10^{12} \text{ m}^{-1}$.

Resistance of the boundary layer

The resistance of the boundary layer can be computed from Figure 7 using eq. (22). This experimental value for R_{bl} , denoted R_{bl}^{exp} , will be compared with the value calculated with eq. (16) and using the sedimentation and diffusion data. The expression for this R_{bl}^{calc} is derived as follows.

According to eq. (13) and (30) we express the permeability of the dissolved Dextran molecules as:

$$p(c_1) = \frac{\eta_0 \cdot s_0}{(1-v_1/v_0) \cdot (c_1 + K_1 \cdot c_1^2 + k_2 \cdot c_1^3)} \quad (37)$$

The concentration of the solute in the boundary layer is a function of the coordinate x and since the rejection is almost 100% we write, see eq. (6):

$$c_1(x) = c_b \cdot \exp(J_v \cdot x/D) \quad (38)$$

Substitution of eq. (38) into eq. (37) yields:

$$p(x)^{-1} = \frac{1-v_1/v_0}{\eta_0 \cdot s_0} \cdot [c_b \cdot \exp(J_v \cdot x/D) + K_1 \cdot c_b^2 \cdot \exp(2 \cdot J_v \cdot x/D) + K_2 \cdot c_b^3 \cdot \exp(3 \cdot J_v \cdot x/D)] \quad (39)$$

The quantity $p(x)^{-1}$ must be integrated over the boundary layer thickness δ and since

$$c_b^n \cdot \int_0^\delta \exp(n \cdot J_v \cdot x/D) \cdot dx = \frac{D}{J_v \cdot n} \cdot c_b^n (\exp(n \cdot J_v/k) - 1)$$

$$= \frac{D}{J_v \cdot n} \cdot (c_m^n - c_b^n) \quad (40)$$

we obtain

$$R_{bl}^{calc} = \int_0^\delta p(x)^{-1} \cdot dx = \frac{D}{J_v} \cdot \frac{1 - v_1/v_0}{\eta_0 \cdot s_0} \cdot [c_m - c_b + \frac{K_1}{2} \cdot (c_m^2 - c_b^2)$$

$$+ \frac{K_2}{3} \cdot (c_m^3 - c_b^3)] \quad (41)$$

Combining eqs. (41), (6) and (22) we obtain a relation in which the permeate flux J_v is the single unknown parameter. In this way J_v can be calculated if the process conditions (ΔP , R_m , c_b and k) and the physical properties of the solute-solvent system (s and D) are known.

Values for the mass transfer coefficient k are obtained in the following way. With the help of eq. (17) the osmotic pressure difference over the membrane is calculated from the permeate flux data. The results are given in Table I. From $\Delta \Pi_m$ and the osmotic pressure data the value of c_m is computed. The maximum value for c_m appears to be 0.364 g/ml (Table I) and since Dextran T70 - water mixtures with concentrations up to 0.7 g/ml are fluid, we conclude that in all experiments reported here no gel layer has been formed.

Using eq. (6) and the c_m values given in Table I the apparent mass transfer coefficient k^{app} can be calculated. In Figure 8 this k^{app} is compared with the mass transfer coefficient k as obtained from the Deissler equation for

TABLE I

V (m/s)	c_b (10^{-3} g/ml)	ΔP (10^5 Pa)	J_V (10^{-5} m/s)	$\Delta \Pi_m$ (10^5 Pa)	c_m (g/ml)	kapp (10^{-5} m/s)	R_{bl}^{exp} (10^{12} m $^{-1}$)	R_{bl}^{calc} (10^{12} m $^{-1}$)	J_{V}^{calc} (10^{-5} m/s)
1.06	0.430	2	2.33	0.56	0.159	0.394	2.65	2.70	2.32
		4	2.78	2.33	0.278	0.417	9.66	9.62	2.71
		6	2.83	4.25	0.348	0.422	16.7	16.5	2.84
	0.935	2	2.06	0.73	0.177	0.394	3.94	3.91	2.06
		4	2.33	2.56	0.288	0.408	12.2	12.1	2.35
		6	2.39	4.52	0.356	0.403	21.2	20.9	2.41
1.420	1.420	2	1.78	0.91	0.194	0.361	5.64	5.68	1.77
		4	1.92	2.82	0.300	0.358	16.4	16.3	1.93
		6	1.97	4.80	0.364	0.356	27.1	26.9	1.99
	0.430	2	2.92	0.18	0.098	0.536	0.729	0.786	2.90
		4	4.00	1.50	0.235	0.633	4.24	4.23	4.00
		6	4.33	3.31	0.317	0.656	8.55	8.45	4.36
0.935	0.935	2	2.67	0.33	0.128	0.542	1.45	1.47	2.65
		4	3.44	1.86	0.255	0.614	6.05	6.01	3.46
		6	3.67	3.71	0.331	0.625	11.4	11.2	3.69
	1.420	2	2.44	0.46	0.147	0.528	2.21	2.19	2.44
		4	3.08	2.08	0.267	0.589	7.57	7.53	3.10
		6	3.22	4.00	0.340	0.589	13.9	12.6	3.25
2.75	0.430	2	3.11	0.05	0.051	0.650	0.250	0.244	3.11
		4	4.92	0.95	0.197	0.803	2.16	2.14	4.92
		6	5.56	2.55	0.288	0.853	5.14	5.08	5.57
	0.935	2	2.86	0.23	0.109	0.600	0.878	0.958	2.83
		4	4.33	1.31	0.223	0.792	3.38	3.38	4.35
		6	4.61	3.14	0.311	0.794	7.61	7.49	4.64
1.420	2	2.75	0.30	0.123	0.617	1.19	1.26	2.72	
	4	3.86	1.60	0.241	0.753	4.65	4.56	3.88	
	6	4.22	3.37	0.319	0.781	8.95	8.90	4.26	

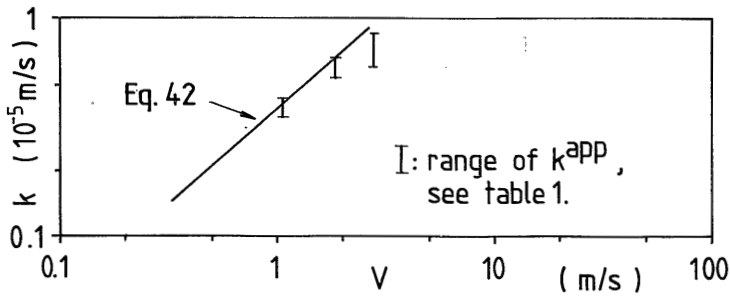


FIGURE 8. Apparent and calculated mass transfer coefficients.
 —: Deissler equation.

turbulent systems:

$$k = 0.023 \frac{D}{d_h} \cdot \left(\frac{V \cdot d_h \cdot \rho_0}{\eta_0} \right)^{0.875} \cdot \left(\frac{\eta_0}{\rho_0 \cdot D} \right)^{0.25} \quad (42)$$

where $d_h = 10.74$ mm is the hydraulic diameter of the thin channel cell and V is the axial bulk velocity. The diffusion coefficient used is the D of the bulk solution which is equal to $4 \cdot 10^{-11}$ m²/s, see Figure 6. The reason why eq. (42) predicts too high values for the mass transfer coefficient is in our opinion that no account has been made for the increase in viscosity in the boundary layer, nor for the effect of the permeate flux on the boundary layer.

The k^{app} values are used to calculate the permeate flux and the result, J_v^{calc} , is displayed in the last column of Table I. The averaged value of $D = 6 \cdot 10^{-11}$ m²/s has been used in this calculation. In Figure 9 the value of J_v^{calc} is plotted as a function of J_v . The value of J_v is calculated with eq. (22) and thus by neglecting the osmotic pressure of the bulk solution. The osmotic pressure data show that this approach is valid. As can be seen from Figure 9 the correlation between J_v^{calc} and J_v is excellent. In the calculation procedure also the values for the boundary layer

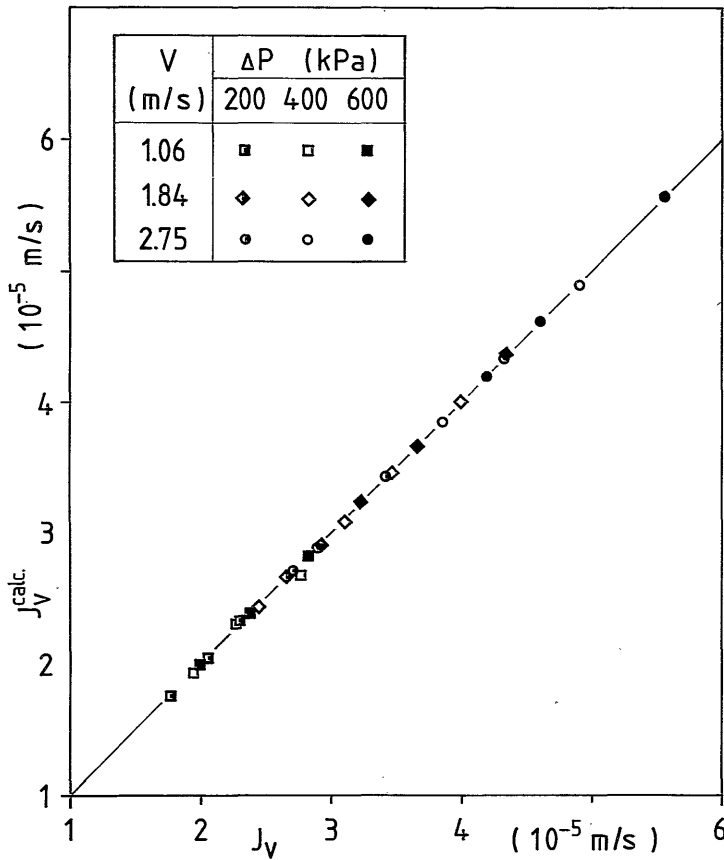


FIGURE 9. Permeate flux calculated from eqs. (41), (6) and (22), J_V^{calc} as a function of the experimental permeate flux J_V .
 —: $J_V^{\text{calc}} = J_V$.

resistance R_{bl}^{calc} are obtained and in Table I these values are compared with R_{bl}^{exp} . The correlation is very good for R_{bl} values varying more than two orders of magnitude, which in view of the close agreement of J_V and J_V^{calc} was expected. These results imply that the approach of calculating the resistance of the boundary layer with aid of the permeability of the Dextran molecules works well. This was already predicted in the theory section. In general one can say that the stationary boundary layer in ultrafiltration can be seen as a diffusion-permeation equilibrium.

CONCLUSIONS

The permeate flux in ultrafiltration applications is smaller than the pure solvent flux due to the formation of a concentration polarization boundary layer. The effect of this concentrated but still fluid boundary layer can be represented in two different ways: *i*) by a reduction of the driving force by an osmotic pressure (the osmotic pressure model), and *ii*) by an increase of the total resistance due to the resistance of the boundary layer (the resistance model). It is shown that these two approaches are essentially equivalent and that the resistance of the boundary layer can be computed with the solvent permeability of the macromolecular solute.

SYMBOLS

A_i	coefficient in eq. (27), $i=1,2,3$ ($\text{Pa}\cdot\text{ml}^i/\text{g}^i$)
c_0	solvent concentration (g/ml)
c_1	solute concentration (g/ml)
c_b	solute concentration in bulk (g/ml)
c_m	solute concentration at membrane surface (g/ml)
d_h	hydraulic diameter (m)
D	diffusion coefficient in volume fixed frame (m^2/s)
D^1	diffusion coefficient in solute fixed frame (m^2/s)
F_0	drag force on solvent (N/g)
F_1	drag force on solute (N/g)
J_v	permeate volume flux (m/s)
J_v^{calc}	J_v from eqs. (6), (22) and (41) (m/s)
k	mass transfer coefficient (m/s)
K_i	coefficient in eq. (30), $i=1,2$ (ml^i/g^i)
M_n	number averaged molecular weight (Dalton)
M_w	weight averaged molecular weight (Dalton)
p	solvent permeability of the solute (m^2)
R	gas constant (J/mol.K)

R_{bl}	resistance of boundary layer (m^{-1})
R_{bl}^{calc}	R_{bl} from eqs. (6), (22) and (41) (m^{-1})
R_{bl}^{exp}	R_{bl} from eq. (22) and flux data (m^{-1})
R_m	resistance of membrane (m^{-1})
s	sedimentation coefficient of the solute (s)
s_0	s at infinite dilution (s)
T	temperature (K) or ($^{\circ}C$)
U_0	velocity of solvent relative to the membrane (m/s)
v_0	partial specific volume of the solvent (ml/g)
v_1	partial specific volume of the solute (ml/g)
V	axial bulk velocity (m/s)
x	coordinate perpendicular to the membrane surface (m)
δ	thickness of boundary layer (m)
ΔP	hydraulic pressure difference (Pa)
$\Delta \Pi$	osmotic pressure difference (Pa)
$\Delta \Pi_b$	$\Delta \Pi$ of bulk solution relative to permeate (Pa)
$\Delta \Pi_{bl}$	$\Delta \Pi$ over boundary layer (Pa)
$\Delta \Pi_m$	$\Delta \Pi$ over membrane (Pa)
μ_0	chemical potential of the solvent (N/m.g)
μ_0^c	concentration part of μ_0 (N/m.g)
μ_1	chemical potential of the solute (N/m.g)
μ_1^c	concentration part of μ_1 (N/m.g)
η_0	viscosity of the solvent (Pa.s)
ρ	solution density (g/ml)
ρ_0	density of the solvent (g/ml)

REFERENCES

- [1] P.F. Mijnlief and W.J.M. Jaspers, *Trans. Faraday Soc.*, 67 (1971) 6 1837.
- [2] S.R. de Groot and P. Mazur, *Non-equilibrium Thermodynamics*, pp. 251, North-Holland Publishing Company,

Amsterdam, 1962.

- [3] P. Dejmek, *PhD Thesis*, Lund Institute of Technology, 1975.
- [4] M. Wales, *ACS Symposium Series*, 154 (1981) 159.
- [5] H. Darcy, *Les fontaines publiques de la ville de Dijon*, 1856.
- [6] T. Svedberg and K.O. Pedersen, *The Ultracentrifuge*, Clarendon Press, Oxford, 1940.
- [7] M.E. McDonnell and A.M. Jamieson, *J. Polym. Sci. Polym. Phys. Ed.*, 18 (1980) 1781.
- [8] F.W. Altena, *PhD Thesis*, Twente University of Technology, Enschede, 1982.
- [9] P.J. Flory, *Principles of Polymer Chemistry*, pp. 531, Ithaca, 1953.
- [10] W. Brown, P. Stilbs and R.M. Johnsen, *J. Polym. Sci. Polym. Phys. Ed.*, 20 (1982) 1771.
- [11] S. Nakao, J.G. Wijmans and C.A. Smolders, will be submitted to *J. Membrane Sci.*
- [12] F.R. Senti, N.N. Hellman, N.H. Ludwig, G.E. Babbcock, R. Tobin, C.A. Glass and B.L. Lamberts, *J. Polym. Sci.*, 17 (1955) 527.
- [13] A.G. Ogston and E.F. Woods, *Trans. Faraday Soc.*, 50 (1954), 635.
- [14] J.W. Williams and W.M. Saunders, *J. Phys. Chem.*, 58 (1954) 854.
- [15] M.J. Clifton, *PhD Thesis*, Université Paul Sabatier, Toulouse, France, 1982.
- [16] J.G. Wijmans, S. Nakao and C.A. Smolders, *J. Membrane Sci.*, 20 (1984) 115.

THE MASS TRANSFER COEFFICIENT IN ULTRAFILTRATION

INTRODUCTION

In a previous paper [1] we reported on a study concerning the permeate flux behaviour in the ultrafiltration of aqueous Dextran T70 solutions. Using the osmotic pressure model we were able to calculate the apparent mass transfer coefficients, k^{app} , and these were compared with the coefficients, K^{D} , obtained through the Deissler equation for mass transfer. The ratio $k^{\text{app}}/k^{\text{D}}$ varies from 0.65 to 1.05 if k^{D} is calculated on the basis of bulk solution properties.

There are a number of factors which may be responsible for the observation that k^{app} is not equal to k^{D} :

i) the influence of the concentration dependence of the diffusion coefficient and the viscosity of the Dextran T70-water system on the mass transfer. A hundred fold increase in macrosolute concentration in the boundary layer is not uncommon.

ii) The influence of the permeate flux through the boundary layer on the mass transfer in that layer.

In this appendix we will analyze the ratio $k^{\text{app}}/k^{\text{D}}$ with respect to these factors.

EFFECT OF VARYING DIFFUSION COEFFICIENT AND VISCOSITY

The mutual diffusion coefficient of the system Dextran T70 - water, D , increases with the Dextran T70 concentration [1]. At very low concentrations the value for D is about $4 \cdot 10^{-11} \text{ m}^2/\text{s}$ and in very concentrated solutions the value is about $8 \cdot 10^{-11} \text{ m}^2/\text{s}$. This implies that mass transfer is enhanced if the average Dextran T70 concentration in the boundary layer increases.

The viscosity of the solution increases with the Dextran concentration [2] as is seen in Figure 1. An increase in viscosity will hamper the mass transfer, so the concentration polarization is responsible for two effects which are counteractive:

- i*) an increase in mass transfer due to an increase in diffusivity;
- ii*) a decrease in mass transfer due to an increase in viscosity.

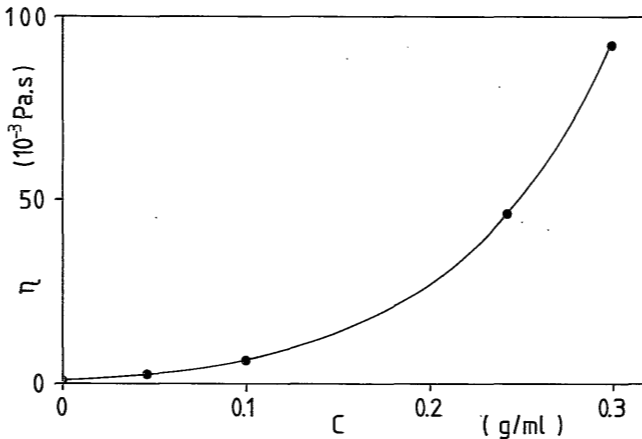


FIGURE 1. Kinematic viscosity, η , of aqueous Dextran T70 solutions as a function of the Dextran concentration, c (2). Temperature: 25 °C.

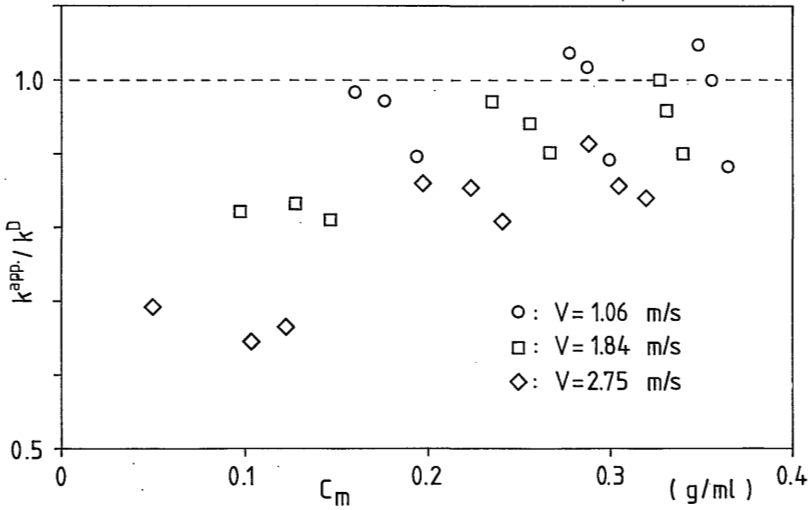


FIGURE 2. Ratio of mass transfer coefficient calculated from the experiments and calculated from the Deissler equation, k^{app}/k^D , as a function of the Dextran T70 concentration at the membrane surface, c_m .

In Figure 2 the ratio k^{app}/k^D is plotted as a function of c_m , the Dextran T70 concentration at the membrane surface. The data on which Figure 2 is based, are given in Table 1. Since the bulk concentrations c_b are negligible compared to c_m , the latter value is indicative for the average concentration in the boundary layer. As can be seen there is hardly any correlation between k^{app}/k^D and c_m : at constant c_m the variation in k^{app}/k^D is at least 25%. This implies that the use of a correction factor based on the value of c_m (analogous to the viscosity correction proposed by Sieder and Tate [3] for heat transfer) is not feasible.

TABLE 1

This table is based on Table 1 of reference 1.

V (m/s)	c_b (10^{-3} g/ml)	ΔP (10^5 Pa)	J_v (10^{-5} m/s)	c_m (g/ml)	k^{app}/k^D (-)	J_v/V (10^{-5})
1.06	0.430	2	2.33	0.159	0.979	2.01
		4	2.78	0.278	1.034	2.32
		6	2.83	0.348	1.048	2.44
	0.935	2	2.06	0.177	0.972	1.77
		4	2.33	0.288	1.014	2.01
		6	2.39	0.356	1.000	2.06
	1.420	2	1.78	0.194	0.897	1.53
		4	1.92	0.300	0.890	1.65
		6	1.97	0.364	0.883	1.70
1.84	0.430	2	1.92	0.098	0.821	1.59
		4	4.00	0.235	0.970	2.17
		6	4.33	0.317	1.004	2.36
	0.935	2	2.67	0.128	0.830	1.45
		4	3.44	0.255	0.940	1.87
		6	3.67	0.331	0.957	1.99
	1.420	2	2.44	0.147	0.809	1.33
		4	3.08	0.267	0.902	1.68
		6	3.22	0.340	0.902	1.75
2.75	0.430	2	3.11	0.051	0.693	1.13
		4	4.92	0.197	0.863	1.79
		6	5.56	0.288	0.916	2.02
	0.935	2	2.86	0.109	0.645	1.04
		4	4.33	0.223	0.851	1.58
		6	4.61	0.311	0.854	1.68
	1.420	2	2.75	0.123	0.663	1.00
		4	3.86	0.241	0.809	1.40
		6	4.22	0.317	0.839	1.54

EFFECT OF PERMEATE FLUX

The permeate flux is responsible for the convection of the not permeating solute towards the membrane surface and thus for the increased solute concentration in the boundary

layer. Taking into account this convective flow [4] and using the film model for the mass transfer near the membrane surface, the concentration polarization can be calculated. However, it is possible that the permeate flux changes the hydrodynamics in the boundary layer and this will then be reflected in a change in the effective mass transfer coefficient.

In Figure 3 the ratio k^{app}/k^D is given as a function of the permeate volume flux, J_v . The points, which were so widely scattered in Figure 2, now fall on three distinct curves, one curve for each axial bulk velocity, V . In Figure 4 the ratio k^{app}/k^D is displayed as a function of J_v/V , the ratio of the permeate flux and the axial velocity. In this plot there seems to be a master curve on which all points lie within an accuracy of 10%.

The influence of a "suction" or "transpiration" flow on the mass transfer has been studied by Johnson *et al.* [5],

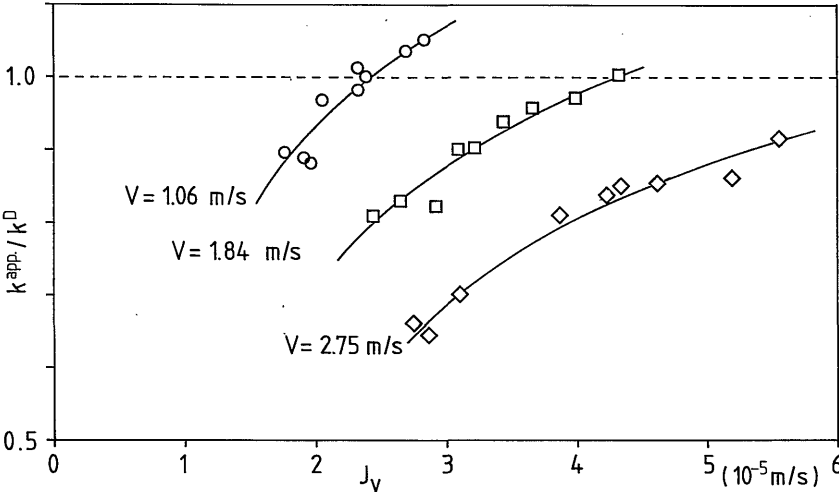


FIGURE 3. The ratio k^{app}/k^D plotted as a function of the permeate volume flux, J_v .

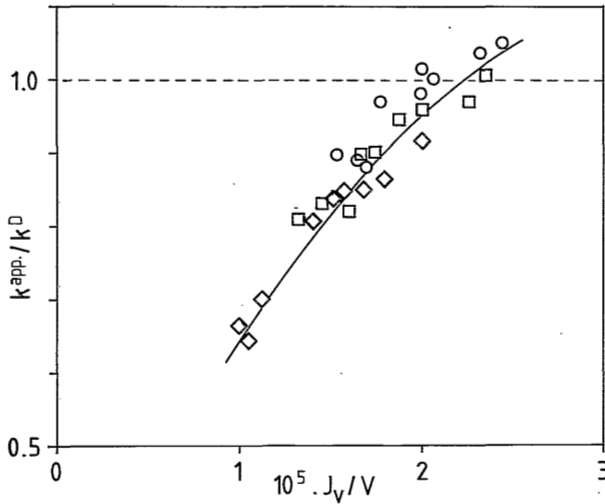


FIGURE 4. The ratio $k^{\text{app}}/k^{\text{D}}$ plotted as a function of the ratio of the permeate volume flux and the axial bulk velocity, J_v/V . The symbols are the same as in the figures 2 and 3.

Thomas [6] and Mizushina *et al.* [7]. Johnson *et al.* and Thomas studied the mass transfer coefficient in hyperfiltration systems and concluded that if $J_v/V < 3 \cdot 10^{-5}$ no effect of J_v on the flow field could be observed. Mizushina *et al.* measured the transport coefficient in a turbulent tube flow by a diffusion-controlled electrode reaction and they observed no deviations from the film model ($J_v/V < 2.13 \cdot 10^{-5}$).

DISCUSSION

Figure 4 suggests that there is a distinct influence of the ratio J_v/V on the apparent mass transfer coefficient in the range $1 \cdot 10^{-5} < J_v/V < 3 \cdot 10^{-5}$. Contrary with this are the findings in the literature cited above. The ques-

tions now is how to explain this contradiction. Finding the answer is not unimportant, since reliable expressions for the mass transfer coefficient in ultrafiltration systems are needed for the prediction of the permeate flux.

We think that in order to solve this problem more work is necessary. In this appendix we will restrict ourselves to the following remarks:

- The experiments of Johnson *et al.* and Thomas are hyperfiltration experiments and ours are ultrafiltration experiments. It is possible that the influence of J_v on k^{app} is more pronounced in an ultrafiltration boundary layer with its high viscosity. Thomas [6] found that at very high permeate fluxes ($J_v/V > 3 \cdot 10^{-5}$) the concentration polarization is less than predicted by the film theory, i.e. k^{app} increases with J_v .

- Since k^D has been calculated on the basis of bulk solution properties, it is possible that the effects of varying diffusivity and viscosity have contributed to the phenomenon shown in Figure 4.

- From Figure 4 one infers that k^{app} differs the most from k^D for low values of J_v/V . This is remarkable as the Deissler equation has been developed for low degrees of concentration polarization, i.e. low values of J_v/V .

- The k^{app} values are calculated with aid of the osmotic pressure model. Systematic errors in the osmotic pressure data and in the J_v versus ΔP data could lead to systematic deviations in k^{app} , especially at low degrees of polarization (low values of J_v/V).

A direct measurement of the membrane surface concentration, c_m , would solve these problems to a large extent. An effective method has not yet been proposed.

- It is worthwhile to perform ultrafiltration experiments with J_v/V values outside the range studied here, and to extend these experiments to other solutes.

REFERENCES AND NOTES

- [1] J.G. Wijmans, S. Nakao, J.W.A. van der Berg, F.R. Troelstra and C.A. Smolders, Chapter 8 of this thesis.
- [2] J.G. Wijmans, MSc Thesis, Twente University of Technology, Enschede, The Netherlands, 1980.
- [3] E.N. Sieder and G.E. Tate, *Ind. Eng. Chem.*, 28 (1936) 1429.
- [4] This is achieved by either incorporating the convection term in the differential mass balance of the boundary layer, or by using the Stewart (*) correction factor for the mass transfer coefficient. The concentration polarization equation obtained is the same for both approaches.
(*) R.B. Bird, W.E. Stewart and E.N. Lightfoot, *Transport Phenomena*, 656-663, Wiley, New York, 1965.
- [5] J.S. Johnson, L. Dresner and K.A. Kraus, in *Principles of Desalination*, K.S. Spiegler Ed., Academic Press, New York, 1966.
- [6] D.G. Thomas, *Ind. Eng. Chem. Fundam.*, 12 (1973) 396.
- [7] T. Muzishina, A. Takeshita, J. Yoshizama and I. Nakamae, *J. Chem. Eng. Jap.*, 5 (1972) 4, 361.

SUMMARY

This thesis concerns the mechanism of formation of synthetic membranes (part I) and the concentration polarization phenomenon in ultrafiltration (part II). In the first chapter a general introduction to membrane separation technology and to the problems treated in this thesis is given.

PART I

In chapter 2 the preparation of membranes by the phase inversion process is discussed and the hypothesis on the formation of membranes as adopted in our laboratory is introduced. Important aspects are the phase separation phenomena of the membrane forming system, i.e. gelation and liquid-liquid demixing, and the mass transfer during the coagulation process. Parameters which determine the membrane structure are identified.

In chapters 3 and 4 detailed investigations into the phase separation phenomena in membrane forming systems containing respectively the polymers polysulfone (PSf) and polyphenyleneoxide (PPO) are described. With the help of turbidimetry, differential scanning calorimetry and pulse induced critical scattering, the phase boundaries in the phase diagrams are determined. Attention is paid to the kinetics of crystallization in the PPO systems. The results are discussed in relation to the properties of PSf and PPO membranes and it is suggested that liquid-liquid demixing is responsible for the formation of pores in the skin layer of ultrafiltration membranes.

Chapters 5 and 6 are directed at the variation of the composition of the casting solution and of the coagulation bath in ternary membrane forming systems. The effect of these parameters on the structure of the top or skin

layer of the membranes is rather strong and there seems to be a common trend for all systems studied. The results are in qualitative agreement with the predictions of a model description in which the ratio of the solvent outflow and the nonsolvent inflow at the first moment of coagulation is related to the ratio of the chemical potential differences at the film/bath interface.

In an appendix to part I a model for the diffusive exchange of solvent and nonsolvent during immersion precipitation as put forward in the literature is discussed and partly criticized. The description of the local composition in a precipitating film at every point of time remains an important and interesting problem.

PART II

In chapter 7 the influence of osmotic pressure on the ultrafiltration permeate flux is analyzed. It is shown that osmotic pressure plays an important role and that this osmotic effect strongly resembles the effect of the formation of a gel layer. It is believed that the possibility of flux limitation by osmotic pressure is generally underestimated.

In chapter 8 it is shown that the effect of concentration polarization on the permeate flux in ultrafiltration can be described *i*) by a reduction of the driving force due to an osmotic pressure (the osmotic pressure model) and *ii*) by an increase of the total resistance due to the resistance of the boundary layer (the boundary layer resistance model). The analysis is restricted to fluid boundary layers with Newtonian behaviour. It appears that these two approaches are essentially equivalent and that the resistance of the boundary layer can be computed with the solvent permeability of the macromolecular solute, as determined by ultracentrifugation experiments.

Finally, in an appendix, attention is paid to the mass transfer near the membrane surface in ultrafiltration applications. Effective methods to predict or directly measure the mass transfer coefficient are not available at this moment.

SAMENVATTING

Dit proefschrift heeft als onderwerpen het vormingsmechanisme van synthetische membranen (deel I) en de concentratie polarisatie in ultrafiltratie toepassingen (deel II). In het eerste hoofdstuk wordt een korte inleiding gegeven in de membraantechnologie en in de behandelde onderwerpen.

DEEL I

In hoofdstuk 2 wordt de vervaardiging van membranen via het fase-inversie proces beschreven en wordt de in onze groep opgestelde hypothese over de vorming van membranen geïntroduceerd. Belangrijke aspecten zijn de fasenovergangen in het membraanvormend systeem, d.w.z. gelering en vloeistof-vloeistof ontmenging, en het massatransport tijdens de coagulatie. Aangeduid worden de parameters die bepalend zijn voor de membraanstructuur.

De hoofdstukken 3 en 4 beschrijven de studies naar de fasenovergangen in membraanvormende systemen, waarbij de polymere component bestaat uit respectievelijk polysulfon (PSf) en polyphenyleenoxide (PPO). Met behulp van turbidimetrie, 'differential scanning calorimetry' en 'pulse induced critical scattering' zijn de fasengrenzen in de verschillende fasediagrammen bepaald. In de PPO systemen is de kinetiek van kristallisatie onderzocht. De resultaten zijn verwerkt in samenhang met de eigenschappen van PSf en PPO membranen en verondersteld wordt dat vloeistof-vloeistof ontmenging verantwoordelijk is voor de vorming van de poriën in de toplaag van ultrafiltratie membranen.

De hoofdstukken 5 en 6 zijn gewijd aan de variatie van de samenstelling van de gietstroop en van het coagulatiebad in ternaire membraanvormende systemen. De invloed van

deze parameters op de structuur van de top laag van de membranen is groot en er blijkt voor de bestudeerde systemen een gemeenschappelijke trend te zijn. De resultaten komen kwalitatief overeen met de voorspellingen van een model waarin de verhouding van de oplosmiddel uitstroom en de nietoplosmiddel instroom in het begin van de coagulatie, beschreven wordt met de verhouding van de chemische potentiaal verschillen over het bad/film grensvlak.

In een appendix van deel I wordt een modelbeschrijving van de uitwisseling van oplosmiddel en nietoplosmiddel tijdens de coagulatie, afkomstig uit de literatuur, besproken en voor een gedeelte bekritiseerd. De beschrijving van de samenstelling van een coagulerende film op elk tijdstip en op elke plaats blijft een belangrijk en interessant probleem.

DEEL II

In hoofdstuk 7 is de invloed van osmotische druk op de permeaatflux in ultrafiltratie onderzocht. De osmotische druk blijkt een belangrijke rol te spelen en het effect van de osmotische druk is vrijwel identiek aan het effect van de vorming van een gellaag. De mogelijkheid van flux limitering door osmotische druk is groter dan in het algemeen wordt aangenomen.

Hoofdstuk 8 laat zien dat het effect van concentratie polarisatie op de permeaatflux in ultrafiltratie beschreven kan worden *i)* door een vermindering van de drijvende kracht door een osmotische druk (het osmotische druk model) en *ii)* door een toename van de totale weerstand ten gevolge van de weerstand van de grenslaag (het grenslaag weerstand model). De beschrijving is beperkt tot vloeibare grenslagen met een Newtons gedrag. Het blijkt dat beide benaderingen volledig gelijkwaardig zijn en dat de weerstand van de grenslaag berekend kan worden met de

permeabiliteit van de opgeloste macromoleculen. De permeabiliteit wordt bepaald met behulp van ultracentrifuge experimenten.

Tenslotte wordt in een appendix aandacht geschonken aan de stofoverdracht bij het membraanoppervlak in ultrafiltratie toepassingen. Effectieve methoden om de transport coëfficiënt te voorspellen of te meten, zijn nog niet voorhanden.

SAMENVATTING VOOR DE LEEK

In het onderzoek dat ik de afgelopen vier jaar heb verricht, hebben membranen centraal gestaan. Wat zijn membranen en waarom wordt er onderzoek aan gedaan?

Membranen zijn in wezen filters die bepaalde stoffen doorlaten en weer andere stoffen tegenhouden. Op die manier is een scheiding van verschillende componenten mogelijk: zoals kippegaas kippen tegenhoudt, houdt een vergiet de macaroni tegen en zoals een koffiefilter het maaisel tegenhoudt, houdt een membraan bepaalde moleculen tegen. Een membraan is dus een filter met een heel fijne structuur en om het maar even heel optimistisch te stellen: met membranen kan in principe elke scheiding bewerkstelligd worden. De eerste voorwaarde is natuurlijk wel dat een membraan met een geschikte structuur voorhanden is. Over het maken van membranen met gunstige eigenschappen gaat deel I van dit proefschrift.

Het merendeel van de membranen wordt gemaakt van kunststof ("plastic") en bij de bereiding worden naast de kunststof twee vloeibare stoffen gebruikt. Het essentiële is dat de combinatie van de drie verschillende stoffen in bepaalde verhoudingen een vloeistof is en in andere verhoudingen een vaste stof. Het membraan wordt nu gemaakt door van de vloeistof een dunne laag te maken en daarna de onderlinge verhouding van de componenten zodanig te veranderen dat de laag vast wordt. De wisselwerking tussen de drie componenten en de manier waarop de onderlinge verhouding wordt veranderd, blijken in grote mate de structuur van het membraan te bepalen. Ik heb deze twee aspecten bestudeerd om een beter inzicht te krijgen in de vorming van de membranen. De resultaten zijn verwerkt in een model dat als leidraad kan dienen voor de ontwikkeling van membranen met zodanige eigenschappen dat scheidingen

(denk bijvoorbeeld aan de afvalwaterproblematiek) op een economische wijze kunnen worden uitgevoerd.

Deel II heeft geen relatie met de vorming van membranen, maar behandelt een probleem dat optreedt als de membranen gebruikt worden en dat concentratie polarisatie genoemd wordt. Dit verschijnsel is te verduidelijken aan de hand van een welbekend proces: het zetten van koffie. Het zal iedereen wel eens zijn opgevallen dat de laag gemalen koffie na afloop dunner en compacter is geworden. Dit komt door het water dat het maalsel heeft meegenomen in de richting van het filter. Het feit dat voor een filter of membraan de tegengehouden stof zich ophoopt, wordt met het begrip concentratie polarisatie aangeduid. Het gevolg van deze opeenhoping is dat het water (de koffie) niet zo snel door het filter stroomt als mogelijk zou zijn: de koffie (?) gezet met een leeg filter is veel sneller klaar. De laag voor het filter of membraan bezit dus een zekere weerstand en bij een specifiek membraanscheidingsproces, de ultrafiltratie, blijkt deze weerstand veel groter te zijn dan de weerstand van het membraan zelf. In deel II ben ik nader ingegaan op de manier waarop de weerstand van de laag kan worden beschreven en het bleek mogelijk de weerstand te berekenen op grond van onafhankelijk gemeten eigenschappen van de tegengehouden stof. Op deze wijze is het mogelijk van te voren een uitspraak te doen over "het tijdstip waarop de koffie klaar is".

LIST OF PUBLICATIONS

- Zoutconcentratie gradiënten als potentiële energiebron: druk gelimiteerde osmose
J.G. Wijmans
Elektrotechniek, 60 (1982) 123
- The mechanism of formation of microporous or skinned membranes produced by immersion precipitation
J.G. Wijmans, J.P.B. Baaij and C.A. Smolders
J. Membrane Sci., 14 (1983) 263
- Removal of a low molecular weight, crystallizable polymer fraction from solutions of polysulfone
J.G. Wijmans and C.A. Smolders
Eur. Polym. J., 19 (1983) 1143
- Diffusion during immersion precipitation
J.G. Wijmans, F.W. Altena and C.A. Smolders
J. Polym. Sci. Polym. Phys. Ed., 22 (1984) 519
- Flux limitation in ultrafiltration:
Osmotic pressure model and gel layer model
J.G. Wijmans, S. Nakao and C.A. Smolders
J. Membrane Sci., 20 (1984) 115
- Hydrodynamic resistance of concentration polarization boundary layers in ultrafiltration
J.G. Wijmans, S. Nakao, J.W.A. van den Berg, F.R. Troelstra and C.A. Smolders
accepted by the J. Membrane Sci.
- Preparation of asymmetric membranes by the phase inversion process
J.G. Wijmans and C.A. Smolders
accepted by NATO Advanced Studies Institute Series
- Preparation of polymeric membranes by the phase inversion process
M.H.V. Mulder, J.G. Wijmans and C.A. Smolders
Textbook European Summer School on Membrane Science and Technology, Cadarache, France, September 3-7, 1984

- Phase separation phenomena in solutions of polysulfone in mixtures of a solvent and a nonsolvent: relationship with membrane formation
J.G. Wijmans, J. Kant, M.H.V. Mulder and C.A. Smolders submitted to Polymer
- Phase separation phenomena in solutions of poly (2,6-dimethyl-1,4-phenyleneoxide) in mixtures of trichloroethylene, 1-octanol and methanol: relationship with membrane formation
J.G. Wijmans, H.J.J. Rutten and C.A. Smolders submitted to J. Polym. Sci. Polym. Phys. Ed.
- The formation of membranes from ternary systems: variation of preparation parameters
J.G. Wijmans, R.J. Johanns and C.A. Smolders submitted to J. Membrane Sci.
- A rationale for the preparation of asymmetric pervaporation membranes
M.H.V. Mulder, J. Oude Hendrikman, J.G. Wijmans and C.A. Smolders submitted to J. Appl. Polym. Sci.
- Diffusion of solvent from a cast cellulose acetate solution during the formation of skinned membranes
F.W. Altena, J. Smid, J.W.A. van den Berg, J.G. Wijmans and C.A. Smolders submitted to Polymer
- Resistance to the permeate flux in unstirred ultrafiltration. Part II. Dissolved macromolecular solutions
S. Nakao, J.G. Wijmans and C.A. Smolders to be submitted to J. Membrane Sci.

LEVENSLLOOP

Hans Wijmans werd op 24 mei 1955 geboren te Amsterdam. In 1972 behaalde hij het HBS-B diploma aan de Thorbecke Scholengemeenschap te Zwolle en begon hij met de studie Chemische Technologie aan de Technische Hogeschool Twente te Enschede. Hij behaalde in 1978 het baccalaureaats diploma (vakgroep Macromoleculaire Chemie en Materiaalkunde) en in 1980 het doctoraal diploma (vakgroep Proceskunde en Industriële Processen).

Van 1 augustus 1980 tot 1 augustus 1984 was hij werkzaam als wetenschappelijk assistent bij de werkgroep Membraanfiltratie van de Technische Hogeschool Twente en verrichtte hij het onderzoek dat in dit proefschrift beschreven is.

